2022-01-04

Probing the Chemistry of Methylmercury in Mammalian Blood Plasma

Bridle, Tristen G.

UNIVERSITY OF CALGARY

Probing the Chemistry of Methylmercury in Mammalian Blood Plasma

by

Tristen Glenn Bridle

A THESIS

SUBMITTED TO THE FACULTY OF GRADUATE STUDIES

IN PARTIAL FULFILMENT OF THE REQUIREMENTS FOR THE

DEGREE OF MASTER OF SCIENCE

GRADUATE PROGRAM IN CHEMISTRY

CALGARY, ALBERTA

JANUARY, 2022

Abstract

A size-exclusion chromatography-inductively coupled plasma-atomic emission spectroscopy (SEC-ICP-AES) technique was developed for the analysis of mammalian blood plasma for endogenous metalloproteins and exogenous metal species. Parameters related to sample preparation, separation, and detection were optimized. The blood plasma was filtered through a 0.45 μm pore size syringe filter to preserve the separation performance of the column. The 1:1 dilution of filtered human and rabbit blood plasma in phosphate-buffered saline (PBS) prior to analysis was needed to prevent peak tailing and shoulder formation. An SRT-10C SEC column from Sepax Technologies Inc., when compared to a previously used Superdex 200 Increase SEC column, gave the same number of peaks with similar resolution, but in approximately half the time and with higher peak intensities. The mass recovery of proteins on the SRT-10C SEC column was 96 ± 2%. To explore the role that small molecular weight plasma thiols play in the delivery of methylmercury (CH_3Hg^+) to transporters located at the placental and blood-brain barriers, the described SEC-ICP-AES technique was applied to the analysis of CH_3Hg^+-spiked rabbit plasma using PBS mobile phases in the absence and presence of the small-molecular weight (SMW) sulfur compounds L-cysteine (Cys), L-homocysteine (hCys), L-glutathione (GSH), and D-methionine (Met). While Met did not affect the binding of CH_3Hg^+ to the main plasma protein, rabbit serum albumin (RSA), Cys, hCys, and GSH did. The presence of 50 μM Cys, hCys, or GSH in the mobile phase resulted in the mobilization of CH_3Hg^+ from RSA in rabbit plasma and from pure RSA in solution. The SMW-Hg species that formed when hCys was present in the mobile phase was qualitatively identified by electrospray ionization mass spectrometry as CH_3Hg-hCys. Using the developed metallomics technique I have found evidence of the formation of SMW-CH_3Hg^+ species under near-physiological conditions that may be involved in the translocation of CH_3Hg^+ from blood plasma to the brain.

Preface

Chapter 1. Portions of the introductory text are used with permission from American Association for the Advancement of Science. Figure 1.2 is modified from Figure 2 in Mertz (1981).

Chapter 4. Figures in this chapter are used with the permission of Multidisciplinary Digital Publishing Institute and Bridle et al. (2021) of which I am an author. Figure 4.1 is taken from Figure 4 in Bridle et al. (2021). Figure 4.5 is modified from Figure 3 in Bridle et al. (2021).

The experiments reported in Chapters 3 and 4 were covered by Ethics ID REB15-1138_REN7, issued by the University of Calgary Conjoint Health Ethics Board for the project "Effect of Albumin Addition to Human Plasma to Alter the Plasma Binding of Cis-Platin" on September 24, 2021.

Acknowledgements

My deepest gratitude is extended towards Dr. Jürgen Gailer, who has provided me with the opportunity to work on a wonderful and important project. His guidance and support have been instrumental to my development as a scientist and as a man. On the door to his office reads a proverb, “A single conversation with a wise man is better than ten years of study.” I have found this to be true.

To the members of my supervisory committee, Dr. Farideh Jalilehvand, Dr. Susana Kimura-Hara, and Dr. Kevin Thurbide, who have provided helpful advice, guidance, and support throughout my degree. To Dr. Hans Osthoff, for sharing his knowledge, feedback, and for serving as the internal-external examiner on my defense committee. To Dr. Todd Sutherland, for serving as the neutral-chair on my defense committee.

To Janice Crawford and Chadwick Dawes, for all of their reliable administrative help and making my degree proceed smoothly.

To Kerri Miller and Wade White, for their invaluable guidance and expertise.

To Dr. Yuen-ying Carpenter, Dr. Julie Lefebvre, Dr. Amanda Musgrove, and Dion Rock, for providing me with a great environment to learn and teach in CHEM 203, 311, and 315.

To Sophia Sarpong-Kumankomah, Maryam Doroudian, and Astha Gautam, for teaching me many things and providing me with great friendship.

To Justin La, for an unwavering friendship throughout our high school and university years.

To my brother Jodi, my parents Bart and Janice, and my grandparents Bob and Eileen, for giving me the opportunity to go to university and their immense love and support.

You have made me who I am today. I am forever grateful.

Table of Contents

List of Tables

List of Figures

List of Symbols and Abbreviations

Symbol/Abbreviation	Definition
Å	Angstrom
AES	Atomic emission spectroscopy
Ar	Argon
AU	Arbitrary units
Au	Gold
As	Arsenic
As^{III}	Arsenite
As^{V}	Arsenate
BBB	Blood-brain barrier
BCA	Bicinchoninic acid
C	Carbon
CA	California
CE	Capillary electrophoresis
Cd	Cadmium
CH_3	Methyl group
CH_3Hg^+	Methyl mercury
Cu	Copper
Cys	Cysteine
c/s	Counts per second
Da	Dalton
DI	De-ionized
DMA^{III}	Dimethylarsinous acid
DMA^{V}	Dimethylarsinic acid
DNA	Deoxyribonucleic acid
EDTA	Ethylenediaminetetraacetic acid
ESI-MS	Electrospray ionization mass spectrometry

e.g.	*exempli gratia*, which means "for example"
eV	Electron volts
EXAFS	Extended x-ray absorption fine structure
Fe	Iron
Ft	Ferritin
g	Gram
GI	Gastrointestinal
GSH	Reduced Glutathione
GS	Oxidized Glutathione
H_2O_2	Hydrogen peroxide
Hb	Hemoglobin
HCl	Hydrochloric acid
hCys	Homocysteine
HEPES	4-(2-hydroxyethyl)-1-piperazineethanesulfonic acid
Hg	Mercury
Hg^0	Metallic mercury
Hg^{2+}	Inorganic mercury
His	Histidine
Hp	Haptoglobin
HPLC	High performance liquid chromatography
HSA	Human serum albumin
hTf	Holo-transferrin
i.e.	*id est*, which means "that is"
ICP	Inductively coupled plasma
I.D.	Inner diameter
ISM	International Symposium of Metallomics
KCl	Potassium chloride

kDa	Kilodalton
kV	Kilovolt
L	Litre
LA	Laser ablation
LAT 1/2	Large-neutral amino acid transporter 1 or 2
LC	Liquid chromatography
LD_{50}	Lethal dose for 50 % of exposed animals
LOD	Limit of Detection (3σ)
M	Molar
MA	Massachusetts
MALDI	Matrix assisted laser desorption ionization
Met	Methionine
min	Minute
mg	Milligram
mL	Millilitre
mM	Millimolar
MMA^{III}	Monomethylarsonous acid
MMA^{V}	Monomethylarsonic acid
MO	Missouri
MOPS	3-(N-morpholino)propanesulfonic acid
MS	Mass spectrometry
MW	Molecular weight
NaCl	Sodium chloride
NaOH	Sodium hydroxide
NH	New Hampshire
nL	Nanolitre
nm	Nanometer
NY	New York

$O_2^{\bullet-}$	Superoxide anions
OH	Hydroxyl group
ON	Ontario
PAGE	Polyacrylamide gel electrophoresis
PAH	Polycyclic aromatic hydrocarbons
Pb	Lead
PBS	Phosphate-buffered saline
PCB	Polychlorinated biphenyls
ppb	Parts per billion (µg/L)
ppm	Parts per million (mg/L)
Psi	Pounds per square inch
QC	Quebec
RBC	Red Blood Cells
RF	Radio frequency
RSA	Rabbit Serum Albumin
RNA	Ribonucleic acid
rpm	Rounds per minute
Se	Selenium
SEC	Size exclusion chromatography
SeO_3^{2-}	Selenite
Sel P	Selenoprotein P
SMW	Small molecular weight
SOD	Superoxide dismutase
Tf	Transferrin
TOF	Time of flight
t_r	Retention time
Tris	Tris(hydroxymethyl)-aminomethane
USA	Unites States of America

% w/v	Percent weight per volume
XAS	X-ray Absorption Spectroscopy
XANES	X-ray Absorption Near Edge Structure
µL	Microliter
µm	Micrometer
µM	Micromolar
µg	Microgram
~	Approximately
%	Percentage
Zn	Zinc

It is worrying that humanity has found itself in a situation of its own doing, where we debate the validity of the scientific analysis of our own near-term extinction.

Travis Ryan (The Great Dying II, Death Atlas, Cattle Decapitation, 2019 LP)

Chapter 1: Introduction

Copyright permission for the use of certain information and figures present in **Chapters 1** and **4** can be found in Appendix B.

1.1 Trace Elements in Biology

In humans, dietary energy is derived from carbohydrates (i.e., sugars, 55-60%), lipids (i.e., fats, <30%), and proteins (i.e., polypeptides/amino acids, 15%).[1] These macronutrients are composed of the "bulk elements" H, C, N, O, and S and are required on the order of grams (g) per day.[2] While these molecules provide the energy that is required for physical activity, mental activity, and growth, a balanced diet also needs to include micronutrients, which includes vitamins and minerals to help facilitate the biochemical processes which sustain life and wellbeing.[3] Vitamins need to be ingested on the order of micrograms (μg) to milligrams (mg) per day and often serve as coenzymes for enzymes responsible for metabolism (e.g., vitamin B_{12}), DNA synthesis and repair (e.g., vitamin B_9), and tissue repair (e.g., vitamin C).[1, 4, 5] Minerals can be further divided into two categories: macrominerals and microminerals. Macrominerals include elements such as Na, Mg, P, Cl, K, and Ca of which the ions Na^+, Mg^{2+}, K^+, and Ca^{2+} are electrolytes that play vital roles in maintaining the transmembrane potential of nerve cells and osmoregulation.[2, 6, 7] Mg^{2+} is also a cofactor that is involved in DNA synthesis.[8] Phosphate, PO_4^{3-}, is a key building block for phospholipids in cell membranes and the backbone of DNA, in addition to forming the high energy bonds in adenosine triphosphate (ATP), biology's energy currency.[9] Microminerals can be further divided into two categories: essential trace elements and essential ultratrace elements (**Fig. 1.1**). Essential trace elements can be defined as elements which have been established to be essential to organismal health by accepted scientific standards (e.g., Mn, Fe, Cu, and Zn) and are required on the order of mg per day.[2, 5] Essential ultratrace elements can be defined

as elements whose tissue concentrations are lower than that of trace elements (e.g., Se, Co, and Mo) and are required on the order of µg per day.[2, 5]

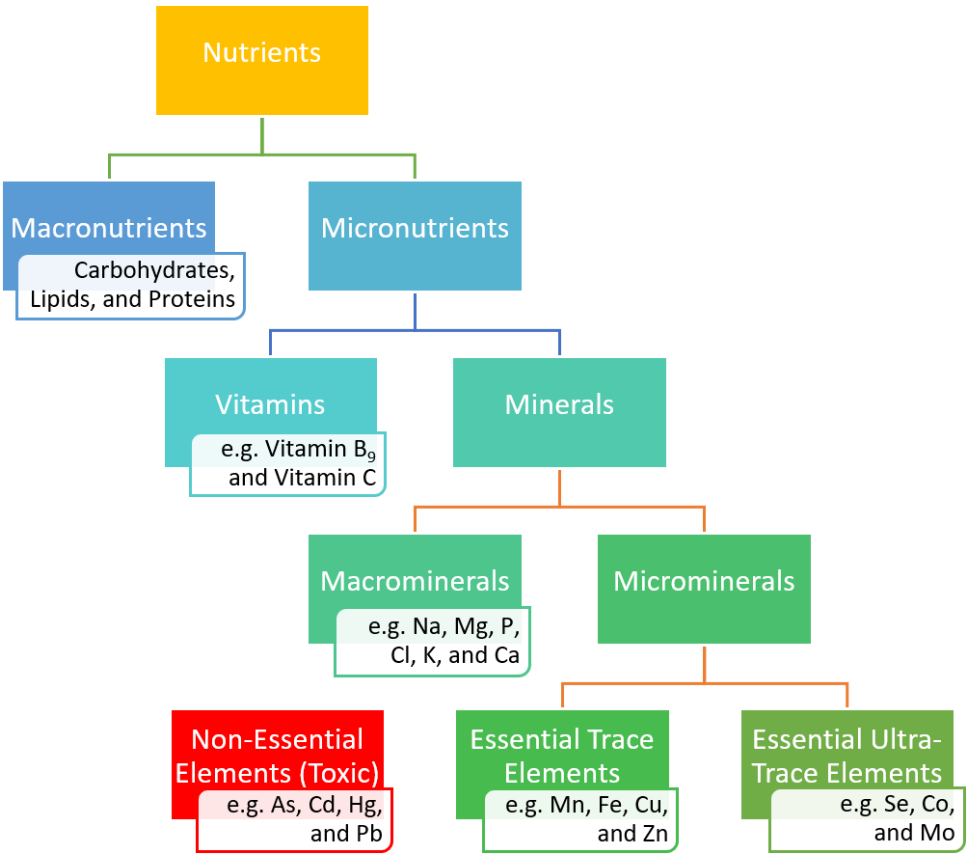

Figure 1.1: Essential nutrients that are important to the maintenance of health and wellbeing and non-essential elements that can be toxic to living organisms at relatively low doses. This figure was created based on the information present in references in **Section 1.1**.[1-9]

1.1.1 Essential Trace and Ultra-Trace Elements in Biology (i.e., Metals)

Approximately one third of all human proteins contain one or more metal ions as cofactors that are vital to the protein's structure and/or function.[10, 11] These metal-containing proteins, called metalloproteins, perform many important biological roles, such as catalysis, transport, and storage.[12] For example, Cu, Zn-superoxide dismutase (Cu, Zn-SOD or SOD1) is a metalloenzyme that is involved in reducing the oxidative stress on cells by catalyzing the conversion of the superoxide radical ($O_2^{\bullet-}$) into hydrogen peroxide (H_2O_2).[13, 14] Transferrin, on the other hand, is a

Fe^{3+}-transporting protein in the bloodstream that delivers Fe^{3+} to cells where it is required for cellular processes, such as DNA synthesis and repair.[15-17] Another metalloprotein, ferritin, serves as an intracellular iron-storage protein.[18] The essential elements that are required by these proteins to function (e.g., Cu, Fe, and Zn) must be effectively absorbed from the gastrointestinal tract into the bloodstream and subsequently transported to "downstream" organs so that bioinorganic chemistry processes, such as metalloprotein assembly can occur.[19, 20]

The dyshomeostasis (i.e., where homeostasis, which stems from the Greek words for "same" or steady", refers to the active maintenance of the stable conditions necessary for survival) of essential metals can have devastating effects on health (**Fig. 1.2**).[18, 21] For example, Wilson's Disease is a genetic disease which adversely affects the metabolism of copper, resulting in the inability of an individual to excrete copper from the body. As a result, copper accumulates in tissues such as the liver, eyes, and brain and can lead to severe neurological symptoms that resemble those of Parkinson's Disease.[22] The essential metal Zn plays important catalytic roles in metalloenzymes such as carbonic anhydrase and those involved in gene regulation (e.g., DNA polymerase).[23] However, factors such as insufficient dietary intake, malabsorption from the diet, or genetics can lead to Zn-deficiency and has been associated with an increased rate of infection due to a reduced lymphocyte count.[23] Additionally, the dyshomeostasis of Zn has been linked to the pathogenesis of Alzheimer's Disease.[24] Evidently, both an excess and a deficiency of an essential element can have severe adverse health effects and it is, therefore, vital that these elements are obtained in sufficient amounts from the diet, their tissue concentration effectively regulated, and that any excess is appropriately excreted from the body.[19]

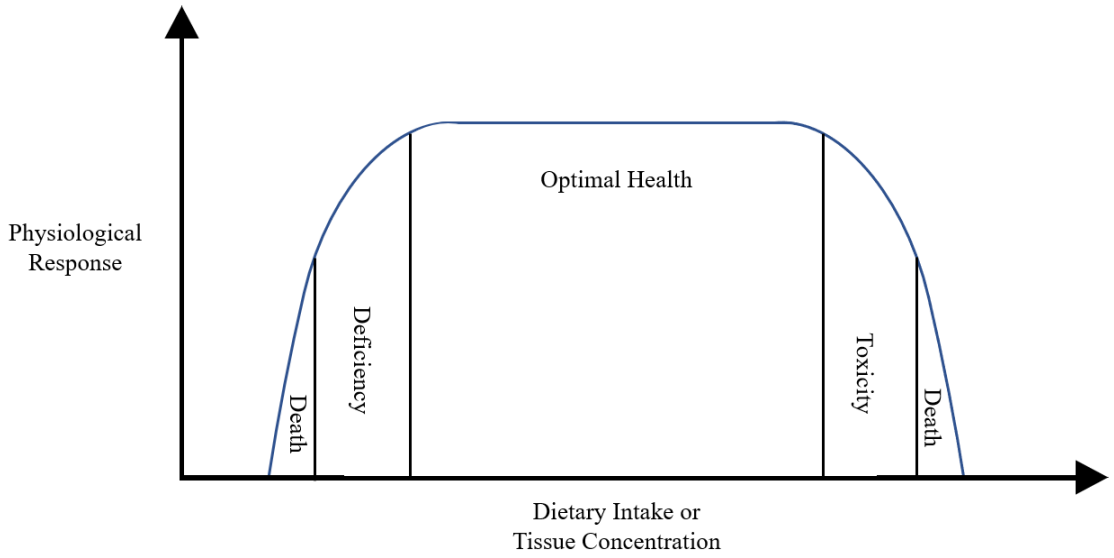

Figure 1.2: Bertrand Diagram illustrating the effect of dietary intake or tissue concentration of an essential element on the health of an organism. Modified from Mertz (1981).[2]

1.1.2 Non-Essential Elements in Biology

While the previously mentioned examples demonstrate the vital roles of certain metals in biology, not all elements serve a biochemical role within an organism. These metals are consequently classified as non-essential elements (**Figure 1.1, red box**). The toxicity of non-essential elements depends on their molecular form, time of exposure (i.e., chronic/acute), route of exposure (e.g., inhalation or ingestion), and exposure dose (i.e., amount).[25, 26] For example, mercury (Hg) exists in multiple forms: the most toxicologically relevant of which include elemental mercury (Hg^0), mercuric ion (Hg^{2+}), methylmercury (CH_3Hg^+), and ethylmercury ($EtHg^+$, from the anti-bactericide thimerosal) and each of these exhibit their own unique mechanisms of toxicity.[25, 27] CH_3Hg^+ is a potent neurotoxin commonly found in fish (e.g., tuna contains 0.12-0.38 ppm CH_3Hg^+) and even low levels of exposure during childhood (e.g., manifesting as a 3-11 µg CH_3Hg^+/g brain tissue) have been linked to neurocognitive damage.[27-30]

The two most toxicologically relevant forms of arsenic (As) are arsenite [$As^{III}(OH)_3$] and arsenate ($As^{V}O_4^{3-}$), which are frequently present in contaminated drinking water; the United States Environmental Protection Agency has established that the maximum permissible As concentration in drinking water is 10 ppb.[31] Human exposure to approximately 200 µg As/day has been linked to an increased risk for a variety of cancers (e.g., lung, bladder, and kidney cancer).[31, 32] Arsenite (As^{III}) and arsenate (As^{V}) are metabolized in mammals to form methylated products, such as the trivalent metabolites monomethylarsonous acid (MMA^{III}) and dimethylarsinous acid (DMA^{III}) and the pentavalent metabolites monomethylarsonic acid (MMA^{V}) and dimethylarsinic acid (DMA^{V}), which collectively determine the toxic effects on the body.[19, 31, 33] However, arsenobetaine [$(CH_3)_3As^+CH_2COO^-$], an organic form of arsenic found in the tissues of mussels and other seafoods, has been demonstrated to be effectively non-toxic to humans.[34] Cd^{2+} is a well known nephrotoxin and has also been classified as a Group 1 human carcinogen by the International Agency for Research on Cancer.[35] Cd also provides an excellent example of ionic mimicry, a term used when an unbound cation (e.g., of a non-essential metal) is able to act as a structural and/or functional homologue of an endogenous essential metal.[36] For example, Cd^{2+} has been shown to displace Zn^{2+} from Zn-binding sites in metalloproteins suggesting a greater binding affinity to those sites than Zn^{2+}.[31, 37]

It should be noted that the ingestion of non-essential elements can disrupt the homeostasis of essential elements. One example of such an occurrence is the interaction between As and Se species in the bloodstream.[19, 38] Se is an essential ultratrace element that, in the form of the amino acid selenocysteine, is incorporated into a number of selenoproteins (e.g., glutathione peroxidases) and whose deficiency has been associated with increased mortality rates in cancer patients.[38, 39] It has been shown that the simultaneous intravenous injection of rabbits with equimolar amounts of

arsenite and selenite (SeO_3^{2-}) resulted in the excretion of an As-Se species in the bile.[40] X-ray absorption spectroscopy (XAS) revealed this As-Se species to be the seleno-bis(*S*-glutathionyl) arsinium ion, $[(GS)_2As\text{-}Se]^-$, and it was later revealed that the formation of $[(GS)_2AsSe]^-$ took place in the cytoplasm of erythrocytes and in hepatocytes, facilitated by the relatively high concentration of reduced glutathione (GSH) therein.[19, 41] This suggests that the formation of the $[(GS)_2AsSe]^-$ species may protect organs from the toxic effects of As^{III}.[19, 42] However, the involvement of the essential trace element Se in this process, of which humans need to ingest ~55 µg/day, indicates that the homeostasis of Se can be perturbed by As^{III} thereby reducing the bioavailability of Se from the diet and, therefore, potentially resulting in Se-deficiency. In such a case, reduced Se-influx means that insufficient amounts of Se are reaching "downstream" target organs for its incorporation into selenoproteins.[38, 42] The ubiquitous nature of metal species in life processes, such as the genomic/proteomic examples previously mentioned, has established the relevance and importance of metals in biology and in recent years has successfully rooted a new field of study. Known as metallomics, this scientific field focusses on delineating the involvement of metals and other trace/ultra-trace elements in life processes and encompasses many disciplines such as biology, chemistry, geology, physics, medicine, and pharmacology.[43] The concept of "Metallomics as Integrated Biometal Science" was proposed by Hiroki Haraguchi in 2004 and will be elaborated upon in the following section.[44]

1.2 Introduction to Metallomics

In 2001, R. J. P. Williams introduced the idea of a "metallome" as the free element content of cells (i.e., the trace element distribution within the cells and tissues of an organism).[45] However, it was not until 2004 that Hiroki Haraguchi's suggested "Metallomics as integrated biometal Science" which eventually resulted in the definition of the field of metallomics.[44] Therein he

outlined the need for another "omics" field that was separate yet complementary to genomics and proteomics since the "syntheses and metabolic functions of genes (DNA and RNA) and proteins cannot be performed without the aid of various metal ions and metalloenzymes." Haraguchi proposed that metallomics be a new scientific field that integrated all research fields that involved "biometals" and defined the metallome as all "metalloproteins, metalloenzymes and other metal-containing biomolecules." In a 2004 paper titled "Metallomics: a new frontier in analytical chemistry", Joanna Szpunar defined metallomics to be the determination of the identity and concentration of metal and metalloid species in biology (note: "metal and metalloid species" will simply be referred to as "metal species" hereafter).[46] She also elaborated to say that the study of a metallome, well defined as the entirety of metal species within a cell or tissue type, will provide information as to (i) the distribution of metal species in subcellular compartments of a given cell type, (ii) the binding/complexation of metals/metalloids to other biomolecules, and (iii) the concentration of these metal species present within a given medium.[46]

Following the publication of Haraguchi's "Metallomics as Integrated Biometal Science", metallomics was officially designated a scientific field in 2004.[43, 44] In 2007 the first International Symposium of Metallomics (ISM) was held in Nagoya, Japan.[43, 47] Since then, the ISM has played a significant role in disseminating metallomics into other scientific disciplines and communities.[43, 47-51] In 2009, the Royal Society of Chemistry launched the journal *Metallomics* whose mission has since been "to publish cutting-edge investigations that consider the metallome (metal, metalloid or trace element) of an entire system, and investigations that may report on the effect of individual metal ions on the organism's other 'omes', such as the genome, proteome or metabolome."[43, 52] Since its inception, Metallomics has published nearly 1600 articles (12 issues/year), accumulated over 6000 citations, and established a 5-year impact factor of 4.69 (Web of Science, **Fig 1.3.**).

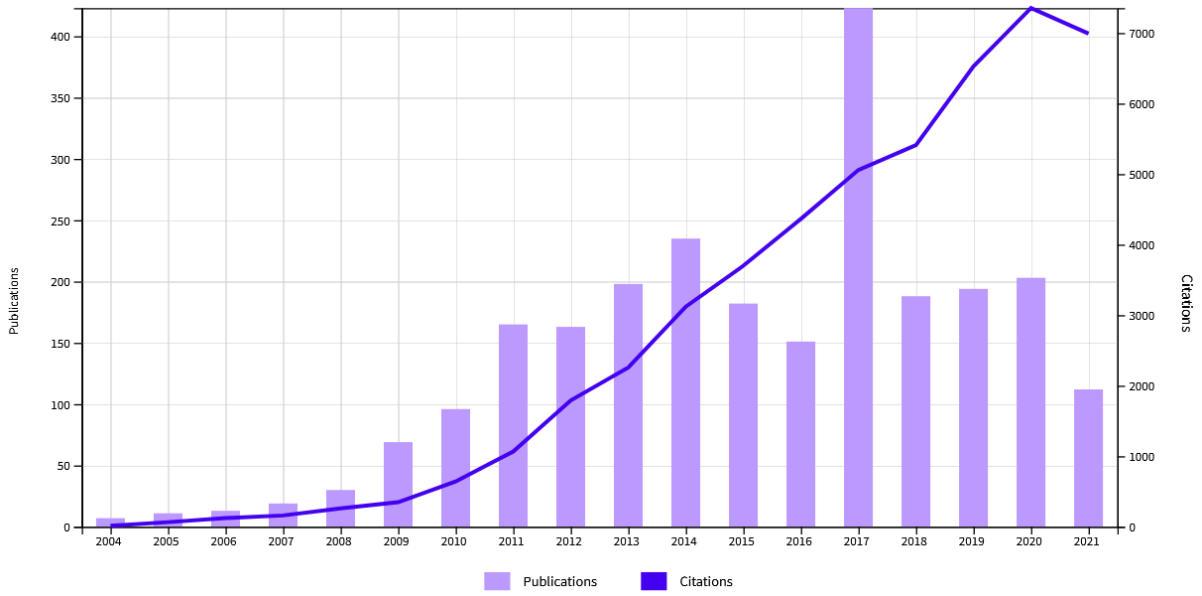

Figure 1.3: Citations and number of articles published in *Metallomics* (Web of Science).

Metallomics embodies many research subjects that utilize different scientific approaches to solve problems or make new discoveries. For example, the analytical approach focuses on the quantitative distribution of elements in biological fluids and tissues, in addition to determining elemental speciation both within and outside the metallome.[43] Alternatively, the structural analysis of the metallome and determining its molecular mechanisms embody a bioinorganic chemistry approach. Other approaches such as that of biochemistry or medicine encompass other focuses such as metalloprotein identification, metabolism of metal-species, or more effective metallodrug design to improve drug efficacy and reduce side-effects. However, all of these approaches embody what can be called the "metallomics approach" where each offers its own unique insight into a problem and come together to provide a comprehensive understanding of metals in biology.

1.3 Metallomics Techniques

The vast number of proteins and other biomolecules that are present in biological fluids makes a comprehensive yet interpretable analysis difficult. For example, the concentration of the

~4800 currently known proteins in blood plasma vary in abundance by up to 10 orders of magnitude, with 99% of total protein mass being accounted for in the most abundant 22 proteins.[53, 54] Therefore, a method that can "filter out" the unwanted information and focus on a subproteome (e.g., the metalloproteome) is desirable as it simplifies the analysis of such a complex biological fluid. Thus, the hyphenation of high-resolution separation techniques (e.g., size exclusion chromatography, polyacrylamide gel electrophoresis, capillary electrophoresis, etc.) to sensitive multi-element detection techniques (e.g., inductively coupled plasma-atomic emission spectroscopy or inductively coupled plasma-mass spectrometry) can provide a comprehensive yet specific analysis of complex biological samples for metalloproteins in what is called analytical elemental 'speciation'. However, the handling and preparation of biological fluids before metallomic analysis also needs to be carefully considered.

1.3.1 Sample Preparation for Metallomic Analysis

Since certain metal-biomolecule interactions may be labile (e.g., the transferrin-iron bond is pH sensitive)[55], it is important to consider the maintenance of physiologically relevant conditions for the metallo-entity during preparation and analysis. If it is only the total metal content of a biological sample that is the primary concern, then, for example, maintaining physiological conditions may not be of importance. However, under certain conditions, metal-protein bonds can become labile and prone to dissociation, and if the purpose of inquiry is to separate and identify metal species within a fluid/tissue, then it is of utmost importance to tailor the method (e.g., choice of buffers, pH, ionic strength, etc.) to ensure that these metal-protein interactions are not disrupted during preparation or analysis. The metal-protein bond is the result of the coordination of metal ions with specific amino acids on proteins which is largely dependent on the

structure/conformation of the protein itself.[10] Therefore, the use of a technique that prevents the denaturation of protein species in solution is essential.[12]

To prevent protein denaturation and maintain key biomolecular interactions, the native environment of the proteins of interest needs to be considered. Molecular crowding is the term used to describe the crowded intracellular environment. The concentration of biomolecules in the cytoplasm can reach up 400 g/L where they occupy up to 40% of the total volume.[56-58] This means that biomolecules, such as proteins, nucleic acids, lipids, and saccharides are always in constant close proximity with other biomolecules and thus there exists a nonspecific steric effect that influences the diffusion rate, structure, stability, and interactions.[57, 58] Therefore, this idea advocates that if a protein is removed from the highly concentrated cytoplasm and placed in a dilute buffer, stabilizing interactions will be lost and the structure of the protein may be compromised. Additionally, physiological pH should be maintained (i.e., pH of the local environment of the metalloprotein) as this directly influences the charges that amino acids that constitute proteins adopt.[59] If, for example, the protonation of acidic metal-binding residues occurs in a low pH buffer, there will be a reduction in the ability of these residues to coordinate metal ions (i.e., lowered binding affinity).[59]

The preparation of blood serum is done by allowing the blood to clot and then subsequently removing the supernatant from the clot after centrifugation.[60] Blood plasma is obtained by the addition of anti-coagulants to blood [e.g., heparin, ethylenediaminetetraacetic acid (EDTA), or citrate], which prevent the blood clotting process. Therefore, since blood plasma contains blood clotting proteins (e.g., blood coagulation factor V), it inherently contains more proteomic information than blood serum.[60, 61] EDTA and citrate function by binding calcium ions thereby preventing proteins involved in coagulation from binding them.[62] Alternatively, heparin binds to

and activates antithrombin, a protein that inactivates proteins involved in the coagulation process.[62, 63] It has been demonstrated that the use of EDTA or citrate as an anticoagulant causes interferences and matrix effects with co-eluting molecules.[62] Additionally, some chelating agents can form complexes with metal ions by abstracting them from metalloproteins, thereby altering the metallomic information that is observed (e.g., altered retention time/peak intensity).[64, 65]

To prevent the degradation of metalloproteins during sample preparation and analysis, the use of protease inhibitors may be necessary. However, certain protease inhibitors, such as 4-benzenesulfonyl fluoride hydrochloride, can form covalent bonds with proteins thus introducing artifacts in the observed molecular weight during certain analyses (e.g., mass spectrometry).[66] Alternatively, undesired protease activity may be avoided by the freezing of the samples in liquid nitrogen and thawing them immediately before analysis.[67-69] However, it must be considered that the freezing of a sample may have adverse effects on the structural integrity of the proteins present. For example, in a study conducted by Cao et al., the thawing of a previously frozen aqueous sample of alcohol dehydrogenase at a rate of >5 ºC/min resulted in irreversible protein damage. However, when the same sample was thawed at a rate of 1 ºC/min, the structure of the protein recovered much more effectively.[70] There must be a careful consideration of the sample preparation to ensure that the analysis of the biological fluid/tissue provides an accurate and meaningful result.

1.3.2 Metallomics Separation Techniques

Just as it is imperative that the metal-protein bond is not disrupted during sample preparation, it is equally important to conserve this bond during the separation process. Therefore, the choice of separation technique will need to be carefully considered. Additionally, the choice of buffers used in the separation needs to be carefully considered to maintain the integrity of the sample molecules in order to provide accurate information. For example, it has been demonstrated

that artifacts can be generated by using different mobile phase-buffers in size exclusion chromatography-inductively coupled plasma-atomic emission spectrometry (SEC-ICP-AES) when rabbit blood plasma was analyzed for Fe, Cu, and Zn metalloproteins.[71] Jahromi et al. studied the effects of four buffers, 150 mM phosphate-buffered saline (PBS, 10 mM NaH_2PO_4, 2.7 mM KCl, and 138 mM NaCl), 100 mM tris(hydroxymethyl)aminomethane (Tris), 100 mM 4-(2-hydroxyethyl)-1-piperazineethanesulfonic acid (HEPES), and 100 mM 3-(N-morpholino)propanesulfonic acid (MOPS) all at pH 7.4, on the SEC-ICP-AES-derived chromatograms of the rabbit blood plasma metalloproteome. It was observed that HEPES and MOPS buffers were causing the abstraction of Fe^{3+} from holo-transferrin (hTf). Additionally, the Zn-specific chromatograms of blood plasma revealed that when HEPES, MOPS, and Tris mobile phases were used, there was a redistribution of the peak area that corresponded to albumin-bound Zn, which was mediated by the buffer ions. Additionally, a small molecular weight Zn peak (<10 kDa) formed when Tris was used and was later identified by ESI-MS as a $Zn(Tris)_2^+$ complex. Meanwhile, when PBS was used as the mobile phase these artifacts were absent, having minimal adverse effects on metalloprotein-metal interactions. This study clearly demonstrates that the mobile phase used in the analysis of metalloproteins may have significant adverse effects on the information obtained from a given analytical method when analyzing blood plasma. As such, there exist numerous separation techniques that can be used, and each lends themselves towards a specific type of analysis. Each of the following methods will be discussed in relation to their use in separation and analysis of metalloproteins.

2-Dimensional Polyacrylamide Gel Electrophoresis (2D-PAGE)

2D Polyacrylamide Gel Electrophoresis (2D-PAGE) is a powerful proteomic tool that is used to separate proteins based on their isoelectric point (pI, the pH at which the protein possesses

a net zero charge) and subsequently their molecular weight (MW) by using a crosslinked polyacrylamide gel. 2D-PAGE is capable of separating and visualizing thousands of proteins in a complex biological sample, such as a tissue extract.[72] The extreme pH and detergent use in traditional 2D-PAGE compromises protein structure and is consequently not suitable to the analysis of metalloproteins since the metal-protein bond, whether it involves essential, trace, or toxic metals, will be broken. However, certain studies, like the one by Becker et al., demonstrated the use of a native-PAGE gel to separate metalloproteins present in rat kidneys and performed an elemental imaging for each protein spot using ICP-MS and matrix-assisted laser desorption/ionization (MALDI)-time of flight (TOF)-MS.[73] Additionally, protein spots on a 2D-PAGE gel can be subjected to laser ablation (LA)-ICP-MS for elemental analysis. However, while effective in separating an impressive number of proteins present in a biological sample, 2D-PAGE is very time consuming. Running one 2D-PAGE can take one to two days, considerably longer than other chromatographic methods (e.g., size exclusion chromatography).[61, 67] Additionally, the nature of 2D-PAGE prevents it from being involved in an online separation and detection technique. The visualization of the proteins by staining (e.g., with Coomassie blue) depends on the amount of protein present in each spot. Therefore, this technique requires a relatively large amount of protein which may not be possible to obtain from a given sample.[72]

Size Exclusion Chromatography (SEC)

Size exclusion chromatography (SEC) uses a porous stationary phase to separate molecules in a sample based on their size (i.e., hydrodynamic radius). In SEC, both the molecular weight of the analytes and the size of the pores in the stationary phase affect a molecule's retention on the column.[74] In a stationary phase with a given pore size, proteins diffuse in and out of the pores at a rate dependant on their size. For example, smaller molecules spend more time in and enter pores

more frequently and, therefore, the smaller molecules will elute from the column later.[75] Ideally, stationary phases in SEC should be inert to prevent direct interactions (i.e., ionic, covalent, or dipole-dipole) with analyte molecules thereby permitting their relatively gentle separation.[60] The theoretical absence of stationary phase-analyte interactions means that the risk of metal-protein bond disruption can be minimized which makes SEC an ideal separation method for metalloproteins.[60] Since SEC offers the ability to conduct isocratic separations (i.e., no salt gradient needed to remove stationary phase-bound proteins), there are minimal structural disruptions in the proteins resulting from extreme changes in ionic strength or polarity of the mobile phase.[61] As elaborated upon previously, PBS is an ideal choice for a mobile phase since it mimics most closely the physiological buffering conditions present in biological samples like blood plasma (pH 7.4) and prevents the formation of artifacts during separation.[61] Therefore, the combination of SEC and a PBS mobile phase presents itself as the optimal separation technique for biological samples containing metalloproteins as the native conformations of metalloproteins and, therefore, metal-protein bonds can be maintained.

Unlike 2D-PAGE, SEC is able to be hyphenated to an online separation-detection method. However, SEC only has a limited ability to provide high resolution separations of metalloproteins of similar molecular weight.[61] Therefore, while the analysis time of SEC is considerably lower than that of 2D-PAGE (hours compared to days), observed protein peaks can contain 'buried' peaks of other proteins present in the sample (i.e., one peak may be the convergence of many smaller peaks of different proteins).[61] Even the most advanced stationary phases (e.g., Superdex 200 Increase, 8.6 µm particle size, fractionation range: 10 – 600 kDa) cannot provide baseline separation of every metalloprotein species present in blood plasma.[71] As stated before, SEC stationary phases should theoretically be inert and, therefore, not interact with the injected

analytes, but protein binding and/or metal abstraction can occur depending on the phases used (e.g., some commercially available media can bind and retain Zn^{2+} ions).[67] During the separation of globular proteins, the relative retention time of each protein can be used to determine their approximate molecular weight. However, since not all proteins adopt a globular shape, the relationship between molecular weight and hydrodynamic radius cannot be assumed to be consistent across all proteins in a given sample. This means that the separation of all protein species in a biological sample will not be perfectly logarithmic with respect to molecular weight. As such, the presence of multiple proteins with similar hydrodynamic radii will result in peak broadening.[61] Similarly, the existence of different conformational states or post-translational modifications (e.g., phosphorylation) of a single protein in solution can broaden the peak.[34, 61]

Capillary Electrophoresis

Alternatively, the use of capillary electrophoresis (CE) as an online separation technique in analytical elemental speciation, specifically of metalloproteins and other metal species, is relatively new, but shows promise.[76-78] A fused silica capillary column, typically 20-100 μm in internal diameter and 20-100 cm in length, utilizes an electrical field (e.g., 10-30 kV), mediated by an appropriate electrolyte/buffer solution, to separate analytes in a sample based on their charge and size.[76] What is known as electrophoretic mobility is responsible for the migration of the analytes from one end of the capillary to the other and corresponds to the attraction of the charged analytes to the oppositely charged electrode. The rate of migration is dependent on the size-to-charge ratio of the analytes which, in combination with the inherent properties of the species, can be altered by controlling the pH of the electrolyte/buffer solution. As such, multiply charged, smaller analytes will move faster that singly charged, larger analytes. Similar to 2D-PAGE, the nature of the buffer solutions used (i.e., extreme pH or ionic strength) has the potential to adversely

affect the analytes in the sample (e.g., protonating/deprotonating amino acids responsible for coordinating metal ions/species). Additionally, the nature of the sample itself, specifically the conductivity of the sample, poses a limiting factor in the ability of CE to separate the analytes therein.[76] Additionally, the salt content of the sample may limit the use of CE and, therefore, require appropriate sample preparation or desalting.[78] However, CE offers the distinct advantages of requiring only small sample sizes/volumes and providing a high resolution of analytes.[76] Due to the small sample volumes (e.g., on the order of 10-2000 nL) a detection technique with a suitable detection limit will need to be coupled with CE (e.g., ICP-MS). As such, it may also be required to pre-concentrate the samples before analysis to ensure the adequate detection of the analytes.[76, 77]

1.3.3 Metallomics Detection Techniques

Upon the separation of the molecular constituents of a biological sample, a suitable detector must be utilized for comprehensive analysis. Metalloproteins can be described as heteroatom-containing proteins such that the bound metal species acts as a unique atomic identifier.[78] Therefore, the use of multielement-specific detectors, such as ICP-AES and ICP-MS, offer selective and sensitive methods for the detection of metallo-entities in biological samples.

The development of Inductively Coupled Plasma-Atomic Emission Spectroscopy (ICP-AES) and Inductively Couple Plasma-Mass Spectrometry (ICP-MS) as highly sensitive instruments capable of simultaneous multielement detection has leant itself towards the comprehensive elemental analysis of a wide variety of biological, environmental, and industrial samples.[43] Here, these technologies will be discussed as they pertain to the analysis of biological samples such as blood, cells, and tissues. While ICP-AES and ICP-MS are competent in the analysis of samples for their quantitative elemental composition, the molecular form or bound-

form of an element is also key to the comprehensive understanding of the roles of metal in biology. Therefore, these techniques are most effective when hyphenated to separation techniques, such as SEC, since they provide molecular information (e.g., molecular weight) to supplement the elemental information of the sample being analyzed.[12] The main advantage of online separation/detection methods, such as SEC-ICP-AES for example, is the rapid analysis time of the sample (e.g., <25 min after sample preparation).[60]

SEC-ICP-AES and SEC-ICP-MS techniques can be employed to simultaneously screen metallo-entities in biological fluids/tissues, selectively detecting individual metals (e.g., Cu, Fe, and Zn), and, therefore, have the potential to provide key insights into the roles that they play in both in health and disease. The detection limits of ICP-AES are 10-300 fold higher for Cu, Fe, and Zn compared to those for ICP-MS.[61] Consequently, the minimum amount of sample that is required for ICP-AES detection is on average higher than for ICP-MS. Similarly, the detection of endogenous ultra-trace elements in biological fluids (e.g., Mo and Se in blood plasma) via ICP-AES is practically impossible and, therefore, more suited to ICP-MS analysis.[67] However, ICP-MS detectors are incompatible with high salt content mobile phases or samples as the detector's orifices will collect salt and clog.[79] Therefore, they cannot be used in the analysis of high salt samples (e.g., blood plasma) or with separation techniques that use high salt mobile phase-buffers. This means that if a PBS buffer-mobile phase (~1% w/v salt content) is being used and blood plasma is being analyzed (0.9% salt content), ICP-AES is the detector of choice for the analysis.[61]

1.3.4 Metalloprotein Identification

Once separated and detected by SEC-ICP-AES or SEC-ICP-MS, metalloproteins or other metal species will need to be qualitatively identified. Prior to sample analysis, a mixture of proteins of known identity and molecular weight may be run on the SEC column in order to provide a size-

calibration.[60] The retention times of these protein standards can be used to provide a scale for the expected molecular weights for eluting molecules based on their retention time. In addition to the retention time, the specific metal that is detected (e.g., Cu) will provide additional information as to the identity of the metal species eluting (e.g., a 100 kDa Cu-containing protein). Based on this information, the identity of the unknown metalloprotein can be confirmed by adding the suspected metalloprotein to the sample and reanalyzing.[80] The subsequent analysis of the "spiked" sample should result in an increase of one metal-peak and, therefore, will be able to determine if the unknown metalloprotein was present the sample (e.g., larger heteroatom peak intensity).[80]

If a peak is expected to contain a protein that has enzymatic activity, then the fractions collected around the retention time of that peak can be subjected to an enzymatic assay. For example, the Cu-containing protein ceruloplasmin has an oxidase activity and can be identified by the appropriate enzymatic assay.[81, 82] The identity of unknown metalloproteins can also be determined via an immunoassay where an antibody specific to an epitope (i.e., amino acid sequence) on the protein of interest is used to qualitatively identify its presence. However, antibodies can be prone to providing false positives due to a lack of specificity (e.g., due to structural similarities between the analyte of interest and other molecules in the sample).[83] As such, it needs to be ensured that the antibody used has a sufficiently high specificity to the epitope of the analyte and that there are no cross-reactivity with other endogenous proteins in the sample.[83, 84] Alternatively, a metal-based immunoassay may be used. In this method antibodies specific to the protein of interest are labeled with metal atoms/ions to provide a heteroatom that can be detected by methods such as SEC-ICP-MS/AES.[78, 84] However, the commercial availability of metal-tagged antibodies are limited and, therefore, it may be necessary to develop one's own metalloprotein-specific antibody and subsequently tag it with the metal of choice, a difficult task.[85]

X-ray absorption spectroscopy (XAS) may also be used to determine the local environment around a specific metal ion in a metalloprotein or other metallo-entity. Analysis of a sample by X-ray absorption near edge structure (XANES) spectroscopy can provide information as to the electronic geometry and oxidation state of the specific metal ion of interest. In addition, extended X-ray absorption fine structure (EXAFS) spectroscopy analysis can be used to determine the bond distances between the absorbing metal ion and its neighbouring atoms (within 0.02 Å accuracy).[84, 86] The primary advantage of XAS is that it is element-specific, allowing one to study the metal of interest without interference from other elements.[86] However, if one metal ion exists in more than one coordination environment within the sample (i.e., found in multiple different metalloproteins) then the data provided by EXAFS will be difficult to interpret. Therefore, the sample must be pure/homogenous with respect to the metallo-entity of interest. Another advantage of XAS is that the sample is not limited to any one physical state. It can be solid, in an aqueous solution, or in a frozen solution. It must be noted, however, that it can be difficult to identify the neighbouring atoms of similar atomic number (e.g., C, N, or O).[86]

Electrospray Ionization-Mass Spectrometry (ESI-MS) is another technique that, when used in parallel with other metallomics techniques, can provide key information to identify metalloproteins. After separation and detection of a metalloprotein by SEC-ICP-AES/MS, further molecular information can be obtained by collecting the eluting fractions and subsequently analyzing them by ESI-MS. This technique can provide information such as the metal-protein stoichiometry and, under certain circumstances, the oxidation state of the metal.[84] However, it must be noted that the compatibility of ESI-MS with certain buffers is limited (e.g., 1% w/v salt, like that of PBS, can interfere with the ionization process) and, therefore, the separation technique

and/or sample preparation must be carefully considered so that neither the applicability of the technique nor the integrity of the sample (i.e., metal-protein bond) is compromised.[78]

1.3.5 Practical Applications of Metallomics Tools for the Analysis of Biological Fluids/Tissues

By using a metallomics approach to analyze biological fluids and tissues, an individual's "metallomic profile" (i.e., concentration/presence of metallo-entities) may be determined which has inherent diagnostic value. Additionally, by being able to identify/quantify the metallo-entities involved in certain diseases, effective treatments (e.g., exploration of new drugs) can be investigated. For example, Zn deficiency has been linked to the development of diabetes mellitus.[23] Both type I and II diabetic individuals exhibit Zn malabsorption from their diet, therefore, the use of analytical tools to measure Zn concentrations in blood plasma and pancreatic tissue can support the diagnosis and suggest certain treatments to help with symptoms (e.g., Zn-supplementation in the diet).[23]

It is also possible to apply a metallomics approach to analyze biological fluids and tissues for toxic metals, such as cadmium (Cd^{2+}), and gain insight into their bioinorganic chemistry. It has been determined that Cd^{2+} interferes with the uptake of intracellular Fe^{2+} by ferritin (Ft), an intracellular iron-storing protein, in the cytoplasm by competing for the same binding sites.[18] As a result, free intracellular Fe^{2+} can accumulate in the cell until it reaches a toxic concentration.[18] Therefore, the analysis of biological tissues (e.g., the liver) by SEC-ICP-AES for Cd and Fe has the potential to confirm that Cd is bound to Ft and that there are high levels of Fe^{2+} within the cytoplasm (bound to small molecular weight molecules). With the increasing exposure of humans (both acute and chronic) to toxic metal species from the environment (i.e., from the diet, drinking water, and polluted air), it is becoming increasingly important to develop methods that are able to

accurately identify and quantify metal species in biological samples and to determine the interactions that they have with (metallo)proteins and other biomolecules.[87, 88] Metallomic techniques that can analyze biological fluids and tissues for metalloproteins and metal-based species, such as SEC-ICP-AES and SEC-ICP-MS, have diagnostic value and the potential to provide key insights into the biochemical mechanisms of disease for the development of effective treatments.

1.4 Human Exposure to Toxic Metal Species

1.4.1 Sources of Toxic Metal Exposure

Following the industrial revolution, the scale of human activity has been continuously increasing thereby contributing to mankind's exposure to toxic metal species.[89] While natural activities, such as volcano eruption, forest fires, and chemical weathering, contribute to harmful pollutants entering the environment, some forms of pollution are being matched and even exceeded by anthropogenic activities.[89, 90] Human activities, such as industry, the manufacturing of goods, mining, and electricity generation has exacerbated the natural release of polluting species into the environment and consequently made the human exposure to toxic metals an imminent public health concern.[91] For example, Zn and Cu mining produces Cd as a by-product when it is extracted from Zn and Cu ores.[31] The large-scale use of inorganic pesticides and fertilizers that contain toxic metal impurities has also contributed to the increased metal content of soil.[90] It has been demonstrated that numerous fertilizers and pesticides contain Cd and Pb and that with repeated application can cause the accumulation of these toxic metals in the soil and the plants that are grown therein, thereby inadvertently introducing these metals into the food chain.[90, 92] Since exceedingly small daily doses of toxic metals and metalloids can adversely affect human health, governments have implemented legislation that limits the amount of metal contaminated fertilizer

and pesticides that can be applied to crops.[92] Additionally, the use of fertilizers such as $(NH_4)_2SO_4$ has resulted in the acidification of rivers and lakes where the low pH promotes the leaching of Cd and Pb from the soil making them more bioavailable to plants and animals.[93]

Increased human exposure to toxic metal species can also be a result of the improper disposal of electronic waste (e.g., leeching of metals into the soil, water sources etc.).[94] Electronic waste refers to any metal-containing technology such as household appliances, computers/televisions and related equipment, power tools, and any other technology that requires electricity for their operation. It is estimated that anywhere between 30 and 50 million metric tonnes of electronic waste are generated each year.[95] Importantly, since technological advancement is occurring very rapidly, obsolete electronic equipment is being replaced more frequently.[96] The sheer amount of electronic waste that is generated and the lack of technologies for effective recycling makes it difficult for governments to deal with their electronic waste in a cost-effective manner.[96] Consequently, electronic waste is often shipped to developing countries that have more lenient regulations ultimately leading to the metals that the waste contains entering the environment.[94] As the technological advancement of mankind increases, so too does the energy needed to power the technology. The burning of fossil fuels has provided the energy required to meet mankind's needs, but has also contaminated the air, water, and earth with toxic metal/chemical species. Coal frequently contains As, Cd, Hg, and Pb in levels ranging anywhere from 1 to 100 ppm and these metals are released into the atmosphere when the coal is burnt.[97] In 1983, global fossil fuel combustion released approximately 332,000 tonnes of Pb into the atmosphere in addition to 18,000 tonnes of As, 7,600 tonnes of Cd, and 3,600 tonnes of Hg.[97]

Bioaccumulation refers to the increase in concentration of a chemical species within an organism relative to the environment over time.[89] Toxic metals accumulate in the tissues of

organisms via their diet and their concentrations become magnified higher up in the food chain.[31] With human activities making toxic metal species more prevalent in the biosphere, coupled with the fact that they do not degrade, chronic human exposure to toxic metal species is becoming an increasingly important issue.[42] For example, rice is a large dietary source of As.[98, 99] Rice-based baby foods being sold in North America today have toxic metals, including As, Cd, Pb, and Hg, at concentrations ranging from 64 to 98 ppb.[100]

Consumer products are also a potential source of human exposure to toxic metal species. Underarm antiperspirants contain aluminium-zirconium salts whose absorption from the skin into the blood stream has been suggested to contribute to the development of Alzheimer's disease and cancer.[101, 102] Smoking is a major source of cadmium exposure with smokers having a blood Cd concentration 4-5 times higher than non-smokers.[103] Toys and inexpensive jewelry can also be a source of exposure to Pb, As, and Cd and teething infants may be at risk for either acute or chronic toxic effects if they swallow such products.[104] While government regulation of toxic metals in consumer products is becoming more stringent and informed regarding the effects of chronic toxic metal exposure, the levels of human exposure is still increasing in the 21st century.[103]

The anthropogenic mobilization of non-essential toxic metals from the earth's crust presents an imminent public health concern due to the limited understanding of the biomolecular mechanisms of chronic metal toxicity in humans. In order to effectively address this issue and develop ways by which to combat it, the biomolecular mechanisms of individual metal and metalloid species toxicity must be elucidated. Additionally, as human exposure is not always limited to a single toxic metal or metalloid species, both the synergistic (the toxicity of two species is greater than the sum of their individual toxic effects) and antagonist effects (the toxicity of two species is less than that of the individual species) of the compound exposure to multiple species

need to be explored to develop a comprehensive understanding of the complex bioinorganic chemistry of toxic metals.

1.4.2 Is Chronic Metal Exposure linked to the Development of Diseases?

In 2015, an estimated 9 million premature deaths were attributed to human exposure to anthropogenic pollution.[91] The scale at which mankind produces pollution (e.g., greenhouse gases, polycyclic aromatic hydrocarbons [PAH], toxic metals, particulate matter etc.) has accelerated with the increased prevalence of industrial processes.[89] Human industrial activity (e.g., mining, fuel combustion etc.) has become the largest source of pollutant materials on earth, outcompeting the release of the same materials via natural activities, such as volcano eruption and forest fires.[89] Furthermore, anthropogenic activities have lead to the introduction of a wide variety of synthetic chemicals that are not found in nature (e.g., polychlorinated biphenyls [PCB], phthalates, etc.), testifying to the devastating effect mankind's actions have on the earth and its inhabitants.[105] While both natural (e.g., volcanic eruption) and anthropogenic (e.g., smelting of ore) processes contribute to the release of chemical pollutants into the environment, these chemical species are disproportionately released into the environment by human industrial activities.[105] The etiology of a number of serious human diseases (e.g., Alzheimer's disease and autism, etc.) appear to be linked to a combination of genetic predisposition and exposure to environmental factors, such as heavy metals.[42, 106-108] Additionally, a number of both organic and inorganic pollutants have been detected, identified, and quantified in the bloodstream.[109] Therefore, the anthropogenic mobilization of toxic metals species from the earth's crust (e.g., via the unprecedented rates of mining and fossil fuel combustion) may be related to the compounded incidence of human health disorders. The chronic human exposure to some toxic metal species (e.g., Pb and Cd) have been linked to the development of adverse health effects, such as cardiovascular and kidney disease.[110,

[111] The acute toxicity of As^{III}, Cd^{2+}, Hg^{2+}, and CH_3Hg^+ has been attributed to their ability to selectively inhibit enzymes (e.g., urease) whose active sites contain vicinal thiol groups.[19, 112] While As^{III} has been shown to irreversibly react with thiol groups and inhibit over 100 mammalian enzymes, the detailed biomolecular mechanisms of inhibition remain unknown.[19] The chronic toxicity of toxic metal species can be associated with the induction of apoptosis, inhibition of ion channels, interference with DNA synthesis/repair, inhibition of protein synthesis, interference with signal transduction, and the generation of free radicals (i.e., oxidative stress).[19] Despite being associated with these biochemical processes, the underlying mechanism by which chronic toxic metal exposure lead to adverse health effects in the long-term (e.g., cancer or neurodegenerative disease) are yet to be fully determined.[19] Chronic human exposure to remarkably low doses of toxic metal species may be implicated in the development of human health disorders for which the etiology remains elusive. Therefore, efforts should be directed towards developing a better understanding of bioinorganic chemistry processes in the bloodstream to gain new insight into the contribution of chronic metal toxicity to the development of adverse health effects and disease.[42]

1.4.3 Chemistry of Toxic Metal Species in the Bloodstream Linked to Adverse Health Effects?

The bloodstream is responsible for the transportation of biomolecules, nutrients, and waste molecules throughout the body. Human blood contains ~4800 plasma proteins, 22 of which make up 99% of total protein mass.[53, 54] Molecular transport via the blood is largely facilitated by transport proteins in the blood plasma, such as transferrin (Tf, Fe^{3+}) and human serum albumin (HSA, fatty acids, Cu^{2+}, Zn^{2+} etc.).[55, 113] Some of these proteins have binding sites for essential metals (trace and ultratrace), some have binding sites for toxic metal species, but toxic metal species can compete for essential metal binding sites (e.g., it has been demonstrated that Cd^{2+} can

displace Zn^{2+} from its native binding sites in proteins, such as the Zn-finger transcription factor, Zn3-Sp1).[37, 42, 114] This is due to these toxic metal species partaking in either ionic or molecular mimicry, defined as the ability of a toxic metal species to "mimic structurally and/or functionally endogenous substrates that normally bind to, or occupy, the active sites of carrier proteins, channels, structural proteins, enzymes, and/or transcription factors."[36] In addition to plasma proteins, the bloodstream carries a large number of metabolites and small molecular weight biomolecules (e.g., over 400 metabolites have been identified in human blood plasma), such as amino acids, peptides, fatty acids, cholesterol, vitamins, carotenoids, and hormones.[115, 116] Red blood cells have also been shown to play a significant role in the chemistry of toxic metal species in the bloodstream.[117, 118] Therefore, the biological complexity of the bloodstream provides a rich source of potential interactions between its constituents and toxic metal species and is critical in determining the 'downstream' toxicological impact on internal organs.[42] The understanding of the *in vivo* biotransformation and metabolism of toxic metal species remains limited and it is, therefore, necessary to determine the bioinorganic chemical processes that occur in the blood stream and their contribution to the development of adverse human health effects.[109]

Human activities (e.g., mining, manufacturing, fossil fuel combustion etc.) contribute significantly to the mobilization of toxic metals and metalloid species from the earth's crust.[109] While many human diseases can be attributed to genetic defects, environmental factors can also contribute to disease by either exacerbating an underlying health condition/genetic predisposition or directly lead to chronically induced adverse health effects and diseases, such as cancer.[119] Chronic human exposure to remarkably low doses of toxic metal species may be involved in the development of more adverse health effects in humans than are currently known.[42] While a number of toxic metal species have been detected and quantified in the bloodstream, the toxicological

meaning that are associated with their concentrations remains in many cases unknown.[20] The bloodstream is a diverse source of biomolecules that can interact with toxic metal species and is critically involved in the mechanism by which a toxic metal species can exert its toxic effects either systemically or selectively.[109] The formation of As-Se and Hg-Se metabolites in erythrocytes, for example, has been proposed to induce systemic Se-deficiency, suggesting that toxic metal species can contribute to organ toxicity without entering an organ themselves.[19, 32, 40, 41, 120, 121] However, knowledge regarding the mechanisms by which toxic metal species lead to adverse health effects is very limited.[42] While the formation of $(GS)_2AsSeHgCH_3$ in erythrocytes has been explored, the structural basis for the antagonism between CH_3Hg^+ and SeO_3^{2-} still needs to be elucidated.[122] Additionally, while the co-administration of SeO_3^{2-} with Cd^{2+} has been demonstrated to negate the Cd^{2+}-induced inhibition of protein synthesis in mouse liver, the structural basis for Cd-SeO_3 interactions remains unknown.[123] Therefore, determining the possible biomolecular mechanisms by which toxic metal and metalloid species lead to the development of adverse health effects within mammalian organisms will provide the leverage that is necessary to implement international legislation aimed at significantly restricting the release of these toxic species into the environment; such efforts being done with the hope of decreasing disease prevalence and advancing the health of mankind.

1.5 Research Objectives

Methylmercury (CH_3Hg^+) is one of the most potent neurotoxins known to man. Human populations are predominantly exposed to this toxin by the consumption of fish from which CH_3Hg^+ is effectively absorbed by the gastrointestinal tract into the bloodstream. Its interactions with plasma proteins, small molecular weight (SMW) molecules, and red blood cells, however, are incompletely understood, but critical as they determine if and how much CH_3Hg^+ reaches

toxicological target organs. To better define the role that SMW plasma thiols play in the delivery of CH_3Hg^+ to known uptake transporters located at the placental and the blood-brain barriers (BBB), I have pursued two objectives. The first objective was to develop a method for the analysis of blood plasma for metalloentities (**Chapter 3**). The second objective was to apply the developed method to investigate the bioinorganic chemistry of methylmercury in mammalian blood plasma (**Chapter 4**). This included determining the binding of CH_3Hg^+ to plasma constituents (e.g., plasma proteins or metabolites) and the elucidation of the effect of SMW thiols (e.g., cysteine, homocysteine, and glutathione) on these binding interactions.

Chapter 2: Experimental Methods and Materials

2.1 Chemicals, Materials, and Solutions

150 mM phosphate-buffered saline (PBS) powder sachets (10 mM NaH_2PO_4, 138 mM NaCl, 2.7 mM KCl, pH 7.4), D, L-homocysteine (hCys, ≥95% purity), L-cysteine (Cys, ≥98% purity), L-glutathione reduced (GSH, ≥98% purity), D-methionine (Met, ≥98% purity), albumin from rabbit serum (RSA, ≥99% purity), bicinchoninic acid kit for protein determination (bicinchoninic acid solution, 4 % w/v $CuSO_4 \cdot 5H_2O$ solution, 1 mg/mL bovine serum albumin protein standard solution), sodium hydroxide (≥97% purity), and blue dextran were purchased from Sigma-Aldrich (St. Louis, MO, USA). 1.0 M $CH_3HgOH_{(aq)}$ was purchased from Alfa Aesar (Haverhill, MA, USA). New Zealand White Rabbit Plasma (sodium heparin, pooled, unspecified gender) was purchased from BIOIVT (Westbury, NY, USA) and stored in liquid nitrogen (-196 °C). Gel Filtration Standard Solution (bovine thyroglobulin - 670 kDa, bovine γ-globulin – 158 kDa, chicken ovalbumin – 44 kDa, horse myoglobulin – 17.5 kDa, and vitamin B_{12} – 1.35 kDa) was purchased from Bio-Rad Laboratories (Hercules, CA, USA). 67-70% w/w HNO_3 (PlasmaPure, trace metal grade) and 34-37 % w/w HCl in (PlasmaPure, trace metal grade) were purchased from SCP Science (Baie D'Urfe, QC, Canada). All mobile phases were filtered through a 0.45 µm pore size nylon membrane filter (Mandel Scientific, Guelph, ON, Canada). All pH measurements were performed with a VWR Symphony SB20 pH meter (Thermo Electron Corporation, Beverly, MA, USA).

2.2 Human blood collection and preparation

The collection of whole blood from a healthy male was collected (after 12 hours of fasting) was approved by the Calgary Conjoint Health Ethics Board (Ethics ID: REB15-1138_REN7). Blood was collected into trace metal grade vacuumized blood collection tubes that contained sodium heparin as an anti-coagulant (Becton Dickinson, Franklin Lake, New Jersey). The blood

samples were then centrifuged at 3000 g for 20 min (4 °C) to separate the whole blood into blood plasma and red blood cells. The supernatants (blood plasma) from different tubes were pooled, mixed, and subsequently transferred in 1.0 mL aliquots to T310 Cryovials (Simport Scientific, Saint-Mathieu-de-Beloeil, QC, Canada) before being stored in liquid nitrogen (-196 °C).

2.3 Mobile Phase and Solution Preparation

PBS was prepared by dissolving one sachet in 1 L of 18.2 MΩ•cm deionized water from a Simplicity water purification system (Millipore, Billerica, MA, USA) and adjusted to pH 7.4 with 4.0 M HCl/NaOH. To prepare PBS that contained a thiol/amino acid, PBS was bubbled through with $N_{2(g)}$ for 60 minutes to reduce the amount of dissolved oxygen and avoid the oxidation of the thiol groups. When necessary, an appropriate amount of either hCys, Cys, GSH, Met, or His was weighed out and dissolved in PBS before adjusting the pH with 4.0 M HCl/NaOH if necessary. The solutions were filled to the appropriate volume before being filtered through a 0.45 µm pore size nylon membrane filter. Thiol/amino acid-containing mobile phases were only used on the day that they were prepared. This, in addition to bubbling $N_{2(g)}$ through the mobile phases during experiments, was meant to avoid/reduce the impact of oxidation of the thiol groups on the obtained results.

2.4 Method Development for the Analysis of Blood Plasma using SEC-ICP-AES

2.4.1 Sample Preparation

Blood plasma (human, rabbit, and rat, stored in liquid nitrogen) was thawed at room temperature (20 °C) for 45 minutes. Blood plasma was initially unfiltered when injected onto the columns, but when deleterious effects on the column's performance were observed, it was decided to filter it through a 0.45 µm pore size syringe filter (Fischer Scientific, Hampton, NH, United States). When determining the appropriate dilution of the plasma with PBS for analysis, the plasma

was then divided into 250 (1 part plasma to 3 parts PBS), 500 (1:1), 750 (3:1), and 1000 µL aliquots before being incubated at 37 °C for 30 minutes before being subsequently diluted to 1.0 mL with PBS if necessary. Once the appropriate dilution factor was determined to be 1:1 (i.e., 500 µL of plasma and 500 µL of PBS, explanation provided in **Chapter 3**), 0, 2, 4, 6, 8, or 10 µL of 0.01 M CH_3HgOH was added to 500 µL of plasma before diluting to 1.0 mL with PBS. A prepacked SRT-10C SEC column (7.8 × 300 mm I.D. × Length, 10 µm particle size, 300 Å pore size, fractionation range: 5 - 1,250 kDa; Sepax Technologies Inc., Newark, DE, USA) or a Superdex 200 Increase SEC column (10 × 300 I.D. × Length, 8.6 µm particle size, fractionation range: 10 – 600 kDa) were utilized for the development of the separation procedure.

2.4.2 Protein Recovery/Mass Balance using Human Plasma

2.4.2.1 SEC-ICP-AES Analysis and Peak Integration

Human plasma aliquots (1.0 mL, stored in liquid nitrogen) were thawed at room temperature (20 °C) for 45 minutes before being pooled and filtered through a 0.45 µm pore size syringe filter (Fischer Scientific, Hampton, NH, United States). The plasma was divided into three 500 µL aliquots and 500 µL of PBS was added to each before being mixed. These three plasma/PBS mixtures were then subsequently analyzed by the SEC-ICP-AES (500 µL sample loop) using the Sepax SRT-10C SEC column. The C-emission of the column effluents were monitored, and the resultant peaks were integrated using the Origin software (Version 2020 b) to get a total carbon signal eluting from the column. Alternatively, human plasma was divided into three 500 µL aliquots and 500 µL of PBS was added to each before being mixed. 500 µL of each of these plasma/PBS mixtures were then added to 9500 µL of PBS. The three 10 mL solutions containing 250 µL of plasma each was directly aspirated into the ICP-AES without the use of a

column. The resultant C-area of the solutions were integrated and compared to the area of the column injections.

2.4.2.2 Bicinchoninic Acid Protein Assay

The bicinchoninic acid (BCA) protein assay functions by the reduction of Cu^{2+} to Cu^{+} and the formation of a complex between the latter and BCA that absorbs maximally at 562 nm.[124] The reduction of Cu^{2+} is attributed to two sources: the temperature-independent oxidation of cysteine, tyrosine, and tryptophan residues and the temperature-dependent oxidation of peptide bonds present in the protein/polypeptide structures.[124] A BCA/$CuSO_4$ solution was prepared by mixing 50 parts BCA with 1 part $CuSO_4$. The 1000 mg/mL bovine serum albumin (BSA) solution was mixed with PBS in appropriate amounts to produce standard solutions of 0, 200, 400, 600, 800, and 1000 mg/mL. Human plasma was thawed and divided into three (i.e., for triplicate measurements) 500 µL to which 500 µL of PBS was added before being mixed. These samples were injected onto the SRT-10C SEC column, and the column effluent was collected into 25 mL volumetric flasks before being diluted to volume with PBS. 250 µL of human plasma was added to three individual 25 mL volumetric flasks before being diluted to volume with PBS. 0.1 mL of each sample was mixed with 2.0 mL of the BCA/$CuSO_4$ solution in triplicate and vortexed to mix. BCA/$CuSO_4$/sample solutions were then incubated at 37 °C for 30 minutes after which they were allowed to cool at room temperature for 10 minutes. The absorbance of the samples was measured in triplicate using a Milton Roy Spectronic 21 spectrophotometer set to 562 nm. A standard curve was generated using the absorbances of the standard BSA solutions to which the plasma samples were compared.

2.5 Toxicologically Relevant Interactions Between Methylmercury and SMW Thiols in Blood Plasma

2.5.1 Sample Preparation

Rabbit plasma aliquots (1.0 mL, stored in liquid nitrogen) were thawed at room temperature (20 °C) for 45 minutes before being pooled and filtered through a 0.45 µm pore size syringe filter (Fischer Scientific, Hampton, NH, United States). The plasma was then divided into 500 µL aliquots before being incubated at 37 °C for 30 minutes. 5 µL of 0.01 M CH_3HgOH was added to each aliquot, followed by an additional 5 minutes of incubation at 37 °C, before being diluted to 1.0 mL with PBS to yield a final [CH_3Hg^+] of 50 µM.

2.6 Instrumentation

The SEC-ICP-AES system was comprised of an Agilent 1200 series Binary Pump SL HPLC pump followed by a Rheodyne 9010 injector equipped with a 500 µL sample loop. A prepacked SRT-10C SEC column (7.8 × 300 mm I.D. × Length, 10 µm particle size, 300 Å pore size, fractionation range: 5 - 1,250 kDa; Sepax Technologies Inc., Newark, DE, USA) or a Superdex 200 Increase SEC column (10 × 300 I.D. × Length, 8.6 µm particle size, fractionation range: 10 – 600 kDa, GE Healthcare, Piscataway, NJ, USA) was utilized at a flow rate of 0.7 (both columns for comparison) or 1.0 L min^{-1} (SRT-10C only) using a PBS mobile phase containing various types and amounts of thiols. Simultaneous multi-element specific detection of Hg (253.652 nm), C (193.091 nm), Cu (324.754 nm), Fe (259.940 nm), Zn (213.856 nm), and S (180.731 nm) in the column effluent was achieved with a Prodigy, high-dispersion, radial-view ICP-AES (Teledyne Leeman Labs, Hudson, NH, USA) using the following parameters: a radio frequency (RF) power of 1.3 kW, an Ar gas coolant flow rate of 19 L min^{-1}, auxiliary flow rate of 0.5 L min^{-1}, and a nebulizer gas pressure of 25 psi.[60, 71] A 240 s delay was implemented between sample injection and the start of the data acquisition, where the data were collected for 660 s. All analyses

were performed in triplicate and the ICP-AES-derived raw data which were acquired using the Prodigy software (SALSA) were imported into SigmaPlot 14.5 and smoothed using the bisquare algorithm. Peak areas and retention times were determined using Origin software (Version 2020 b).

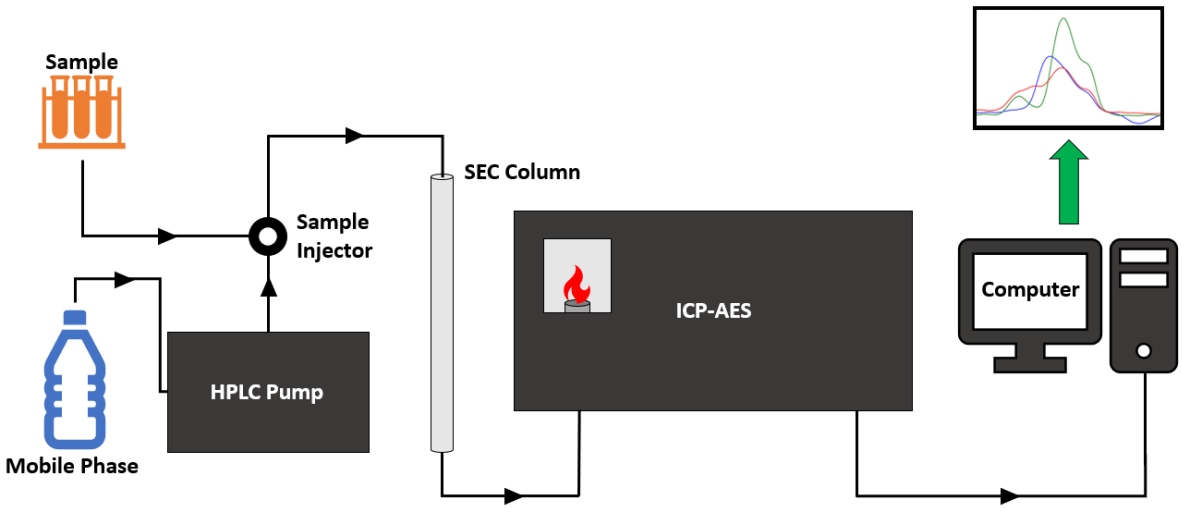

Figure 2.1: Schematic representation of the Size-exclusion Chromatography-Inductively Coupled Plasma-Atomic Emission Spectroscopy system which was used for the analysis of rabbit plasma.

2.7 Electrospray Ionization Mass spectrometry

An CH_3Hg-RSA complex (synthesis same as outlined above) was injected onto the SRT-10C SEC column using 50 mM Tris-buffer which contained 50 µM of hCys (pH 7.4) as the mobile phase. The obtained Hg-specific chromatogram was used to determine the retention time of the on-column formed CH_3Hg-SMW thiol complex. Thereafter, another aliquot of the CH_3Hg-RSA complex was injected and the fraction that contained the CH_3Hg-SMW thiol complex was collected (t_r = 651 s) and submitted for analysis by electrospray ionization-mass spectrometry (ESI-MS). The optimal conditions for the qualitative identification of CH_3Hg-SMW thiol complexes by HPLC-ESI-MS were informed from previous studies.[125] In brief, part of the buffer matrix was removed before MS analysis by injecting the fraction onto an Agilent 1200 series

HPLC system comprised of a ZORBAX Eclipse Plus C_{18} HPLC column (2.1 x 50 mm ID x Length, 1.8 µm particle size, Agilent Technologies, Santa Clara, CA, USA) using gradient elution with 0.1% formic acid in water and MeOH (0-1 min: 20% MeOH; 1-9 min: gradient elution up to 90% MeOH; 9-10 min: 90% MeOH). The eluting Hg-containing analyte was qualitatively identified using an Agilent 6520 LC-Q-TOF mass spectrometer.

Chapter 3: Development of a Method to Analyze Blood Plasma for Metalloproteins using SEC-ICP-AES

3.1 Introduction

To accurately and reproducibly (e.g., triplicate analysis) analyze biological samples for metal species it is vital that the analytical method used is sensitive enough to detect metal species at the concentrations at which they are present *in vivo* (e.g., transferrin is present in plasma/serum between 1.8-3.7 g/L).[60] The structure of a protein is key to its function. Therefore, if the structure of a protein is denatured then the function of the protein (e.g., ability to bind a metal ion that is responsible for its enzymatic or redox activity) is compromised. As such, keeping experimental conditions (e.g., pH, physiologically relevant mobile phase, etc.), such that the metal-protein bond is not disturbed, is essential.[60] Manley et al. developed a hyphenated technique that successfully analyzed and determined rabbit blood plasma for 12 Cu, Fe, and Zn metalloproteins using size exclusion chromatography (SEC), which is a gentle separation technique due to the fact that analytes do not chemically interact with the stationary phase during the separation process, and the employed PBS mobile phase has been shown to produce fewer artefacts than other 'biological buffers', before being fed into an ICP-AES to achieve multielement-specific detection of the metal species of interest.[60, 71, 126] SEC-ICP-AES has since been used to gain insight into the fate of Cd and Hg species in erythrocyte lysate and has proven to be invaluable in providing insight into the bioinorganic chemistry of toxic metal species in the bloodstream and other biological fluids.[117]

The interaction of CH_3Hg^+ with plasma proteins and SMW metabolites in the bloodstream is incompletely understood. However, such an understanding is critical to establish the mechanisms which deliver this species to the BBB for subsequent translocation into the brain. Studies with rats have shown that SMW thiols (e.g., L-cysteine), when coadministered with CH_3Hg^+ intravenously, resulted in the increased accumulation of CH_3Hg^+ in the liver, kidneys,

and cerebrum, suggesting that SMW thiols may be directly involved in the translocation process.[127] It has been suggested that CH_3Hg^+ can cross the BBB via molecular mimicry when bound to cysteine as the CH_3Hg-Cys complex structurally resembles Met and, therefore, may be a substrate for the corresponding transport protein.[128, 129] While EXAFS and computational studies have demonstrated that the structural resemblance between these molecules is limited, (i.e., while the number of atoms is similar, the 3D geometry of the molecules are very different) the authors of this study do suggest that the translocation of the CH_3Hg-Cys complex across the BBB may involve the chiral alpha-carbon end of the amino acid complex.[130] To better understand the bioinorganic chemistry of CH_3Hg^+ in the mammalian bloodstream, and its interactions with small molecular weight thiols, the following chapter describes the development of an SEC-ICP-AES method suited to the task.

Previously, our lab used a Superdex 200 Increase SEC column (10 × 300 mm I.D. × Length, 8.6 or 13 µm particle size, fractionation range: 10 – 600 kDa; GE Healthcare, Piscataway, NJ, USA) for the analysis of blood plasma with SEC-ICP-AES. I was provided the opportunity to work with a new company, Sepax Technologies Inc., who offered a SEC column that is cheaper than the one previously used. Ultimately, it was decided that the SEC column of choice would be the SRT-10C SEC column (7.8 × 300 mm I.D. × Length, 10 µm particle size, 300 Å pore size, fractionation range: 5 - 1,250 kDa; Sepax Technologies Inc., Newark, DE, USA). Compared to the Superdex 200 Increase SEC column, the SRT-10C SEC column has a wider fractionation range (5 - 1,250 kDa compared to 10 – 600 kDa). Additionally, since the column volume was smaller (7.8 × 300 mm compared to 10 × 300 mm I.D. × Length) less mobile phase would be required to equilibrate the column, reducing material costs, and achieving a faster separation. Furthermore, the cost of the SRT-10C SEC column is approximately 60% that of the Superdex 200 Increase

SEC column. Therefore, the following chapter describes the development of a method to analyze blood plasma for metalloentities with the SRT-10C SEC column, comparing its performance with that of the Superdex 200 Increase SEC column for its ultimate use in the analysis of blood plasma for methylmercury (CH_3Hg^+)-derived species.

3.1 Results and Discussion

3.1.1 Sample Preparation

To achieve reproducible and representative results, appropriate sample preparation is key. In all of my experiments I used New Zealand White Rabbit Plasma (sodium heparin, pooled, unspecified gender, 100 mL in individual 1.0 mL cryovials) which was purchased from BIOIVT (Westbury, NY, USA), stored in liquid nitrogen (-196 °C), and thawed immediately prior to use. Prior to the analysis of rabbit plasma, a gel filtration standard solution (bovine thyroglobulin - 670 kDa, bovine γ-globulin – 158 kDa, chicken ovalbumin – 44 kDa, horse myoglobulin – 17.5 kDa, and vitamin B_{12} – 1.35 kDa) was injected onto the column and the C-specific chromatogram (**Figure 3.1**) was used to size-calibrate the column. This provided an indication of the column performance prior to plasma analysis. Additionally, as will be seen below, some problems that were encountered when rabbit plasma was injected had to be overcome.

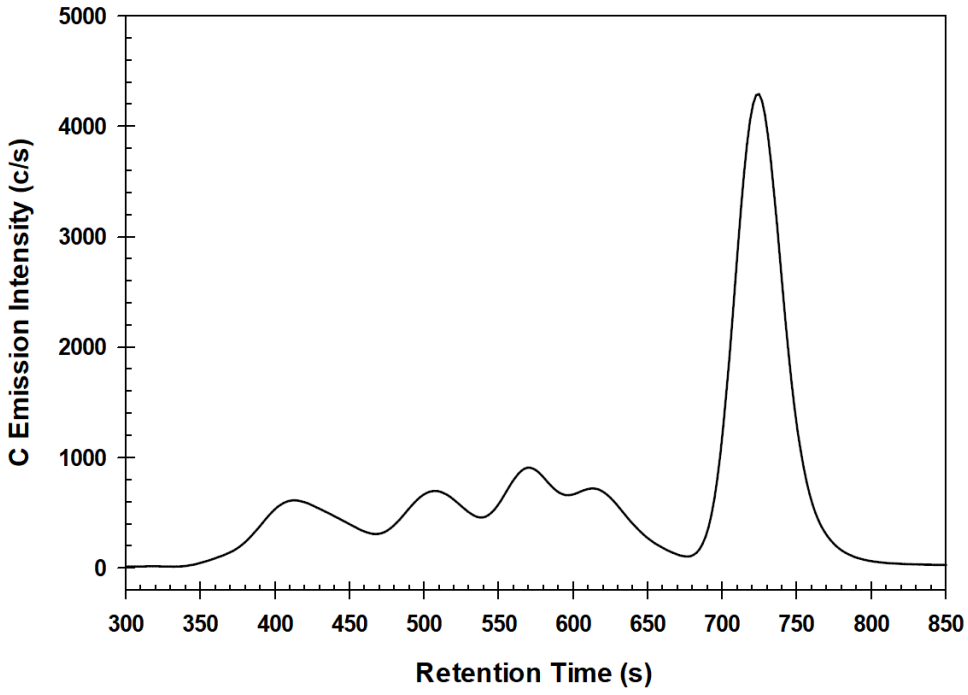

Figure 3.1: C-Specific chromatogram obtained by SEC-ICP-AES for the analysis of gel filtration standard solution (bovine thyroglobulin - 670 kDa, bovine γ-globulin – 158 kDa, chicken ovalbumin – 44 kDa, horse myoglobulin – 17.5 kDa, and vitamin B_{12} – 1.35 kDa) which are used to calibrate the column and provide molecular weight markers for subsequent figures. Column: Sepax SRT-10C SEC-300 column (7.8 × 300 mm I.D. × Length, 10 µm particle size, 300 Å pore size); Mobile phase: 150 mM PBS (pH 7.4); Temperature: 20 °C; Flow rate: 1.0 mL/min; Injection volume: 500 µL; Detector: ICP-AES (C-emission wavelength - 193.091 nm).

3.1.1.1 Filtration of the Plasma

Initially, rabbit plasma was directly injected onto an old, previously used Superdex 200 Increase SEC column (i.e., 1.0 mL cryovials of rabbit plasma were thawed before being directly injected). **Figure 3.2** shows the C-specific chromatogram of the analysis of five subsequent injections of unfiltered rabbit plasma. It can be seen that the peak shape quickly deteriorates (e.g., loss of gaussian shape, development of shoulder, and introduction of peak artefacts at ~1700 s), which suggests that there is something in the samples that adversely affects the separation of the proteins.

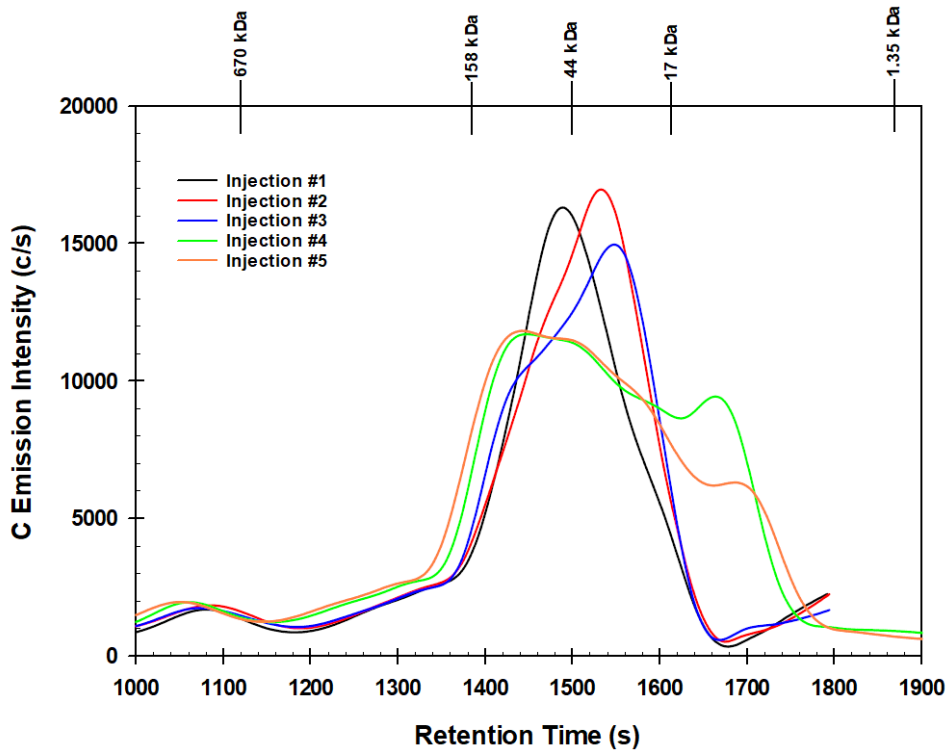

Figure 3.2: C-specific chromatograms obtained by SEC-ICP-AES for the analysis of unfiltered rabbit blood plasma (five subsequent injections). Column: Superdex 200 SEC column (10 × 300 mm I.D. × Length, 8.6 µm particle size, fractionation range: 10 – 600 kDa); Mobile phase: 150 mM PBS (pH 7.4); Temperature: 20 °C; Flow rate: 0.7 mL/min; Injection volume: 500 µL; Detector: ICP-AES (C-emission wavelength - 193.091 nm). The retention times of molecular weight markers are indicated at the top of the figure.

To check the performance of the column, a solution of blue dextran was injected onto the column, which is shown in **Figure 3.3.** The asymmetrical shape of the blue dextran dye indicated that the integrity of the chromatographic bed was compromised. To look further into the issue, the top cap of the column was removed, and the top of the stationary phase bed was examined. As seen in **Figure 3.4**, there were black solids and a yellow discolouration of the stationary phase that appears more prevalent on one side. This observation may explain the shape of the blue dextran dye peak that was observed in **Figure 3.3** where the one side of the dye plug migrated through the column faster than the other. To attempt to clear a potential blockage of the top of the column bed, a small portion of the stationary phase was removed from the top of the column. The first couple

of centimeters of the stationary phase were suspended in water and allowed to settle overnight. The column was recapped and equilibrated with PBS at 0.7 mL/min allowing the column to pack/settle with pressure. **Figure 3.5** shows a second injection of a blue dextran solution where the shape of the dye peak is significantly more uniform. To validate the results of the blue dextran injection that suggest that column performance has been restored, the gel filtration standard solution was injected followed by the triplicate injection of rabbit plasma. However, it was decided that the rabbit plasma needed to be filtered (0.45 µm pore size syringe filter) before these three injections and the resultant chromatograms are shown in **Figure 3.6**. While this figure shows that some separation performance had been restored, the peaks were not gaussian in shape. Despite this, it was determined that filtration of the plasma is key to preserve the performance of the column if rabbit plasma is repeatedly injected. This is most likely due to the removal of aggregated proteins (e.g., with hydrodynamic radii > 0.45 µm) present in the plasma that can accumulate on the surface of the stationary phase, potentially clogging it, and/or resulting in an altered peak shape.[131]

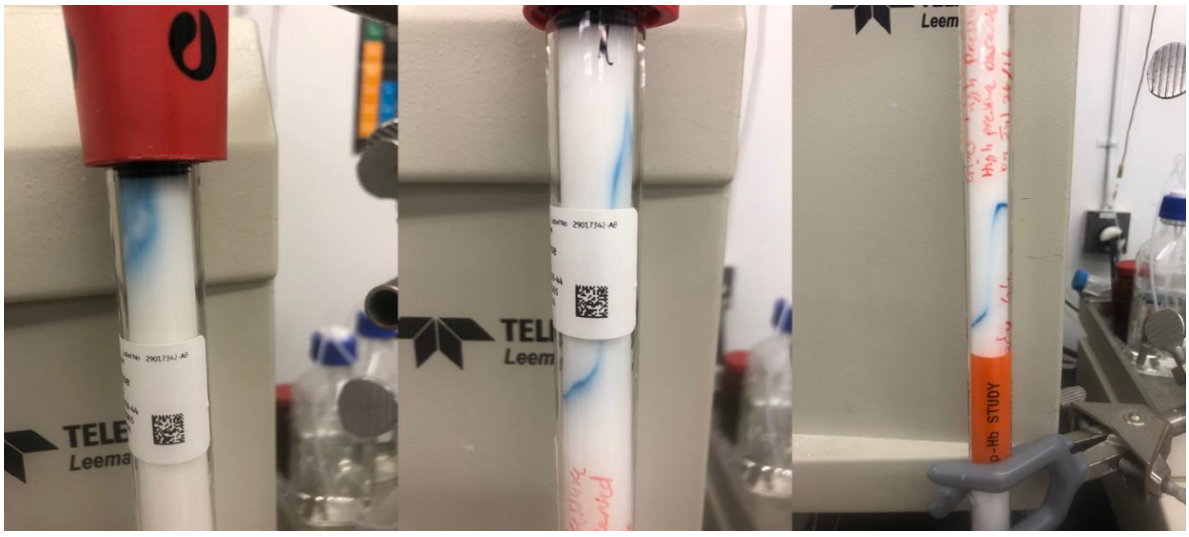

Figure 3.3: Image of non-uniform blue dextran dye migrating through the SEC column after the column performance has been adversely affected by five subsequent injections of unfiltered rabbit plasma.

Figure 3.4: Image of the surface of the column bed after five injections of unfiltered rabbit plasma and one injection of blue dextran. A yellow discolouration and black solids are clearly visible.

Figure 3.5: Image of improved uniform shape of blue dextran dye migrating through the SEC column after removing some of the stationary phase from the top of the column bed and repacking.

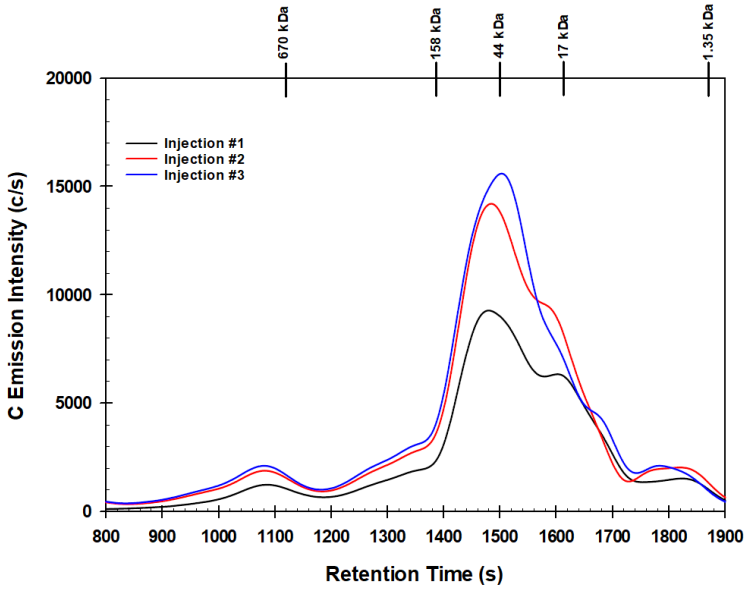

Figure 3.6: C-specific chromatograms obtained by SEC-ICP-AES for the analysis of filtered rabbit blood plasma (three subsequent injections). Column: Superdex 200 Increase SEC column (10 × 300 mm I.D. × Length, 8.6 µm particle size, fractionation range: 10 – 600 kDa); Mobile phase: 150 mM PBS (pH 7.4); Temperature: 20 °C; Flow rate: 0.7 mL/min; Injection volume: 500 µL; Detector: ICP-AES (C-emission wavelength - 193.091 nm). The retention times of molecular weight markers are indicated at the top of the figure.

3.1.1.2 Column Comparison

An SRT-10C SEC column (7.8 × 300 mm I.D. × Length, 10 µm particle size, 300 Å pore size, fractionation range: 5 - 1,250 kDa; Sepax Technologies Inc., Newark, DE, USA) was evaluated for its ability to analyze rabbit plasma for metalloproteins. It was decided to compare the performance of this column to that of the Superdex 200 Increase SEC column with respect to the separation of Cu, Fe, and Zn-containing metalloproteins in rabbit plasma. All parameters were kept the same between experiments (e.g., mobile phase, temperature, flow rate, injection volume etc.). The manufacturer recommended flow rate for the Superdex 200 Increase SEC column was 0.75 mL/min. Therefore, the performance of the two columns were compared at this flow rate. However, despite the display of the HPLC system showing 0.75 mL/min, the actual flow rate was 0.7 mL/min, determined by collecting column effluent in a graduated cylinder for five minutes and

measuring the volume delivered. When it was decided to switch to the SRT-10C SEC column for future experiments, the flow rate was increased to 1.0 mL/min, which was Sepax Technologies Inc.'s recommended flow rate for the column (see **Section 3.1.4**), and this flow rate was verified before every experiment.

The analysis of rabbit plasma for Cu, Fe, and Zn species using both the Superdex 200 Increase and the SRT-10C SEC columns is shown in **Figure 3.7.** The scale of the x- and y-axis in **Figure 3.**7 were adjusted to compare the peak shapes. The number of peaks, peak resolution, and peak shapes between the two columns are similar. However, the peak width with the Superdex 200 Increase SEC column were wider (e.g., the main Fe-peak in **Figure 3.7** was 100 s wider in the Superdex 200 Increase chromatogram) and not as intense (e.g., the main Fe-peak in **Figure 3.7** was ~50 c/s less intense in the Superdex 200 Increase chromatogram). These observations can be explained by the differences in the column width (Superdex 200 Increase – 10 mm, SRT-10C – 7.8 mm) and the stationary phase. Additionally, it should be noted that the total analysis time was significantly shorter with the SRT-10C SEC column, by ~850 s. With regard to the molecular weight markers at the top of each Figure, the 158, 44, and 17 kDa markers are closer together in the Superdex 200 Increase SEC column and all markers appear more evenly spaced out with the SRT-10C SEC column suggesting superior resolution within this molecular weight range. **Figure 3.8** shows the same data as **Figure 3.7**, but with the same x- and y-axis scales to better demonstrate the reduced analysis time and increased peak intensity using the SRT-10C SEC column. Given that the SRT-10C SEC column shows the same number of peaks with similar resolution as the Superdex 200 Increase SEC column, but in approximately half the time and with higher peak intensities, it was decided that the SRT-10C SEC column was appropriate for the analysis of blood

plasma and in fact also improved sample throughput. All following experiments were performed with the SRT-10C SEC column.

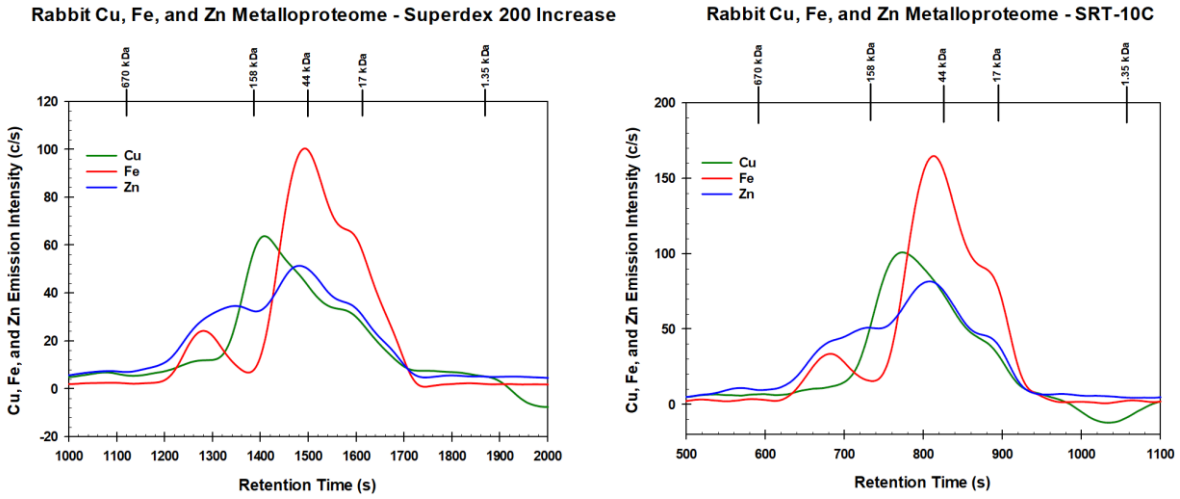

Figure 3.7**:** Comparative Cu-, Fe-, and Zn-specific chromatograms obtained by SEC-ICP-AES for the analysis of New Zealand White Rabbit blood plasma. Columns: Superdex 200 Increase SEC Column (Left) (10 × 300 mm I.D. × length, 8.6 µm particle size) and Sepax SRT-10C SEC-300 column (Right) (7.8 × 300 mm I.D. × Length, 10 µm particle size, 300 Å pore size); Mobile phase: 150 mM PBS (pH 7.4); Temperature: 20 °C. Flow rate: 0.7 mL/min for both columns; Injection Volume: 500 µL; Detector: ICP-AES (Cu-emission wavelength - 324.754 nm, Fe-emission wavelength – 259.940 nm, Zn-emission wavelength – 213.856 nm). The retention times of molecular weight markers are indicated at the top of the figure.

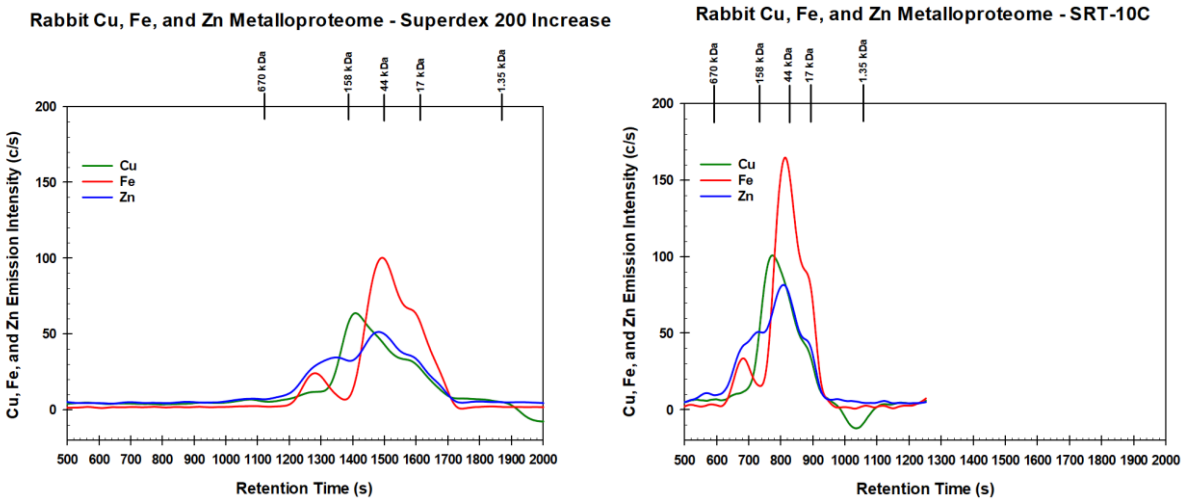

Figure 3.8: Comparative Cu-, Fe-, and Zn-specific chromatograms (adjusted chromatographic window) obtained by SEC-ICP-AES for the analysis of New Zealand White Rabbit blood plasma. Columns: Superdex 200 Increase SEC Column (Left) (10 × 300 mm I.D. × length, 8.6 µm particle size) and Sepax SRT-10C SEC-300 column (Right) (7.8 × 300 mm I.D. × Length, 10 µm particle

size, 300 Å pore size); Mobile phase: 150 mM PBS (pH 7.4); Temperature: 20 °C. Flow rate: 0.7 mL/min for both columns; Injection Volume: 500 µL; Detector: ICP-AES (Cu-emission wavelength - 324.754 nm, Fe-emission wavelength – 259.940 nm, Zn-emission wavelength – 213.856 nm). The retention times of molecular weight markers are indicated at the top of the figure.

3.1.1.3 Comparison of Rat, Rabbit, and Human blood plasma analysis using SRT-10C

Using the SRT-10C SEC column, the C-, Cu-, Fe-, and Zn-specific chromatograms of three mammalian species' (i.e., Sprague-Dawley Rat, New Zealand White Rabbit, and human) blood plasma were compared in order to gain insight into differences in their Cu, Fe and Zn-metalloproteomes. **Figure 3.9** shows the C-emission of rat, rabbit, and human plasma when they were analyzed by SEC-ICP-AES. All three species have a similar number of peaks (i.e., four, but with the peaks around 44 kDa exhibiting a double peak or bearing shoulders on the long retention end) with slightly different retention times (t_r). The most intense peak in rabbit plasma, just to the left of the 44 kDa MW marker, at t_r = 813 s, has been previously identified RSA, the most abundant protein in plasma.[60] While rat, rabbit, and human serum albumins have a similar number of amino acids and % helical content, it can be seen in **Figure 3.9** that differences in their structure exist (e.g., hydrodynamic radius) that may explain the differences in the observed retention times.[132, 133] The albumin peak in rabbit plasma displays a shoulder while the corresponding human and rat peaks exhibit additional peaks that are not baseline separated from their respective albumin peaks.

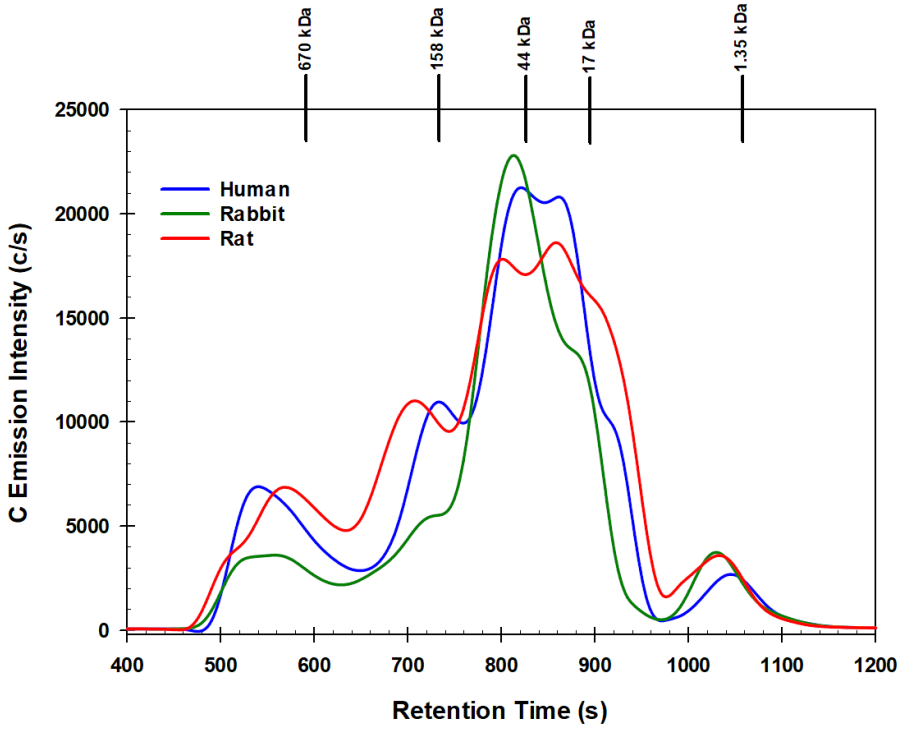

Figure 3.9: Comparative C-specific chromatograms obtained by SEC-ICP-AES for the analysis of human (blue), New Zealand White Rabbit (green), and Sprague-Dawley rat (red) blood plasma. Column: Sepax SRT-10C SEC-300 column (7.8 × 300 mm I.D. × Length, 10 µm particle size, 300 Å pore size); Mobile phase: 150 mM PBS (pH 7.4); Temperature: 20 °C; Flow rate: 0.7 mL/min; Injection volume: 500 µL; Detector: ICP-AES (C-emission wavelength - 193.091 nm). The retention times of molecular weight markers are indicated at the top of the figure.

The Cu-specific chromatograms for these three species are shown in **Figure 3.10**. The peak that elutes at t_r = 765 s in rabbit and human plasma has been previously identified as ceruloplasmin.[60, 80] Peaks with similar retention times exist for both human and rat plasma. However, at t_r = 845 s, rat plasma appears to have another large Cu-containing peak that was not identified. In **Figure 3.9** at $t_r \approx 1140$ s, there is a small decrease or "dip" in the emission intensity of Cu. This has been seen in previous experiments and may be explained by the coelution of a multitude of other SMW species (e.g., Ca^{2+}) that may reduce the Cu-emission intensity.[71] **Figure 3.11** illustrates the plasma Fe-metalloproteomes of these three species. All three species have a Fe-peak at t_r = ~810 s and it has been identified in rabbit and human plasma as hTf.[60, 80] All three

species possess considerable shoulders/peaks that are not separated from the hTf peak. The peak in human plasma at t_r = 620 s was recently identified as a haptoglobin-hemoglobin (Hp-Hb) complex.[80] This species forms when red blood cells rupture and release free Hb into the blood plasma. Hp subsequently binds Hp-dimers to preclude kidney toxicity by free Hb. Thus, the rat and rabbit Fe-peaks with t_r = 698 and 682 s, respectively, correspond to the species-specific Hp-Hb complexes.

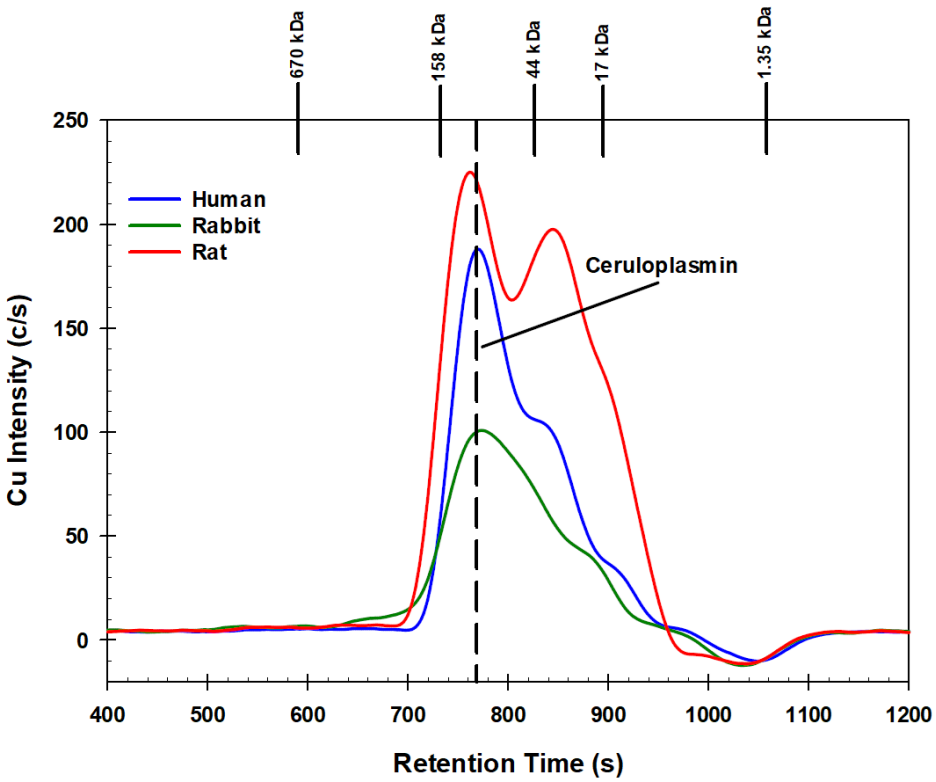

Figure 3.10: Comparative Cu-specific chromatograms obtained by SEC-ICP-AES for the analysis of human (blue), New Zealand White Rabbit (green), and Sprague-Dawley rat (red) blood plasma. Column: Sepax SRT-10C SEC-300 column (7.8 × 300 mm I.D. × Length, 10 µm particle size, 300 Å pore size); Mobile phase: 150 mM PBS (pH 7.4); Temperature: 20 °C; Flow rate: 0.7 mL/min; Injection volume: 500 µL; Detector: ICP-AES (Cu-emission wavelength - 324.754 nm, Fe-emission wavelength – 259.940 nm, Zn-emission wavelength – 213.856 nm). The retention times of molecular weight markers are indicated at the top of the figure.

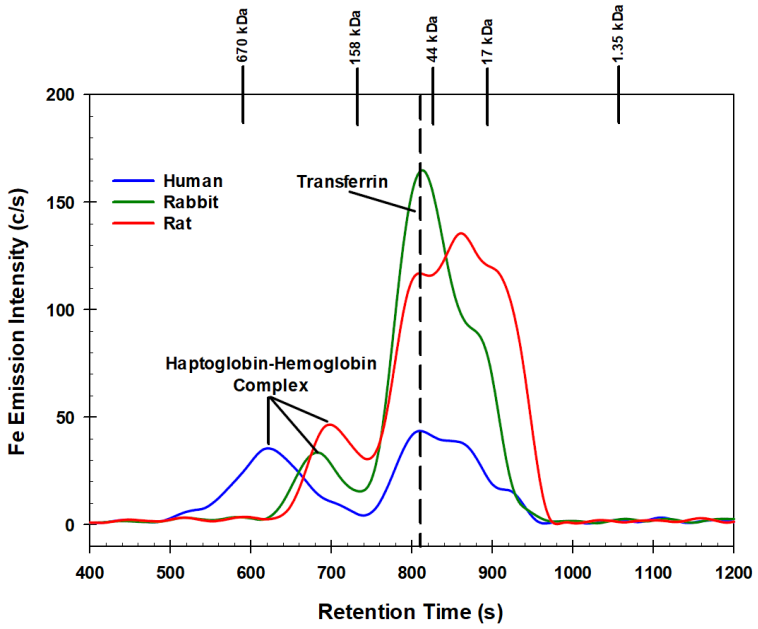

Figure 3.11: Comparative Fe-specific chromatograms obtained by SEC-ICP-AES for the analysis of human (blue), New Zealand White Rabbit (green), and Sprague-Dawley rat (red) blood plasma. Column: Sepax SRT-10C SEC-300 column (7.8 × 300 mm I.D. × Length, 10 µm particle size, 300 Å pore size); Mobile phase: 150 mM PBS (pH 7.4); Temperature: 20 °C; Flow rate: 0.7 mL/min; Injection volume: 500 µL; Detector: ICP-AES (Fe-emission wavelength - 259.940 nm). The retention times of molecular weight markers are indicated at the top of the figure.

The Zn-specific chromatograms in **Figure 3.12** showcase one major Zn-containing species for human, rabbit, and rat plasma (t_r = 813, 807, and 797 respectively) that corresponds to albumin-bound Zn.[60] Much like the **Figures 3.9-3.11** there are large shoulders/unresolved peaks on the long-retention end. Previous studies within the group have reported on the analysis of human and rabbit plasma using SEC-ICP-AES.[34, 60, 65, 71, 80] However, the presence of shoulder peaks and peaks that are not baseline separated in the above data has not been seen in previous studies to the extent seen here. This information suggests that these shoulders/peaks are artefacts that are generated due to sample preparation or the properties of the SRT-10C SEC column, or both. To investigate this phenomenon and attempt to remedy the poor peak shapes, the next section outlines the progressive and systematic dilution of human and rabbit plasma with PBS and investigating the effect of the flow rate on the separation of the metalloproteins.

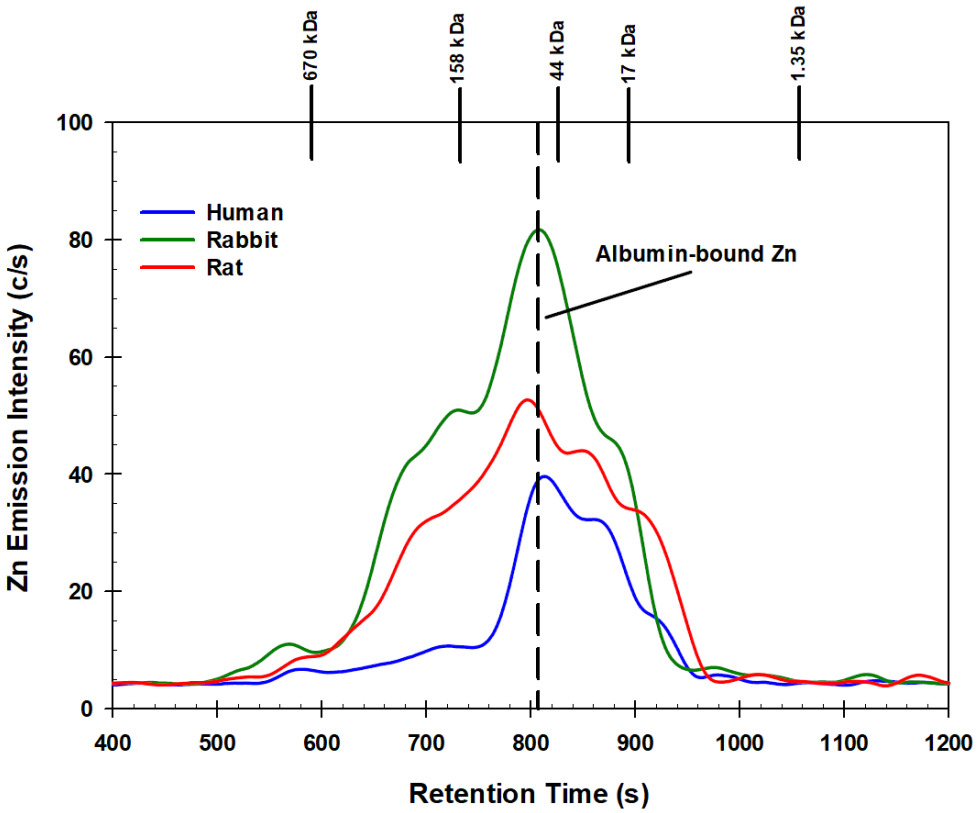

Figure 3.12: Comparative Zn-specific chromatograms obtained by SEC-ICP-AES for the analysis of human (blue), New Zealand White Rabbit (green), and Sprague-Dawley rat (red) blood plasma. Column: Sepax SRT-10C SEC-300 column (7.8 × 300 mm I.D. × Length, 10 µm particle size, 300 Å pore size); Mobile phase: 150 mM PBS (pH 7.4); Temperature: 20 °C; Flow rate: 0.7 mL/min; Injection volume: 500 µL; Detector: ICP-AES (Zn-emission wavelength - 213.856 nm). The retention times of molecular weight markers are indicated at the top of the figure.

3.1.1.4 Dilution of Plasma with PBS

Due to the presence of shoulders on the previously discussed peaks, the effect of diluting the blood plasma prior to analysis was investigated. Instead of diluting plasma with water, which could induce too drastic a change in ionic strength of the plasma, potentially causing the denaturation of protein structure, the addition of 150 mM PBS to plasma was investigated to reduce the viscosity prior to injection while maintaining a physiological pH. **Figure 3.13** illustrates the effect of the dilution of both human and rabbit plasma with PBS on retention time, signal intensity, and peak shape. Human plasma has a noticeably darker yellow colour and is more viscous than rabbit plasma. Therefore, both plasma types were progressively diluted, and the results compared

in **Figure 3.13**. The albumin peak in the undiluted rabbit plasma (**Figure 3.13A**, black line, t_r = 804 s) had a signal intensity of ~28,000 c/s and a shoulder at t_r = 885 s. When the rabbit plasma was diluted 3:1 (750 µL plasma:250 µL PBS, **Figure 3.13A,** red line), the intensity of the albumin peak increased to ~31,000 c/s and the shoulder disappeared. The peak shapes of subsequent dilutions (1:1, blue line and 1:3, green line) of rabbit plasma were very similar to 3:1 with the exception that the signal intensity decreased (~24,000 and ~17,000 c/s respectively) as dilution was increased.

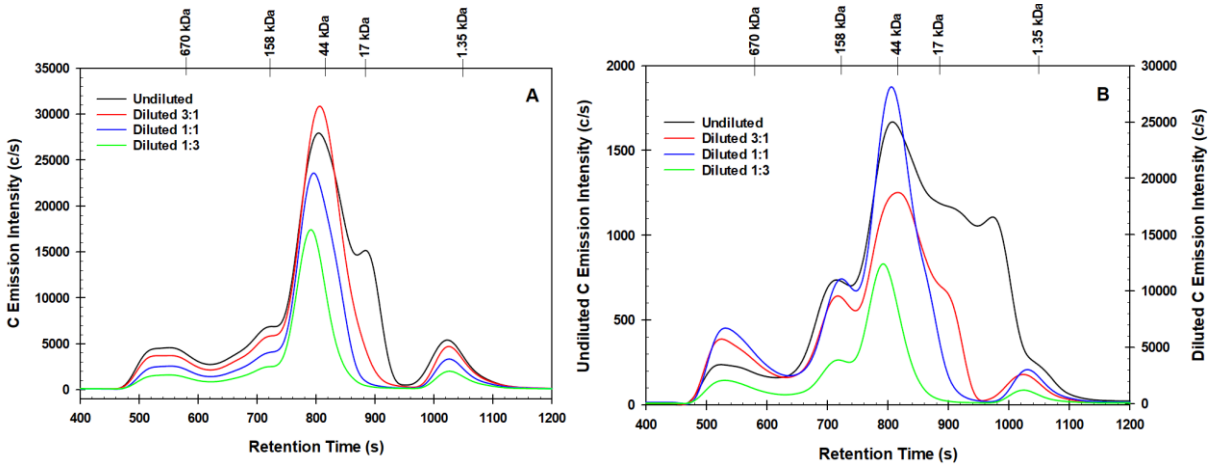

Figure 3.13: Comparative C-specific chromatograms obtained by SEC-ICP-AES for the analysis of New Zealand White Rabbit (A) and human (B) blood plasma. Plasma of each species was mixed with the appropriate volumes of PBS to achieve 3:1 (750 µL plasma and 250 µL PBS), 1:1 (500 µL and 500 µL), and 1:3 (250 µL and 750 µL) ratios of Plasma:PBS. Column: Sepax SRT-10C SEC-300 column (7.8 × 300 mm I.D. × Length, 10 µm particle size, 300 Å pore size); Mobile phase: 150 mM PBS (pH 7.4); Temperature: 20 °C; Flow rate: 0.7 mL/min; Injection volume: 500 µL; Detector: ICP-AES (C-emission wavelength – 193.091 nm). The retention times of molecular weight markers are indicated at the top of the figure.

In **Figure 3.13B** undiluted human plasma (black line) had a maximum C-emission intensity, corresponding to the albumin peak, of ~1600 c/s. This peak also contained extreme tailing and shoulders that extend all the way until the inclusion volume at 1.35 kDa. When the human plasma was diluted 3:1 with PBS (**Figure 3.13B**, red line) the intensity of the albumin peak increased to ~19,000 c/s and the tailing disappeared only leaving a minor shoulder. The 1:1 dilution

of human plasma (**Figure 3.13B**, blue line) further increased the intensity of the albumin peak to ~28,000 c/s and resulted in the shoulder disappearing completely. Further dilution to 1:3 (**Figure 3.13B**, green line) resulted in peaks with the same shapes as with the 1:1 dilution, but with lower signal intensity (albumin - ~12,000 c/s). The information in **Figure 3.13** demonstrates the strong effect that dilution has on peak shape and intensity. It may be related to the large amount of material being injected onto the column, such that diffusion into the stationary phase impeded and peaks are effectively split, resulting in the formation of artefacts. An alternate explanation is that the dilution of the plasma reduces the number of non-specific interactions between proteins in plasma, potentially preventing the formation of aggregates that interfere with the separation, or reducing the viscosity due to variations in lipid concentration.[131, 134] It is interesting to note that when the plasma of either species is diluted (3:1 for rabbit and 1:1 for human) that there was a significant increase in the signal intensity of the albumin peak. This is counterintuitive since less material is being injected onto the column. However, a possible explanation lies in the operating principle of the ICP-AES. If the concentration of protein is extremely high in the albumin peak that is eluting from the column it may be that the viscosity of the solution as this peak leaves the column is high enough such that the nebulization efficiency is reduced (i.e., the nebulizer may be incapable of effectively producing an aerosol) such that the mass transfer into the plasma is significantly reduced. Similarly, it is also possible that as the viscosity of the effluent increased for the peak, the effective flowrate of the pump decreased, resulting in a lower overall mass transfer into the torch.[135]

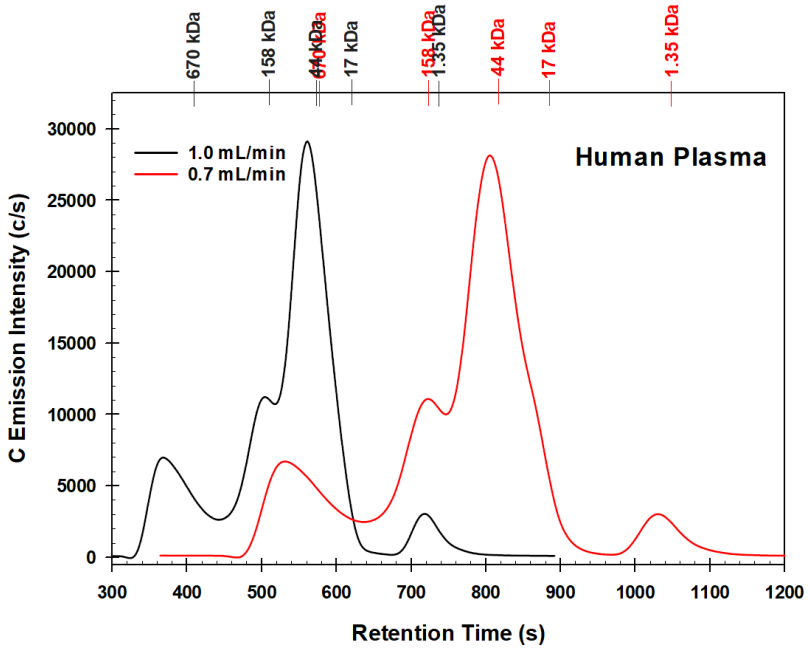

Figure 3.14: Comparative C-specific chromatograms obtained by SEC-ICP-AES for the analysis of human blood plasma. Column: Sepax SRT-10C SEC-300 column (7.8 × 300 mm I.D. × Length, 10 µm particle size, 300 Å pore size); Mobile phase: 150 mM PBS (pH 7.4); Temperature: 20 °C; Flow rate: 0.70 or 1.0 mL/min; Injection Volume: 500 µL; Detector: ICP-AES (C-emission wavelength – 193.091 nm). The retention times of molecular weight markers are indicated at the top of the figure.

The manufacturer's recommended flow rate for the SRT-10C SEC column is 1.0 mL/min. All of the previous Figures have been obtained using a flow rate of 0.7 mL/min to effectively compare this column to the Superdex 200 Increase SEC column. The reason the flow rate was not increased before now was that data accumulated during the column comparison (**Section 3.1.1.2**) was used in the species comparison (**Section 3.1.1.3**) and the dilution analysis (**Section 3.1.1.4**). **Figure 3.14** shows the analysis of human plasma, monitoring the C-emission line, at both 0.7 (red line) and 1.0 mL/min (black line). Increasing the flow rate to 1.0 from 0.7 mL/min reduced the total analysis time by ~30% while still maintaining the same resolution and peak shape (i.e., no shoulders or peak splitting). The molecular weight markers at the top of the chromatogram for both flow rates maintain a similar relative separation from each other. In the remaining sections, the flow rate when using the SRT-10C SEC column was 1.0 mL/min.

3.1.2 SRT-10C SEC Column Mass Recovery Determination

To verify sufficient mass recovery (i.e., to determine to what extent any blood plasma constituents may irreversibly bind to the stationary phase and, therefore, not elute from the column) of the SRT-10C SEC column, two methods were employed. The first method compared the total peak area of the C-emission line for the analysis of human plasma via SEC-ICP-AES and comparing it to the total carbon-peak area for the direct injection analysis of the same amount of human plasma by ICP-AES. The second method utilized the BCA assay that can be used to quantify proteins in solution based on the reaction of certain amino acids and peptide bonds with Cu^{2+} in solution, complexation of the formed Cu^{+} ions by BCA, followed by measuring the absorbance of the resultant purple colour at 562 nm.[60, 136]

3.1.2.1 Mass Recovery Using ICP-AES

Figure 3.14 shows the ICP-AES analysis of 250 µL human plasma after passing through a column (black line) and the direct analysis of 250 µL of the same plasma (diluted to 10 mL with PBS) by direct aspiration into the ICP-AES system. The areas under each curve (obtained by the analysis of the raw ICP-AES data using Origin 2020b software) are compared in **Table 3.1**. Using this method, the mass recovery of the SRT-10C SEC column was 80.0%. While it is possible that 20% of the injected material was retained on the column, there may be an alternative explanation. The C-emission intensity of the direct analysis (red line) reaches a maximum of ~6100 c/s, while the albumin peak in the column analysis approaches 32,000 c/s. It may be possible that the intensity of the albumin peak (t_r = 572 s) exceeds the linear range for the C-emission line resulting in a lower total carbon area for this analysis. While the linear range of the Prodigy ICP-AES for C-emission is not commonly determined, other elements, depending on the monitored wavelength, have linear dynamic ranges that range from 1 to 1000 mg/L.[137] Alternatively, the viscosity and

surface tension of the column effluent when the albumin peak elutes may alter the effectiveness of the nebulizer to form the aerosol or the reduce the evaporation of the solvent.[138] However, in the following section the BCA assay was used to corroborate these results.

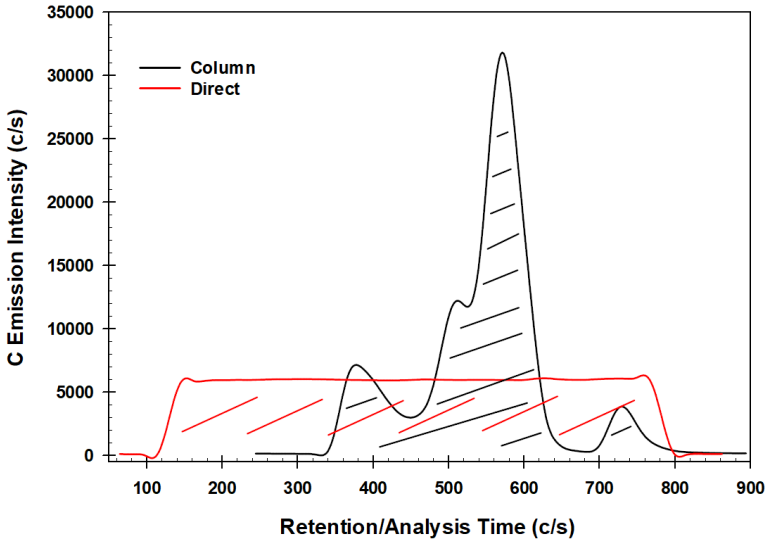

Figure 3.15: Comparative C-specific chromatograms of human blood plasma analyzed directly by ICP-AES (red line, 250 µL plasma diluted to 10 mL in PBS) or analyzed after passing through a Sepax SRT-10C SEC-300 column (black line, 250 µL plasma mixed with 250 µL PBS) (7.8 × 300 mm I.D. × Length, 10 µm particle size, 300 Å pore size). Mobile phase: 150 mM PBS (pH 7.4); Temperature: 20 °C; Flow rate: 1.0 mL/min; Injection volume: 500 µL; Detector: ICP-AES (C-emission wavelength – 193.091 nm). The retention times of molecular weight markers are indicated at the top of the figure.

Table 3.1: Mass recovery determination of SRT-10C SEC column using (SEC)-ICP-AES and determining area counts with the Origin 2020b software. C-emission intensity was monitored for both the direct aspiration analysis of human plasma and the effluent of the SRT-10C SEC column.

Analysis Type	Direct (ICP-AES)			Sepax SRT-10C (SEC-ICP-AES)		
Replicate	1	2	3	1	2	3
Peak Area	3.85×10^6	3.97×10^6	4.05×10^6	3.29×10^6	3.04×10^6	3.16×10^6
Average Peak Area	$3.96 \pm 0.104 \times 10^6$			$3.16 \pm 0.121 \times 10^6$		
Mass Recovery (%)	80.0%					

3.1.2.2 Mass Recovery Determination Using BCA Assay

To verify the results presented in **Section 3.1.1.5.1** a BCA assay was performed on the column effluent after the injection of 250 µL human plasma on the SRT-10C SEC column and

comparison was made to a solution of 250 µL human plasma diluted in PBS (25 mL final volume for each solution). The BCA assay utilizes a standard curve (**Figure 3.15**) produced by solutions of known protein concentrations and the resultant line of best fit is used to determine protein concentrations in the samples. The column effluent from three different injections of human plasma onto the SRT-10C SEC column were collected (C1, C2, and C3) and compared to three solutions prepared by diluting human plasma (D1, D2, and D3) in PBS to 25 mL. Each resultant solution was analyzed in triplicate by the BCA assay.

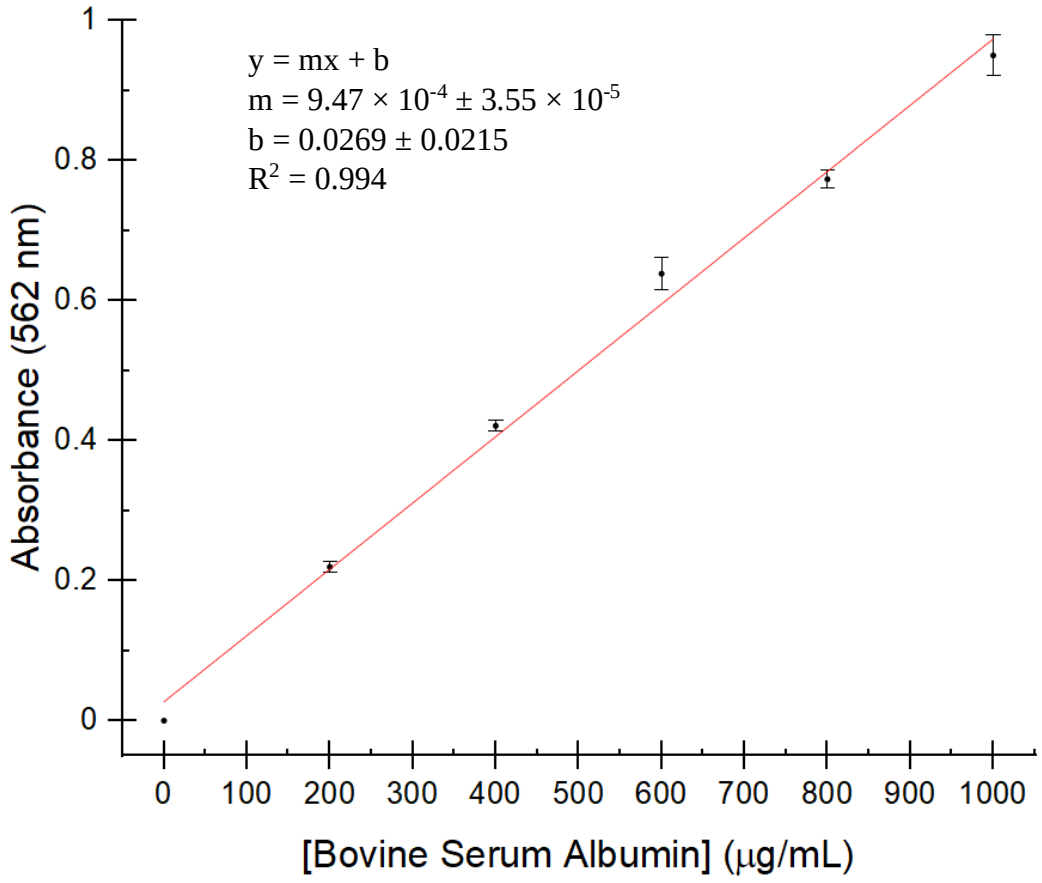

Figure 3.16: Standard curve for bovine serum albumin (BSA) solutions. Solutions were prepared using a 1000 mg/mL BSA stock that was diluted appropriately with 150 mM PBS. 0.1 mL of each solution was mixed with 2.0 mL of a 50:1 bicinchoninic acid (BCA)/$CuSO_4$ before being incubated at 37 °C and absorbance subsequently measured at 562 nm.

As shown in **Table 3.2,** the average protein concentration of the column effluent (C1-3) was 329 µg/mL, and the average protein concentration of the human plasma dilutions (D1-3) was 341 µg/mL. These numbers indicate a 96 ± 2% recovery of injected protein, a 16% increase from the results in the previous section. Taken together, these results suggest that there was minimal protein binding (<4%) to the stationary phase of the column and, therefore, this column is appropriate for the analysis of blood plasma constituents.

Table 3.2: Mass recovery determination of SRT-10C SEC column using BCA assay. Protein concentration was determined for both a solution prepared from 250 µL of plasma diluted to 25 mL with PBS (D1-3) and collecting the effluent of the SRT-10C SEC column (250 µL human plasma injected) and diluting to 25 mL with PBS (C1-3).

Sample	Average [Protein] (µg/mL)	Mass Recovery (%)	Average Mass Recovery (%)
C1	**320**	**94**	**96 ± 2**
D1	**340**		
C2	**318**	**97**	
D2	**329**		
C3	**348**	**98**	
D3	**354**		

3.1.1.6 Addition of CH_3HgOH to Human, Rabbit, and Rat Plasma

Human exposure to CH_3Hg^+ is most commonly associated with the ingestion of fish (e.g., tuna, swordfish) and concerning since chronic low dose exposure to this neurotoxin will result in CH_3Hg^+ entering the blood plasma where concentrations up to 20 µg/L (ppb) have been observed.[29, 139] Therefore, it would be ideal to investigate the bioinorganic chemistry of CH_3Hg^+ at these physiologically relevant concentrations. However, the detection limit (smallest amount of a material that can be distinguished from a blank/noise) of our ICP-AES for Hg is 30 ppb.[140] Additionally, if a 30 ppb Hg solution was injected onto the SRT-10C SEC column, when it elutes, the concentration of Hg will be diluted even further in the mobile phase (e.g., 500 µL of 30 ppb

Hg eluting from the column in peak widths of 100 s at a flow rate of 1.0 mL/min would yield a concentration of ~9 ppb, assuming this fraction was collected and mixed). As such, this section investigates the concentration of CH_3Hg^+ that would be appropriate for detection in blood plasma on the instrument given the sample preparation and separation parameters established in the following sections.

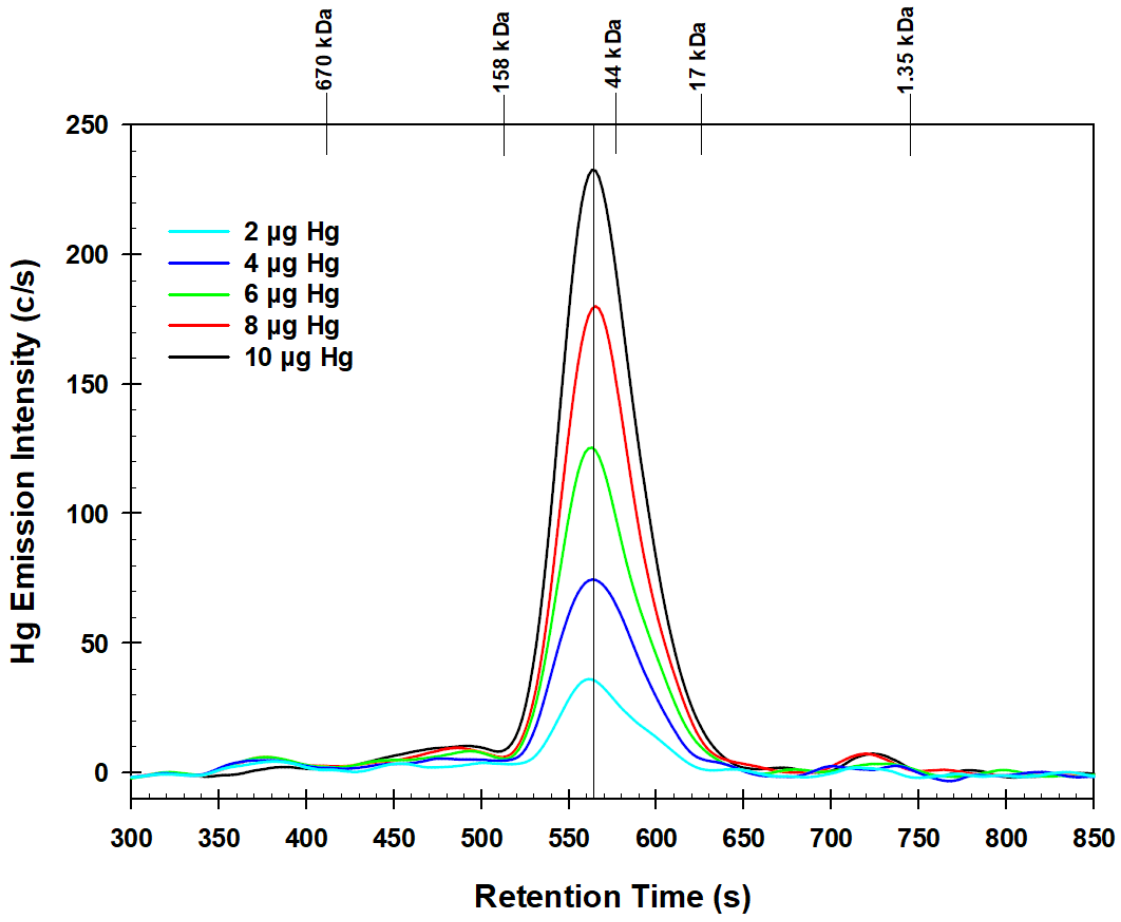

Figure 3.17: Hg-specific chromatogram obtained by SEC-ICP-AES for the analysis of human blood plasma with added CH_3HgOH. 500 µL of plasma was incubated at 37 ºC for 30 minutes (150 rpm) before adding 10, 8, 6, 4, or 2 µL of 0.01 M CH_3HgOH solution followed by the addition of 500 µL PBS. Column: Sepax SRT-10C SEC-300 column (7.8 × 300 mm I.D. × Length, 10 µm particle size, 300 Å pore size); Mobile phase: 150 mM PBS (pH 7.4); Temperature: 20 °C; Flow rate: 1.0 mL/min; Injection volume: 500 µL; Detector: ICP-AES (Hg-emission wavelength – 253.652 nm). The retention times of molecular weight markers are indicated at the top of the figure.

Figure 3.16 shows the SEC-ICP-AES analysis of 500 µL human plasma with 2, 4, 6, 8, and 10 µL of a 0.01 M (~2 µg/µL) CH_3HgOH solution being added, before being diluted to 1.0 mL with PBS and analyzed. Given that the plasma is diluted 1:1 with PBS and that the injection volume is 500 µL, the mass of elemental Hg actually entering the column is indicated in **Figure 3.16**. As expected, increased amounts of the CH_3HgOH solution added to human plasma increases the intensity of the detected Hg peak (t_r = ~564 s, peak intensity = 36, 73, 124, 180, and 231 c/s). Interestingly, in the 8 and 10 µg Hg chromatograms (red and black lines respectively), a small Hg peak appears at t_r = 722 s suggesting that more than one Hg-species may be forming in the plasma, possibly with small molecular weight metabolites (e.g., amino acids), but may only be forming appreciably at these higher concentrations, such that they are detectable.[28]

The Hg-peaks in **Figure 3.16** elute at a retention time consistent with serum albumin. To corroborate this, **Figure 3.17** shows both the Hg (red) and C (black) emission lines for the same analysis in human plasma, but also compares it to the results of CH_3Hg^+-spiked rabbit and rat plasma (10 µL of 0.01 M CH_3HgOH added). While each Hg-peak coelutes with the most intense C-peak (suggesting that CH_3Hg^+ binds to serum albumin), subtle differences exist between species. The retention time of human, rabbit, and rat Hg-peaks are 561, 563, and 567 s respectively. The slightly different retention times are likely due to interspecies variation in the molecular weight, amino acid composition, and hydrodynamic radius of serum albumin.[132] It is possible that the binding site of CH_3Hg^+ on serum albumin is a conserved Cys-34 residue.[132, 141] To achieve a strong Hg signal given the parameters of the sample preparation and separation, while not introducing so much CH_3Hg^+ such that artefacts are introduced by achieving super-physiological concentrations, the information presented in both **Figures 3.16** and **3.17** which suggest a "middle of the road" amount of Hg that may be used to obtain good results. Given that the average human

serum/plasma concentration of albumin ranges from ~35-50 mg/L, equivalent to approximately 250-375 µM when diluted 1:1 with PBS, and that 5 µL of the 0.01 M CH_3HgOH added to 500 µL plasma and 495 µL of PBS results in a concentration of 50 µM CH_3HgOH, this information indicates that there is at most a 1:5 molar ratio of the concentrations of CH_3Hg^+ and albumin.[60, 142] This means that the CH_3Hg^+ concentration is sufficiently low in solution that binding sites on albumin are not being saturated with CH_3Hg^+ and suggests that what is being seen are actual physiologically relevant interactions and not super-physiological artefacts. Therefore, the addition of 5 µL of the 0.01 M CH_3HgOH solution to plasma samples provides a peak of sufficient intensity while not unreasonably exceeding physiological conditions.

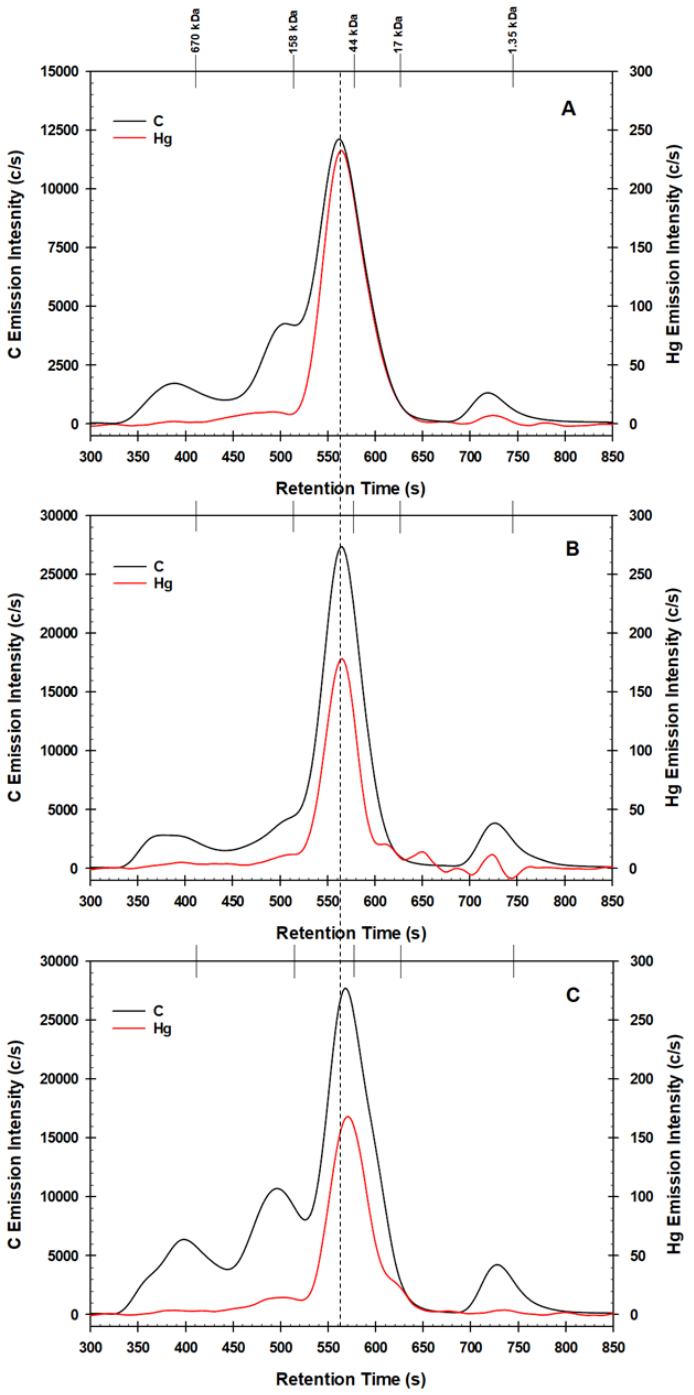

Figure 3.18: C- and Hg-specific chromatograms obtained by SEC-ICP-AES for the analysis of human (A), New Zealand White Rabbit (B), and Sprague-Dawley rat (C) blood plasma spiked with 10 µL of 0.01 M CH_3HgOH solution followed by the addition of 490 µL PBS. Column: Sepax SRT-10C SEC-300 column (7.8 × 300 mm I.D. × Length, 10 µm particle size, 300 Å pore size); Mobile phase: 150 mM PBS (pH 7.4); Temperature: 20 °C; Flow rate: 1.0 mL/min; Injection volume: 500 µL; Detector: ICP-AES (C-emission wavelength – 193.091 nm, Hg-emission wavelength – 253.652 nm). The retention times of molecular weight markers are indicated at the top of the figure.

3.2 Conclusion

This chapter has described the results that were obtained in the context of developing a more cost-effective method to analyze blood plasma using SEC-ICP-AES by optimizing a number of parameters involving sample preparation (**Section 3.1.1**), column suitability (**Section 3.1.1.2**), and elemental detection (**Section 3.1.1.6**). It was determined that filtering commercially available blood plasma through a 0.45 µm pore size filter prior to injection on the column was essential for maintaining the separation performance of the SEC stationary phase. The comparison of the chromatograms produced by the analysis of blood plasma on both the Superdex 200 Increase and SRT-10C SEC columns demonstrated that the same number of peaks were produced with comparable resolution, but with the SRT-10C SEC column providing improved separation times and peak intensities. The analysis of three mammalian species' blood plasma demonstrated that shoulders were being artificially produced in the chromatogram. Diluting blood plasma 1:1 with PBS was determined to be critical to prevent the formation of chromatographic artefacts during separation. Increasing the flow rate of the HPLC pump to 1.0 from 0.7 mL/min further improved the separation time while maintaining the same number of peaks and resolution. The recovery of plasma proteins from the SRT-10C SEC column was determined to be 96 ± 2% indicating minimal irreversible protein binding to the stationary phase. CH_3Hg^+ behaved similarly in human, rabbit, and rat plasma, appearing to bind to serum albumin. While measuring physiologically relevant concentrations of CH_3Hg^+ in blood plasma (0-20 µg/L) was not achievable with our instrument, with the limit of detection (LOD, 3σ) for Hg being 30 ppb, the addition of 5 µL of 0.01 M CH_3HgOH to 500 µL of plasma before diluting to 1.0 mL with PBS provided a Hg-peak with a strong intensity that didn't saturate the proposed binding site on serum albumin.[29, 139, 140] These results provided the foundation for the experiments presented in **Chapter 4**.

Chapter 4: Toxicologically Relevant Interactions between Methylmercury and SMW Thiols in Blood Plasma

4.1 Introduction

Methylmercury (CH_3Hg^+) is one of the most potent known neurotoxins.[143, 144] From a public health point of view human exposure to CH_3Hg^+ is not only relevant to adults, but also to children as this pollutant can have serious adverse effects on the development and functioning of the human central nervous system.[145] The on-going anthropogenic release of Hg into the atmosphere combined with climate change and overfishing has contributed to an increase in the CH_3Hg^+ concentration in Atlantic bluefin tuna by approximately 56% over the past five decades.[146] Since human exposure to CH_3Hg^+ is predominantly attributed to the ingestion of CH_3Hg^+-containing fish, communities where fish is the primary food source are often adversely affected.[147-149] Over the past decades toxicological research has provided important insight into the complex mechanisms that deliver environment-derived CH_3Hg^+ to the human brain.[150] After CH_3Hg^+ enters the bloodstream, it will interact with a plethora of plasma proteins, small molecular weight (SMW) molecules and red blood cells.[42, 151] Although these interactions fundamentally determine if and how much of CH_3Hg^+ that enters the bloodstream will eventually reach the brain and other toxicological target organs, significant knowledge gaps remain.[152] Probing interactions between CH_3Hg^+ and relevant biomolecules in the bloodstream under near physiological conditions represents a molecular toxicological approach to possibly identify factors which play an important role in terms of determining how much of this neurotoxin reaches the brain following the exposure of various human populations to realistic doses of this potent neurotoxin.[149, 153, 154] Gaining insight into these processes thus represents an important first step in terms of to reducing the staggering costs of environmental disease, possibly by implementing low-cost nutritional interventions.[155, 156] To establish the mechanism which governs the translocation of CH_3Hg^+ from the bloodstream to

the brain one needs to probe CH_3Hg^+'s interactions with biomolecules in blood plasma as well as in red blood cells (RBCs) to establish which CH_3Hg^+-derived molecular species represent the substrates for uptake into the brain via the BBB.[157] With regard to interactions of CH_3Hg^+ with constituents of the bloodstream it has been shown that in plasma CH_3Hg^+ forms adducts with human serum albumin (HSA) in aqueous solution.[158] Based on the structure of HSA and the high affinity of CH_3Hg^+ for thiols, Cys-34 – which is located in a crevice on the protein (**Figure 4.1**)- is the most likely binding site, but it cannot be entirely excluded that the hydrophobic moiety of CH_3Hg^+ binds to a hydrophobic pocket on the protein.[159] Biological thiols are known to play an important role in the metabolism of CH_3Hg^+.[160] ^{1}H-NMR spectroscopy has been employed to demonstrate that CH_3Hg^+ rapidly crosses the red blood cell membrane, where it subsequently binds to glutathione (GSH) and hemoglobin (Hb) in the cytosol.[118, 151] These results exemplify the importance of understanding the partitioning of CH_3Hg^+ between blood plasma and RBCs in the bloodstream, as an effective sequestration within RBCs would preclude its translocation to the brain and the associated adverse neurotoxic effects.[161-163] In terms of knowledge gaps, the number of proteins in human blood plasma that bind CH_3Hg^+, the sequence of biochemical mechanisms that deliver this neurotoxin across the BBB and the actual species that is/are translocated are unknown, but studies with rats have shown that small molecular weight (SMW) thiols appear to be implicated in the translocation process.[127]

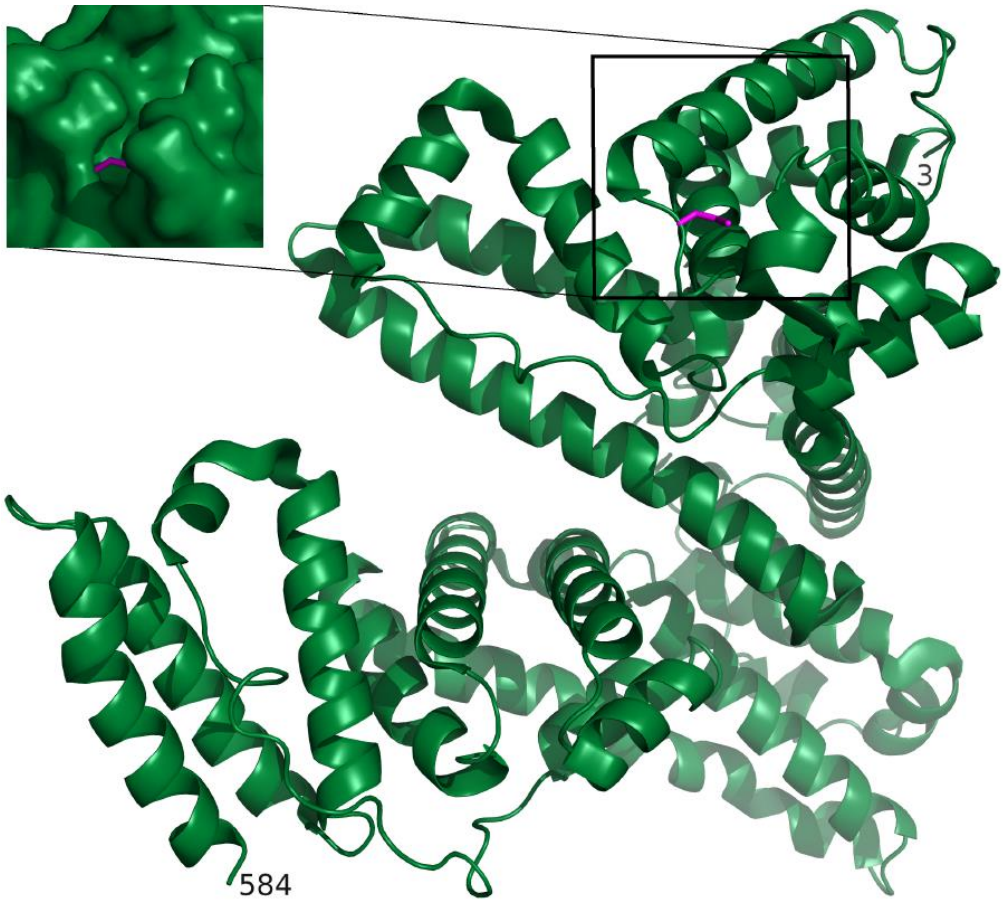

Figure 4.1: A modelled ribbon diagram of HSA (green) bound to CH_3Hg^+ (purple). The inset on the top-left of the figure shows the zoomed-in location of CH_3Hg^+ bound to the Cys-34 residue of HSA. Taken from Bridle et al. (2021).[157] Information regarding how this figure was generated can be found therein.

Direct experimental evidence in support of this involvement comes from studies which have demonstrated that a CH_3Hg-cysteine (Cys) complex is recognized by molecular transport pumps (LAT-1 and LAT-2) located at the BBB which specifically recognizes amino acids, such as L-methionine, and infuse the CH_3Hg-Cys complex into the brain.[128, 129] Detailed structural investigations of the CH_3Hg-Cys complex by extended X-ray absorption fine structure (EXAFS) spectroscopy, however, have provided evidence that the translocation cannot be attributed to 'molecular mimicry', but that it may rather involve a more localized mimicry of the amino acid part of the complex.[130] This notion is supported by the fact that while the coadministration of

CH_3Hg^+ and L-cysteine enhanced the uptake of CH_3Hg^+ into oocytes that expressed LAT-1 and LAT-2 transporters, the coadministration of CH_3Hg^+ and D-cysteine did not.[129] This suggests that the transportation of amino acids via the LAT-1/2 transporters is stereoselective (D-cysteine is the corresponding stereoisomer of L-cysteine).

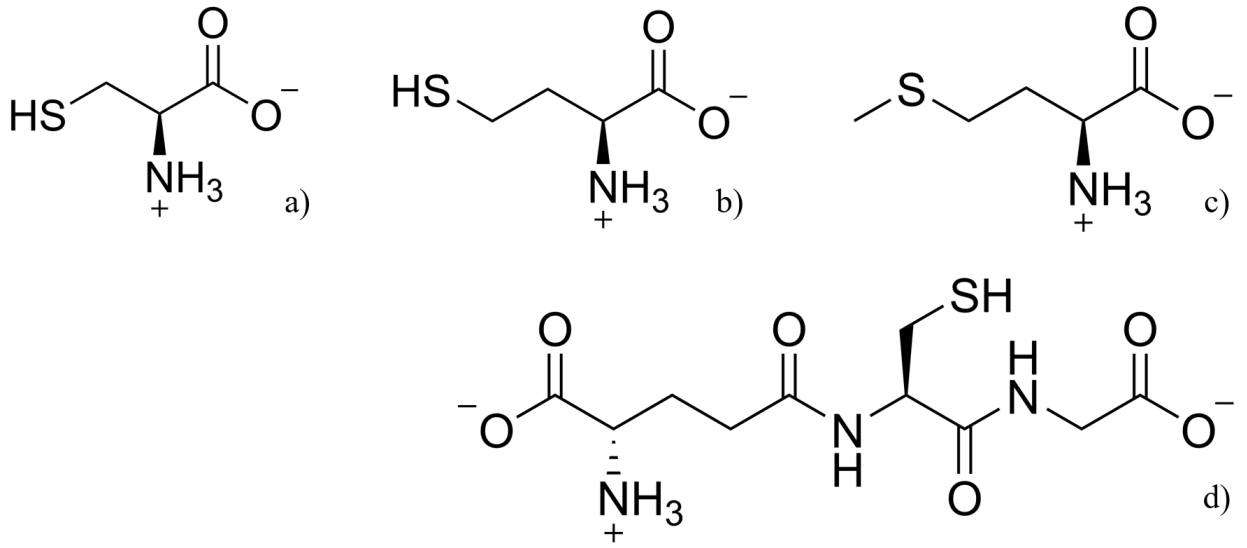

Figure 4.2: Chemical structures of L-cysteine (a), L-homocysteine (b), L-methionine (c) and L-glutathione (d) at pH 7.4.

To better define the biochemical mechanisms, which govern the translocation of CH_3Hg^+ from the bloodstream to the brain size exclusion chromatography coupled on-line to an inductively coupled plasma atomic emission spectrometer (SEC-ICP-AES) was utilized. Specifically, this metallomics tool was used to probe the effect of Cys, hCys, Met and GSH (**Figure 4.2**) on CH_3Hg^+ bound to proteins in rabbit plasma since all of these amino acids are present in blood plasma at µM concentrations (hCys 5–15, Cys 200–300, and GSH 1–5 µM) or have been shown to form complexes with CH_3Hg^+ *in vivo*.[164, 165] After spiking rabbit blood plasma with CH_3Hg^+, the obtained mixture was analyzed using PBS as the mobile phase as the latter has been shown to minimize artefacts when plasma is analyzed.[166] The derived Hg-specific chromatograms revealed

the binding of CH_3Hg^+ to RSA. Thereafter, physiologically relevant concentrations of each SMW thiol were added to the mobile phase and CH_3Hg^+-spiked rabbit plasma was analyzed again. Changes in the Hg-specific chromatograms allowed the systematic investigation into the effect of each thiol on the binding of CH_3Hg^+ to plasma proteins. Since the plasma concentration of hCys is elevated in certain human conditions, this SMW thiol was the primary focus and was compared the results to those obtained for the structurally related Cys, Met and GSH.[167-169] Furthermore, the results that were obtained with rabbit blood plasma were corroborated with an aqueous solution of pure rabbit serum albumin (40 g/L, ~600 µM) to which CH_3Hg^+ had been added. Taken together, the fact that the top-down results were confirmed by bottom-up results demonstrate that the plasma concentration of hCys and Cys play an important role in the metabolism of CH_3Hg^+ in the bloodstream which could be implicated in its translocation to the brain.

Chronic low dose exposure to CH_3Hg^+ can result in blood plasma concentrations that range from 0-20 µg/L (ppb) and above.[29, 139] Therefore, it would be ideal to investigate the bioinorganic chemistry of CH_3Hg^+ at these physiologically relevant concentrations. However, the detection limit of our ICP-AES for Hg is 30 ppb, so higher levels of Hg are herein considered.[140] Given that the average human serum/plasma concentration of albumin ranges from ~35-50 mg/L, equivalent to approximately 250-375 µM when diluted 1:1 with PBS, and that 5 µL of the 0.01 M CH_3HgOH added to 500 µL plasma and 495 µL of PBS results in a concentration of 50 µM CH_3HgOH, this information indicates that there is at most a 1:5 ratio of the concentrations of CH_3Hg^+ and albumin.[60, 142] This means that the CH_3Hg^+ concentration is sufficiently low in solution that binding sites on albumin are not being saturated with CH_3Hg^+ and suggests that what is being seen are physiologically relevant interactions and not super-physiological artefacts. For additional

figures that were generated from the experiments performed in **Chapter 4**, which may aid in providing additional understanding of the results therein, please see Appendix A.

4.2 Results and Discussion

To overcome the inherent difficulty that is associated with delineating the interactions of CH_3Hg^+ with relevant biomolecules in the bloodstream, metallomics tools can provide valuable insight.[170, 171] To this end, the effect of Cys, hCys and GSH on the interaction of CH_3Hg^+ bound to plasma proteins in rabbit plasma and in a solution of pure rabbit serum albumin (RSA) spiked with CH_3Hg^+ was investigated. In view of the fact that the plasma concentration of hCys is elevated in certain human health conditions and in hyperhomocysteinemia, it is important to investigate if the exposure of these individuals to dietary CH_3Hg^+ (e.g., via the consumption of tuna) may make them more susceptible to the neurotoxic effects of CH_3Hg^+ based on the bioinorganic processes that unfold in the bloodstream. [167, 169, 172] With the exception of some preliminary experiments in human plasma (**Section 4.2.1**), rabbit blood plasma from BIOIVT (Westbury, NY, USA) was used to conduct all experiments (the experimental details for the results in this chapter are outlined in **Sections 2.3** and **2.5**).

4.2.1 Analysis of Human Plasma for CH_3Hg^+ with Small Molecular Weight Thiols in the Mobile Phase

Figure 4.3 shows the analysis of human plasma spiked with CH_3Hg^+ and analyzed by SEC-ICP-AES using PBS as the mobile phase with the addition of 500 µM Cys, hCys, or GSH in said mobile phase. The Hg-peak that coeluted with human serum albumin (t_r = 563 s) is no longer seen and there appears another set of Hg-peaks in the SMW range of the chromatogram. The ligand-exchange of CH_3Hg^+ between thiol-containing molecules is well established in the literature, but here it is observed in the biological context of blood plasma and with physiologically relevant

molecules (e.g., amino acids) that seem to be capable of abstracting CH_3Hg^+ from albumin.[28] All three peaks that appear with Cys (t_r = 722 s), hCys (t_r = 733 s), or GSH (t_r = 699 s) have a smaller shoulder on their long retention ends. This suggests the formation of more than one SMW Hg-species, possibly between CH_3Hg^+ and the added thiols (e.g., CH_3Hg-(h)Cys or CH_3Hg-GS), or other biomolecules present in human blood plasma (e.g., CH_3Hg-(h)Cys species interacting with other peptides/proteins in plasma). The higher intensity of the Hg-peaks when the mobile phase contained 500 µM hCys (**Figure 4.3**, blue line) is attributed to the changing of the adapter (O-ring) that connects the concentric nebulizer to the spray chamber in between the hCys and subsequent Cys and GSH experiments. The stock of human plasma had run out after these experiments and, due to the restrictions of COVID-19, fresh human plasma was not able to be obtained. Therefore, the following experiments in **Chapter 4** were conducted in New Zealand White Rabbit blood plasma obtained from BIOIVT (Westbury, NY, USA).

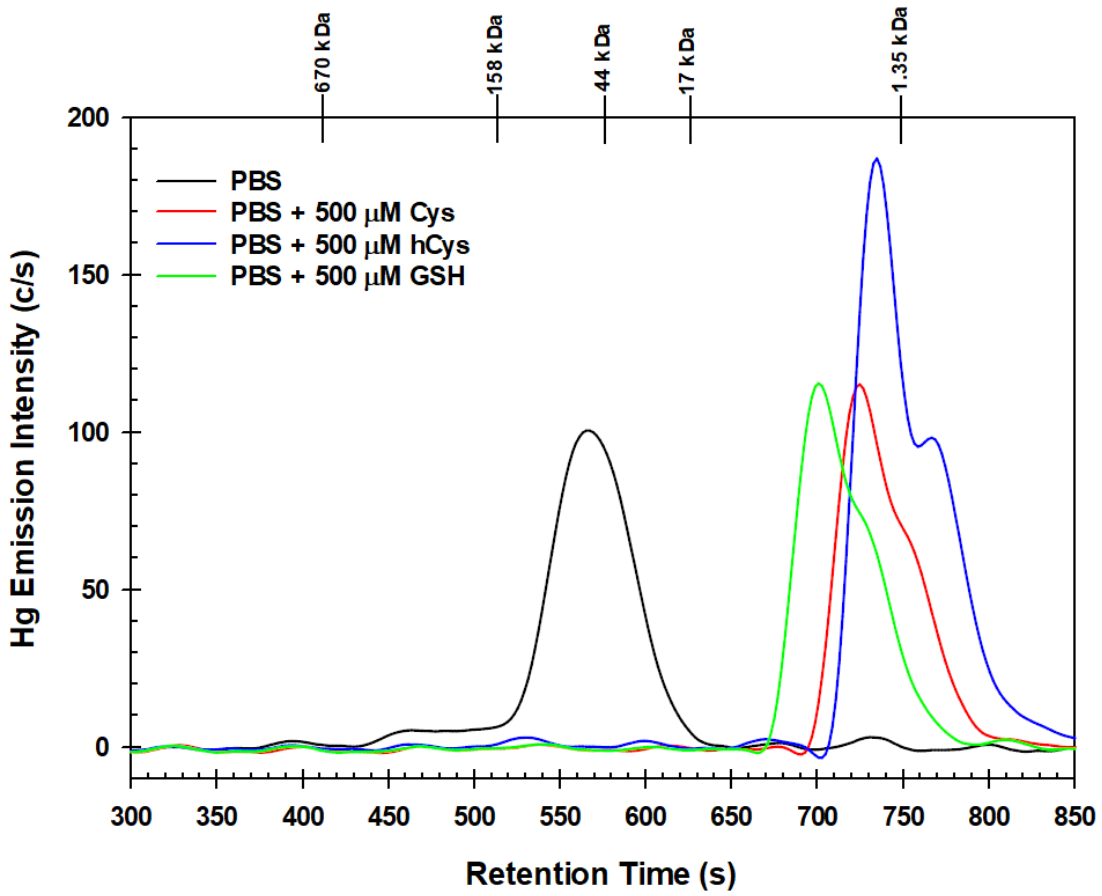

Figure 4.3: Representative Hg-specific chromatograms obtained by SEC-ICP-AES for the analysis of human blood plasma spiked with 5 µL of 0.01 M CH_3HgOH solution followed by the addition of 495 µL PBS. Column: Sepax SRT-10C SEC-300 column (7.8 × 300 mm I.D. × Length, 10 µm particle size, 300 Å pore size); Mobile phase: 150 mM PBS (pH 7.4) with 500 µM Cys, hCys, or GSH; Temperature: 20 °C; Flow rate: 1.0 mL/min; Injection volume: 500 µL (250 µL blood plasma and 250 µL of PBS containing 5 µg Hg, 50 µM CH_3Hg^+); Detector: ICP-AES (Hg mission wavelength – 253.652 nm). The retention times of molecular weight markers are indicated at the top of the figure.

4.2.2 Analysis of Rabbit Plasma for CH_3Hg^+ with Small Molecular Weight Thiols in the Mobile Phase

The analysis of CH_3Hg^+-spiked rabbit plasma revealed a single Hg-peak (t_r= 556 ± 1 s, total Hg peak area 7033 ± 211 area counts/AU) which eluted shortly before the 44 kDa molecular weight marker (**Figure 4.4A**, black line). Based on the high affinity of CH_3Hg^+ for serum albumin [158] and the fact that rabbit serum albumin (RSA) is also the most abundant protein, the detected

Hg-peak is tentatively identified as a CH_3Hg-RSA complex. Indeed, the analysis of a mixture which was obtained by the addition of CH_3Hg^+ to a solution of pure RSA resulted in the detection of a Hg-peak which had an identical retention time (**Figure. 4.5**, bottom) compared to that observed for CH_3Hg^+-spiked rabbit plasma (**Fig. 4.4A**, black line).

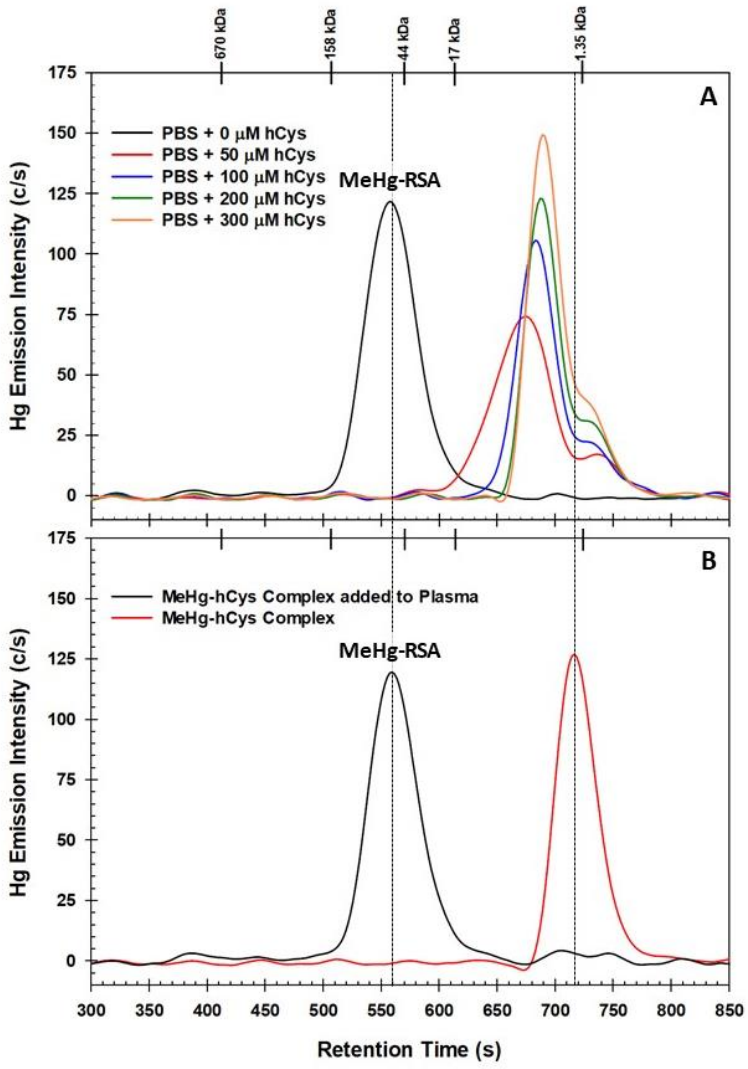

Figure 4.4: Representative Hg-specific chromatograms obtained by SEC-ICP-AES for the analysis of rabbit blood plasma spiked with CH_3HgOH (A) or an equimolar CH_3Hg.hCys solution in PBS and after its addition to rabbit blood plasma (B). Column: Sepax SRT-10C SEC column (7.8 × 300 mm I.D. × Length, 10 µm particle size, 300 Å pore size); Mobile phase: 150 mM PBS (pH 7.4) with 0, 50, 100, 200, 300 µM hCys; Temperature: 20 °C; Flow rate: 1.0 mL/min; Injection volume: 500 µL (250 µL blood plasma and 250 µL of PBS containing 5 µg Hg, 50 µM CH_3Hg^+); Detector ICP-AES (Hg-emission wavelength – 253.652 nm). The retention times of molecular weight markers are indicated at the top of the figure.

The addition of increasing concentrations of hCys to the mobile phase was associated with a reduction in the total area counts for the Hg peak area to 5345 ± 187 AU (50 µM), 5207 ± 224 AU (100 µM), 5388 ± 194 AU (200 µM) and 5985 ± 314 AU (300 µM) (**Table 4.1**), which can be attributed to effects of the sulfur-content of the mobile phase on the emission of Hg from the ICP which is not well understood.[173] The addition of 50 µM of hCys to the mobile phase resulted in the detection of two Hg-peaks with significantly increased retention times. The first, major Hg-peak (t_r= 674 ± 1 s) exhibited a considerable peak width (> 100 s) and had a shoulder (t_r = 733 ± 3 s) (**Figure 4.4A**, red line). These results imply that this hCys concentration mobilizes CH_3Hg^+ from RSA to form SMW Hg-species. The relative retention times of these Hg-peaks suggests that the first Hg-peak that eluted possibly corresponds to a CH_3Hg-hCys complex that is weakly bound to other small molecular weight peptides that are present in plasma (t_r = 674 ± 1 s), while the second Hg-peak may represent a CH_3Hg-hCys complex that has a small affinity for the stationary phase as it eluted past the inclusion volume of 1.35 kDa (t_r =733 ± 3 s).

Table 4.1: Total Hg-area counts and corresponding standard deviations for the peaks shown in Figure 4.3.

Mobile Phase (PBS)	0 µM hCys	50 µM hCys	100 µM hCys	200 µM hCys	300 µM hCys
Hg Peak Area (AU, × 10^3)	7.03 ± 0.21	5.35 ± 0.19	5.21 ± 0.22	5.39 ± 0.19	5.99 ± 0.31

Increasing the hCys concentration of the mobile phase from 50 to 100, 200 and 300 µM resulted in a gradual increase in the S-emission baseline in the obtained S-specific chromatograms (data not shown) and also resulted in the detection of two Hg-peaks (**Figure 4.4A**, blue, green and orange lines), which had the same relative intensity compared to those observed with the 50 µM mobile phase. The first Hg-peak that eluted with the 100 µM hCys mobile phase was notably

sharper and had a 10 s increased retention time compared to the corresponding peak with the 50 µM mobile phase. The first Hg-peak became progressively narrower with higher intensities as the hCys concentration increased and the same was observed for the shoulder.

In an attempt to qualitatively identify the observed Hg-peaks that were observed when CH_3Hg^+-spiked rabbit plasma was analyzed with the 50 µM hCys mobile phase (**Figure 4.4A**), a CH_3Hg-hCys complex obtained by mixing equimolar (5×10^{-7} mol) amounts of CH_3Hg^+ and hCys in PBS (50 µM) was injected onto the SEC column. The results revealed a single Hg-peak (**Figure 4.4B**, red line), which eluted close to the inclusion volume and can be assigned to a CH_3Hg-hCys complex, which had a different retention time than the Hg double-peaks that were observed when CH_3Hg^+-spiked rabbit plasma was analyzed with different hCys concentration in the mobile phases (**Figure 4.4**, dotted vertical line close to the 1.35 kDa MW marker). The shorter retention time of the first Hg-peak for rabbit plasma with hCys in the mobile phase (**Figure 4.4A**) is attributed to the formation of a CH_3Hg-hCys complex that weakly interacts with small molecular weight species in plasma (e.g., peptides and sugars) and, therefore, elutes earlier than the 'unbound' CH_3Hg-hCys complex (**Figure 4.4B**, red line).

To investigate if CH_3Hg^+ is translocated from a synthetic CH_3Hg-hCys complex to RSA in rabbit plasma, the synthetic CH_3Hg-hCys complex was added to rabbit plasma. The analysis of the obtained mixture revealed a single Hg-peak (**Figure 4.4B**, black line), which had an identical retention time as the Hg-peak that was observed when CH_3Hg^+-spiked rabbit plasma was analyzed (**Figure 4.4A**, black line, dotted vertical black line before the 44 kDa MW marker). These results demonstrate a rapid translocation of the CH_3Hg^+ moiety from the CH_3Hg-hCys complex to RSA and support the notion that CH_3Hg^+ binds to a Cys residue since the CH_3Hg-S bond in thiols is known to be thermodynamically stable, but kinetically labile (e.g., the binding affinity of CH_3Hg^+

to thiol groups is significantly stronger than other nucleophilic groups, however, the average lifetime of the CH_3Hg-SG complex is less than 0.01 s).[28, 118, 174-176] Accordingly, the CH_3Hg^+ moiety from the synthetic CH_3Hg-hCys complex was rapidly translocated to RSA owing to the extremely rapid exchange of CH_3Hg^+ with thiol groups and the higher concentration of RSA that the CH_3Hg-hCys complex encountered after it was added to rabbit plasma.

To demonstrate that thiols in the mobile phase cause the shift of CH_3Hg^+ to larger retention times, CH_3Hg^+-spiked rabbit plasma was analyzed using mobile phases that contained 300 µM of Met, Cys or GSH in the mobile phase (**Figure 4.5**, top). The results that were obtained for Met (**Figure 4.5**, top, black lines) revealed a single Hg-peak (t_r = 557 ± 1 s) that had the same retention time (t_r = 556 ± 1 s) as the Hg-peak of the CH_3Hg-RSA complex (**Figure 4.4A**, black line), which shows that CH_3Hg^+ was not mobilized from RSA owing to the lack of a thiol group in Met (**Figure 4.2**). Similar results for 500 µM Histidine (His) were observed (data not shown). Conversely, the Hg-specific chromatograms that were obtained for Cys (**Figure 4.5**, top, red line) and GSH (**Figure 4.5**, top, blue line) revealed a single Hg-peak that eluted close to the inclusion volume and had a very minor Hg-shoulder on its long retention end, which is reminiscent to the results obtained for hCys (**Figure 4.4A**, orange line). These observations can be readily explained as Cys and GSH contain thiol groups which are able to mobilize CH_3Hg^+ from RSA in a similar manner as hCys (**Figure 4.4A**). The ~30 s shorter retention time of the Hg-peak that was observed with the GSH compared to the Cys-containing mobile phase can be attributed to a larger hydrodynamic radius of the potentially formed CH_3Hg-GS species compared to the CH_3Hg-Cys species.

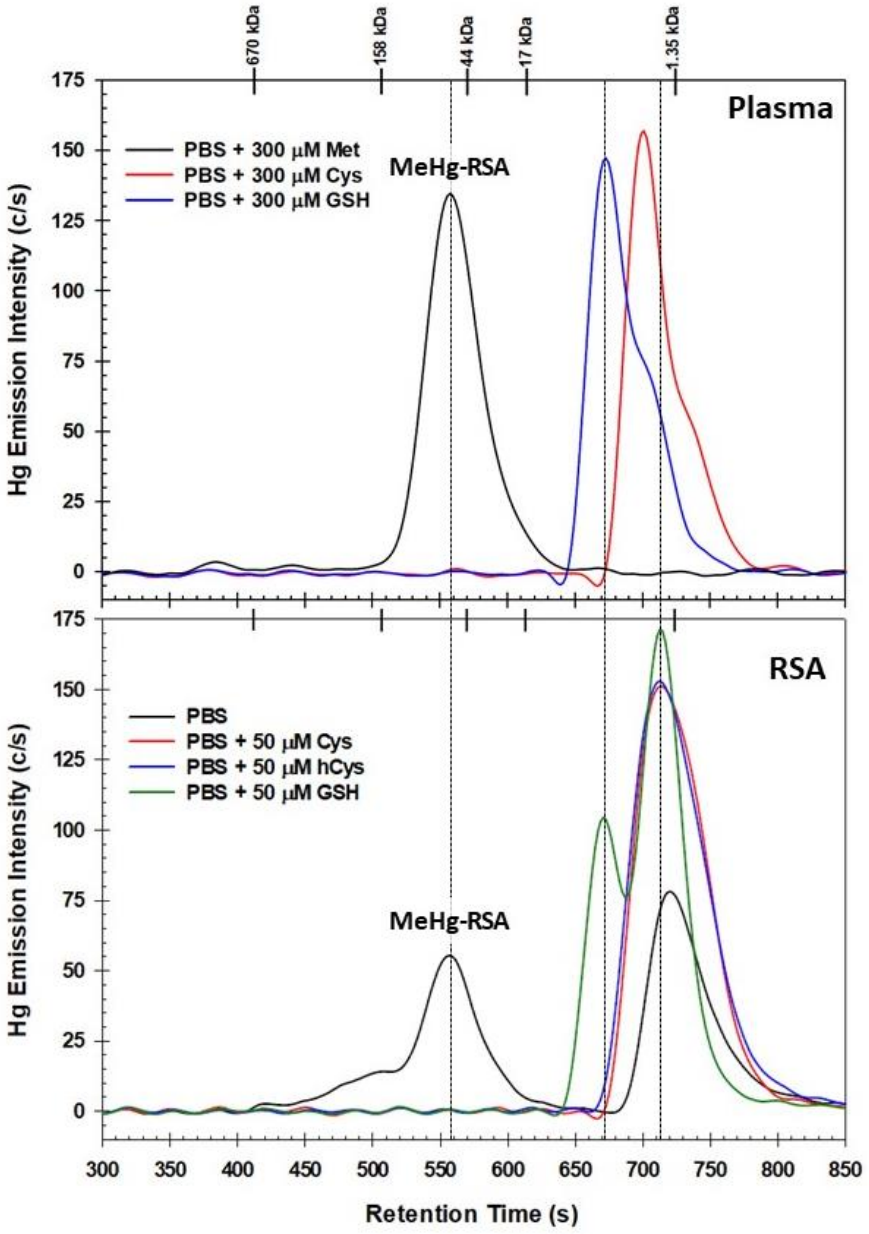

Figure 4.5: Representative Hg-specific chromatograms obtained by SEC-ICP-AES for the analysis of rabbit blood plasma spiked with CH_3HgOH which was analyzed with mobile phases which contained 300 µM of methionine (Met), cysteine (Cys) or glutathione (GSH) (Plasma) or an aqueous solution of a CH_3Hg^+-spiked solution of 40 g/L (~600 µM, ~300 µM after 1:1 dilution with PBS) of rabbit serum albumin (RSA) in PBS which was analyzed with mobile phases that contained 50 µM of cysteine (Cys), homocysteine (hCys) or glutathione (GSH). Column: Sepax SRT-10C SEC column (7.8 × 300 mm I.D. × Length, 10 µm particle size, 300 Å pore size, fractionation range: 5 - 1,250 kDa); Mobile phase: 150 mM PBS (pH 7.4) with 50 or 300 µM Met, Cys, hCys, or GSH; Temperature: 20 °C; Flow rate: 1.0 mL/min; Injection volume: 500 µL (250 µL blood plasma and 250 µL of PBS containing 5 µg Hg, 50 µM CH_3Hg^+); Detector: ICP-AES (Hg-emission wavelength – 253.652 nm). The retention times of molecular weight markers are indicated at the top of the figure.

To directly observe the effect of physiologically more relevant concentrations of SMW thiols on CH_3Hg^+ bound to pure RSA, the latter mixture was analyzed with mobile phases that contained 50 µM of Cys, hCys and GSH (**Figure 4.5**, bottom; red, blue and green lines). Without thiols in the mobile phase two Hg-peaks of about equal peak area and peak width were observed, with the first one displaying fronting, which it is attributed to protein-protein interactions. The first Hg-peak (t_r = 557 ± 1 s) is tentatively identified as a CH_3Hg-RSA complex, while the second Hg-peak (t_r = 721 ± 1 s) essentially eluted in the inclusion volume and, therefore, corresponds to a SMW Hg-species. These results imply that ~50% of CH_3Hg^+ was not able to bind to Cys-34 on RSA, possibly due to it being oxidized or otherwise bound, or that CH_3Hg^+ was mobilized from RSA during the analysis by the constituents of the PBS-buffer, possibly the Cl^- ions. When the CH_3Hg-RSA complex was analyzed with a mobile phase that contained 50 µM of Cys (**Figure 4.5**, bottom; red line) or hCys (**Figure 4.5**, bottom; blue line), a single and exceedingly broad Hg-peak eluted in the inclusion volume in each case, which had a nearly identical retention time as the Hg-peak detected when a solution that contained equimolar CH_3Hg^+ and hCys was analyzed (**Figure 4.4B**, red line). This finding implies that all CH_3Hg^+ was mobilized from RSA at this comparatively low Cys/hCys concentration. To obtain direct experimental evidence for the formation of CH_3Hg-SMW thiol complexes, the aforementioned experiment (**Figure 4.5**, bottom; blue line) was repeated with 50 mM Tris-buffer (50 µM hCys) as the mobile phase and the collected Hg-containing fraction (t_r = 721 ± 1 s) was analyzed by ESI-MS. As is evident from the obtained ESI-MS spectra (**Figure 4.6)**, a CH_3Hg-hCys complex was detected by its m/z ratio and the close match between the observed and the calculated Hg-isotope pattern. These results unequivocally confirm that the CH_3Hg-hCys complex was formed on the column at near physiological conditions.

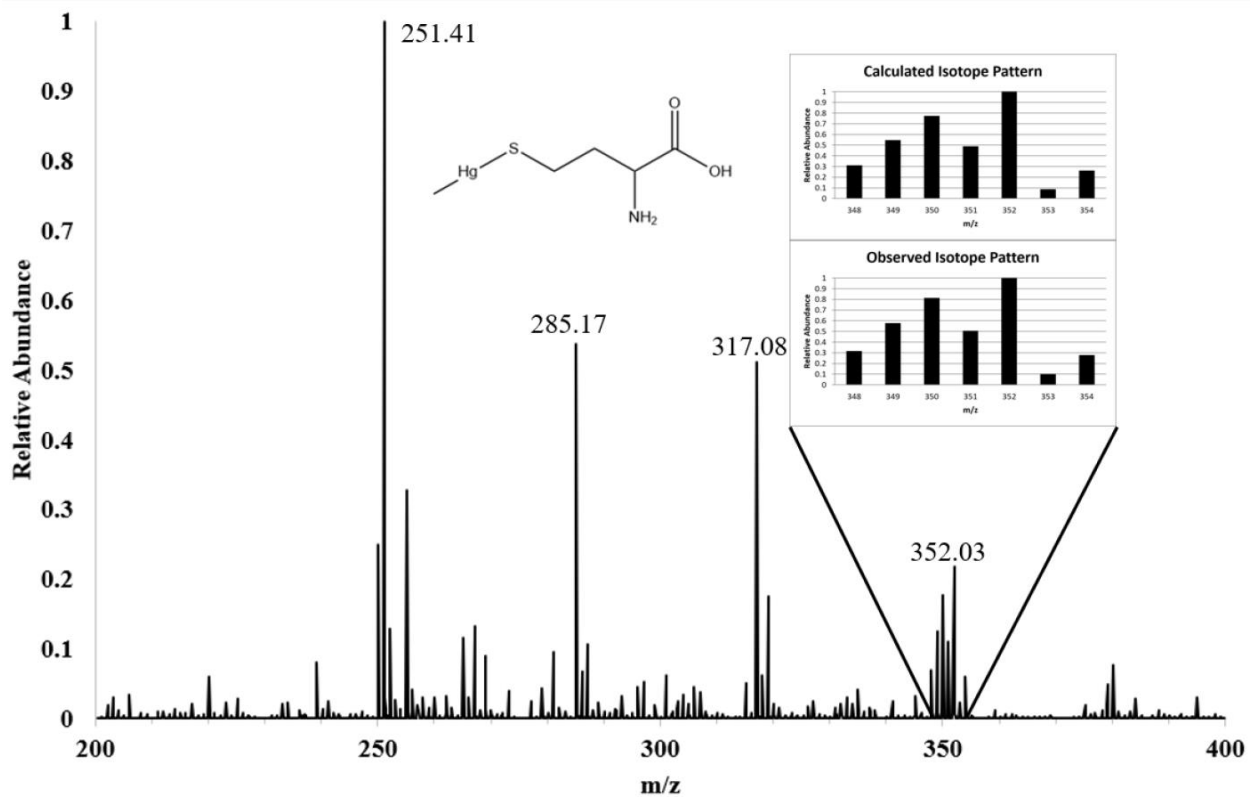

Figure 4.6: ESI-MS identification of the Hg-species that eluted in the SMW range after the analysis of a CH_3Hg-spiked RSA solution by SEC-ICP-AES using 50 mM Tris-buffer (pH 7.4, 50 µM hCys) as the mobile phase.

In contrast to these results, the analysis of the CH_3Hg-RSA complex with a mobile phase that contained 50 µM of GSH produced two Hg-peaks (t_r = 671 ± 1 and 713 ± 1 s) that were not baseline separated. The first Hg-peak had the same retention time as the Hg-peak that was detected when CH_3Hg^+-spiked rabbit plasma was analyzed with a 300 µM GSH mobile phase (**Figure 4.5**, top, blue line), while the second Hg-peak had a retention time that aligned with the Hg-shoulder. These results are somewhat surprising since GSH has been shown to form a 1:1 complex with CH_3Hg^+ that is excreted from the liver to the bile.[118, 177] The formation of two Hg-peaks may be attributed to the formation of multiple coordinate species of CH_3Hg^+ (e.g., CH_3Hg-GS or CH_3Hg-$(GS)_2$ much like the formation of GS_2Hg and GS_3Hg species, which have demonstrated to exist in aqueous solution.[178]

The observed mobilization of CH_3Hg^+ from RSA by 50 µM SMW thiols in the mobile phase can also be rationalized based on the fact that the CH_3Hg-S bond in thiols (i.e., CH_3Hg-RSA and CH_3Hg-hCys) is thermodynamically stable, but kinetically labile.[28, 118] As a RSA-CH_3Hg^+ complex travels through the column it will encounter hCys molecules and the CH_3Hg^+, even though it is bound to RSA, will statistically interact with hCys molecules and form a CH_3Hg-hCys complex for a small fraction of time.[174, 175] If this event unfolds in the vicinity of the BBB, which contains the LAT-1 and LAT-2 transporters, the CH_3Hg^+ cargo can then be translocated into the brain. Although a new, previously uncharacterized ligand binding site has been identified in RSA, the overall similarity of the amino acid sequence between RSA and human serum albumin (HSA)[179] suggests that these results are of relevance to humans.

Taken together, these results allow us to propose a model which describes the biochemical events that unfold in rabbit plasma after CH_3Hg^+ enters the bloodstream and its translocation to the BBB for uptake into the brain (**Figure 4.7**). In brief, the ingestion of CH_3Hg^+-containing fish, such as tuna or swordfish will result in the absorption of a CH_3Hg-Cys complex either from the stomach and/or the GI-tract into the bloodstream, where it will readily react with RSA to form a CH_3Hg-RSA complex (**Figure 4.4B**).[180] Since CH_3Hg^+ is likely bound to Cys-34 in a crevice of RSA, it does not appear feasible that this CH_3Hg-RSA complex is able to donate CH_3Hg^+ to the LAT-1 and LAT-2 transporter located at the BBB to mediate its uptake into the brain.[181] The above results provide direct experimental evidence that 50 µm of Cys and hCys can mobilize CH_3Hg^+ from RSA contained in rabbit plasma and from pure RSA at near physiological conditions, which supports previous *in vivo* studies that have shown SMW thiols to play an important role in the distribution of this neurotoxin to organs in mammals.[127] Therefore, it appears feasible that CH_3Hg-Cys and/or CH_3Hg-hCys species are implicated in the translocation of CH_3Hg^+ across the BBB by

known amino acid transporters, namely the LAT-1 and the LAT-2 transporter.[128, 182, 183] One limitation of our approach is that it is not feasible to prepare mobile phases which contain a thiol below 50 µM owing to the rapid oxidation of these SMW thiols at neutral pH, which could render the free thiol concentration effectively zero.[184]

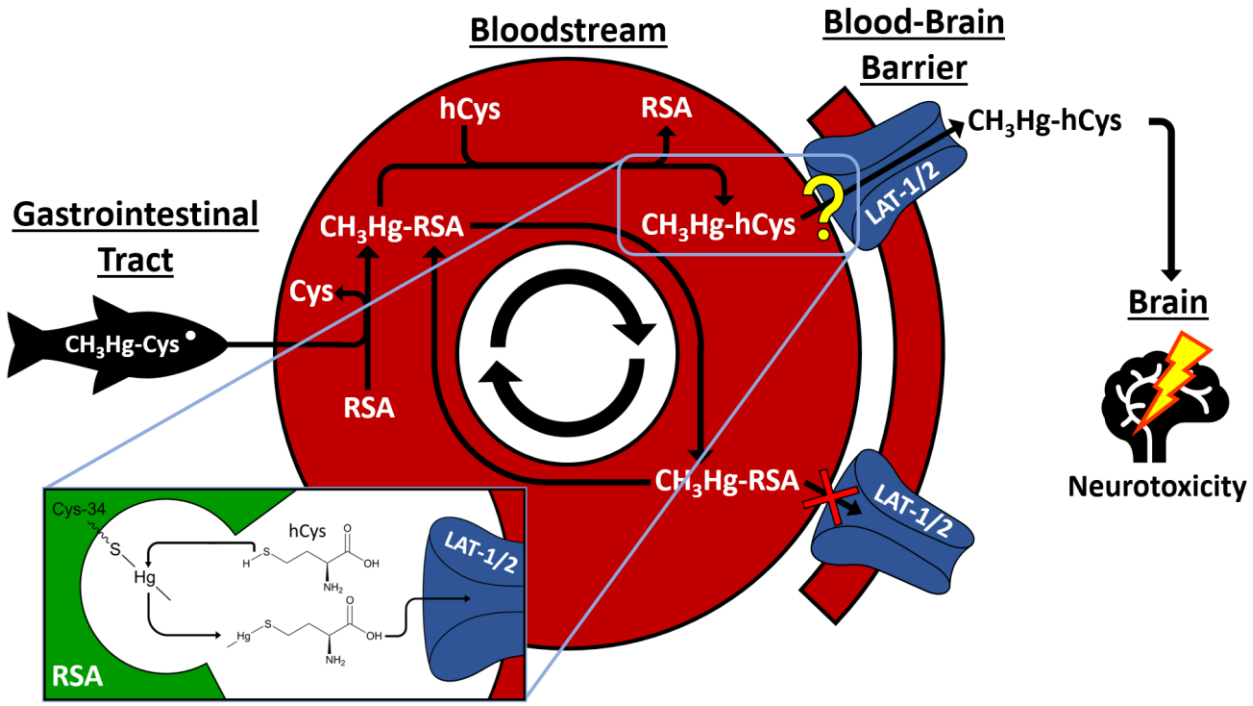

Figure 4.7: Model which depicts the delivery of CH_3Hg^+ after its absorption from the GI-tract into the bloodstream to the brain. The proposed location of the CH_3Hg^+ binding site is in a crevice on RSA precludes the direct delivery of the toxic cargo to the mechanisms which mediate its uptake across the blood-brain barrier (BBB) into the brain. The kinetic instability of CH_3Hg-thiol bonds suggests that in the presence of sufficient plasma concentrations of Cys and/or hCys, CH_3Hg^+ forms complexes with these small molecular weight thiols which are substrates for its translocation into the brain. Modified from Bridle et al. (2021).[157]

In light of the known association between elevated plasma concentrations of Cys and hCys and the development of neurotoxicity in humans, one needs to consider the possibility that these particular SMW thiols can critically modulate the metabolism of CH_3Hg^+ in these individuals in a manner that makes them more susceptible to the neurotoxic effects of this and possibly other toxic metals, such as cadmium.[169, 185] Considering that a significant fraction of the population is chronically exposed to CH_3Hg^+ via the diet and that there is a considerable delay before the onset

of adverse effects in humans, further studies are warranted to better understand the mechanism which orchestrate the translocation of this neurotoxin from the bloodstream to the brain.[186] It will be necessary to identify and structurally characterize all CH_3Hg-SMW thiol complexes which are substrates for the transporters that mediate their uptake into the brain and to better understand the interaction of CH_3Hg^+ with dietary Se compounds in the bloodstream as the latter represent detoxification mechanisms that may reduce the amount that reaches the brain.[187] In addition, the design of studies to directly observe the uptake of specific CH_3Hg-complexes into cells and or tissues slices represents a valuable challenge that metallomics researchers may address in the future.

4.3 Conclusion

The bioinorganic chemistry of toxic metal species that unfolds in the bloodstream fundamentally determines if and how much of any given toxin will reach specific toxicological target organs and is, therefore, directly implicated in the development organ-based toxic effects in mammals.[42, 188] To probe the bioinorganic processes of CH_3Hg^+ that unfold in blood plasma, a metallomics tool has been applied to study its binding in rabbit plasma and to investigate the effects of SMW sulfur compounds on the binding of CH_3Hg^+ to the major plasma protein, which was identified as RSA. The fact that a synthetic CH_3Hg-hCys complex readily donated its CH_3Hg-moiety to RSA in rabbit plasma implied Cys-34 as the binding site. Since a Met-containing mobile phase did not mobilize CH_3Hg^+ from RSA, but Cys and GSH-containing mobile phases did, revealed that its abstraction is driven by thiols. Since 50 µM Cys, hCys and GSH effectively mobilized CH_3Hg^+ from pure RSA and the same concentration of hCys mobilized CH_3Hg^+ from RSA in rabbit plasma suggests, the formed CH_3Hg-SMW thiol complexes can be delivered to the uptake mechanisms which are located at the BBB and translocate CH_3Hg^+ into the brain. ESI-MS

analysis of the CH_3Hg-containing species that eluted in the SMW elution range when 50 µM hCys was present in the mobile phase unequivocally identified a CH_3Hg-hCys complex. These studies are the first of their kind to systematically explore the effect of relevant SMW thiols on the stability of a CH_3Hg-RSA complex in blood plasma at near physiological conditions and represent an important first step to uncover the biochemical mechanisms which link human CH_3Hg^+ exposure to its neurotoxicity.

Chapter 5: Conclusions

5.1 Thesis Conclusion

The anthropogenic mobilization of toxic metal and metalloid species from the Earth's crust (e.g., via mining and the burning of fossil fuels) and consequent chronic human exposure may be related to the etiology of more human diseases than are currently understood. To push industrial and environmental policy towards the stricter regulation and restriction of the release of toxic species into the environment, the underlying biochemical mechanisms by which these species contribute to the development of disease and adverse health effects need to be determined. Carefully planned and executed science is critical to convince policy makers and inform the public as to the dangers of pollution. Additionally, human exposure is not limited to one toxic metal species at a time, and the synergistic or antagonistic effects of concomitant exposure is incompletely understood. Therefore, appropriate analytical tools need to be used to accurately investigate the effects of chronic metal exposure on human health. Gaining insight into the bioinorganic chemistry of toxic metal and metalloid species will place another stone on the bridge to possibly linking exposure and disease. To this end, I have developed a SEC-ICP-AES method for the analysis of mammalian blood plasma for endogenous metalloproteins and applied it to probe exogenous metal species (e.g., methylmercury) as to their binding to endogenous plasma proteins.

Chapter 3 summarizes the development of this method, which includes the optimization of various parameters (sample filtration/dilution, chromatographic flow-rate, etc.) and it was determined that the filtration (0.45 µm pore size syringe filter) of mammalian blood plasma prior to separation on an SEC column was crucial to maintain the performance of the column over repeated injections. The separation performance of a Superdex 200 Increase SEC column (GE

Healthcare, Piscataway, NJ, USA) was compared to a newly obtained SRT-10C SEC column (Sepax Technologies Inc., Newark, DE, USA) for the analysis of mammalian blood plasma for metalloproteins. It was determined that the SRT-10C SEC column afforded essentially the same peak resolution as the Superdex 200 Increase SEC column, but it half the analysis time, at a reduced cost, and with higher peak intensities improving sample throughput significantly. The 1:1 dilution of blood plasma with PBS removed significant tailing and undesirable peak shoulders from the chromatograms. The BCA assay was employed to demonstrate that minimal irreversible binding of proteins to the stationary phase of the SRT-10C SEC column occurred.

In **Chapter 4**, the developed SEC-ICP-AES method was applied to the analysis of human and rabbit plasma that had been spiked with CH_3Hg^+ where it was observed that CH_3Hg^+ bound to serum albumin in both plasma types. A synthetic CH_3Hg-hCys species, when added to rabbit plasma readily donated the CH_3Hg^+ moiety to rabbit serum albumin (RSA). Given that the thiol-containing Cys-34 in the amino acid sequence of this protein is conserved between rabbit and human serum albumin, it is likely that this is the binding site for CH_3Hg^+. The introduction of physiologically relevant concentrations of SMW thiols (Cys, hCys, and GSH) to the PBS mobile phase resulted in the mobilization of CH_3Hg^+ from RSA in plasma and its elution in the SMW range, whereas a 300 µM Met-containing mobile did not mobilize CH_3Hg^+ from RSA suggesting that the abstraction from RSA is facilitated by reduced thiol groups. In a solution of pure RSA in PBS, 50 µM Cys, hCys, and GSH also mobilized CH_3Hg^+ from RSA in a very similar way to rabbit blood plasma. I have found evidence of the formation of SMW-CH_3Hg^+ species under near-physiological conditions that may be critically involved in the translocation of CH_3Hg^+ from blood plasma to the brain.

5.2 Future Work

Within the scope of this work there are two research directions that can be further explored. Since the developed method was successful in probing the bioinorganic chemistry of CH_3Hg^+ in blood plasma, it is feasible that similar experiments can be performed with other toxic metal and metalloid species. For example, manganese (e.g., Mn^{2+} in $MnCl_2$ dust) is a known mammalian neurotoxin, the occupational inhalation of which has been associated with high levels of Mn in the brain leading to the development of Parkinson's Disease-like symptoms. However, the mechanisms of translocation of Mn^{2+} from the bloodstream to the brain is not fully understood. By investigating the bioinorganic chemistry of Mn^{2+} in blood plasma, it is possible to elucidate the details of the mechanism that are involved in translocation to the brain and other target organs. Similarly, cerebrospinal fluid may be analyzed by this method to gain insight into the bioinorganic chemistry of toxic metals (e.g., CH_3Hg^+, Mn^{2+}, Pb^{2+} etc.) on the other side of the BBB and their involvement in disease processes by investigating to which proteins these metals may be bound to. The complimentary nature of the information gained in both blood and cerebrospinal fluid could then help to gain a more complete understanding of the mechanisms of toxic metal species translocation and neurotoxicity. Since the oxidation state of a given metal or metalloid is a determining factor in its toxicity (e.g., the LD_{50} of Cr^{III} is ~300 times larger that Cr^{VI}) the application of the developed method to study the binding of Mn^{2+} to plasma proteins in plasma would require the determination of the oxidation state of the metal during the experiment. Therefore, X-ray Absorption Near Edge Structure (XANES) spectroscopy could be employed to observe changes in the oxidation state of the metal in such experiments that may provide insight into the translocation of these toxic metal species to target organs.

References

1. Cordain, L.; Eaton, S. B.; Sebastian, A.; Mann, N.; Lindeberg, S.; Watkins, B. A.; O'Keefe, J. H.; Brand-Miller, J., Origins and evolution of the Western diet: health implications for the 21st century. *Am. J. Clin. Nutr.* **2005,** *81* (2), 341-54.
2. Mertz, W., The essential trace elements. *Science* **1981,** *213* (4514), 1332-8.
3. Best, C.; Neufingerl, N.; Del Rosso, J. M.; Transler, C.; van den Briel, T.; Osendarp, S., Can multi-micronutrient food fortification improve the micronutrient status, growth, health, and cognition of schoolchildren? A systematic review. *Nutr. Rev.* **2011,** *69* (4), 186-204.
4. Lewis, M. J., Alcoholism and nutrition: a review of vitamin supplementation and treatment. *Curr. Opin. Clin. Nutr. Metab. Care* **2020,** *23* (2), 138-144.
5. *Dietary Reference Intakes for Vitamin A, Vitamin K, Arsenic, Boron, Chromium, Copper, Iodine, Iron, Manganese, Molybdenum, Nickel, Silicon, Vanadium, and Zinc*. National Academies Press (US) Copyright 2001 by the National Academy of Sciences. All rights reserved.: Washington (DC), 2001.
6. Khan, M. U.; Patel, A. G.; Wilbur, S. L.; Khan, I. A., Electrocardiographic changes in combined electrolyte depletion. *Int. J. Cardiol.* **2007,** *116* (2), 276-8.
7. Hosseiniyan Khatibi, S. M.; Zununi Vahed, F.; Sharifi, S.; Ardalan, M.; Mohajel Shoja, M.; Zununi Vahed, S., Osmolytes resist against harsh osmolarity: Something old something new. *Biochimie* **2019,** *158*, 156-164.
8. Vormann, J., Magnesium and Kidney Health - More on the 'Forgotten Electrolyte'. *Am. J. Nephrol.* **2016,** *44* (5), 379-380.
9. Kraft, M. D., Phosphorus and calcium: a review for the adult nutrition support clinician. *Nutr. Clin. Pract.* **2015,** *30* (1), 21-33.
10. Tainer, J. A.; Roberts, V. A.; Getzoff, E. D., Metal-binding sites in proteins. *Curr. Opin. Biotechnol.* **1991,** *2* (4), 582-91.
11. Bren, K. L.; Pecoraro, V. L.; Gray, H. B., Metalloprotein folding. *Inorg. Chem.* **2004,** *43* (25), 7894-6.
12. Mounicou, S.; Szpunar, J.; Lobinski, R., Metallomics: the concept and methodology. *Chem. Soc. Rev.* **2009,** *38* (4), 1119-38.
13. McCord, J. M.; Fridovich, I., Superoxide dismutase. An enzymic function for erythrocuprein (hemocuprein). *J. Biol. Chem.* **1969,** *244* (22), 6049-55.
14. Zelko, I. N.; Mariani, T. J.; Folz, R. J., Superoxide dismutase multigene family: a comparison of the CuZn-SOD (SOD1), Mn-SOD (SOD2), and EC-SOD (SOD3) gene structures, evolution, and expression. *Free Radical Biol. Med.* **2002,** *33* (3), 337-49.
15. Gammella, E.; Buratti, P.; Cairo, G.; Recalcati, S., The transferrin receptor: the cellular iron gate. *Metallomics* **2017,** *9* (10), 1367-1375.
16. Puig, S.; Ramos-Alonso, L.; Romero, A. M.; Martinez-Pastor, M. T., The elemental role of iron in DNA synthesis and repair. *Metallomics* **2017,** *9* (11), 1483-1500.
17. Zhang, C., Essential functions of iron-requiring proteins in DNA replication, repair and cell cycle control. *Protein Cell* **2014,** *5* (10), 750-60.
18. Carmona, F.; Palacios, O.; Galvez, N.; Cuesta, R.; Atrian, S.; Capdevila, M.; Dominguez-Vera, J. M., Ferritin iron uptake and release in the presence of metals and metalloproteins: Chemical implications in the brain. *Coord. Chem. Rev.* **2013,** *257* (19-20), 2752-2764.
19. Gailer, J., Arsenic-selenium and mercury-selenium bonds in biology. *Coord. Chem. Rev.* **2007,** *251* (1-2), 234-254.

20. Gailer, J., Probing the bioinorganic chemistry of toxic metals in the mammalian bloodstream to advance human health. *J. Inorg. Biochem.* **2012,** *108*, 128-32.
21. Pfeiffer, R. F., Wilson's Disease. *Semin. Neurol.* **2007,** *27* (2), 123-32.
22. Ala, A.; Walker, A. P.; Ashkan, K.; Dooley, J. S.; Schilsky, M. L., Wilson's disease. *Lancet* **2007,** *369* (9559), 397-408.
23. Jurowski, K.; Szewczyk, B.; Nowak, G.; Piekoszewski, W., Biological consequences of zinc deficiency in the pathomechanisms of selected diseases. *J. Biol. Inorg. Chem.* **2014,** *19* (7), 1069-79.
24. Xu, Y.; Xiao, G.; Liu, L.; Lang, M., Zinc transporters in Alzheimer's disease. *Mol. Brain* **2019,** *12* (1), 106.
25. Broussard, L. A.; Hammett-Stabler, C. A.; Winecker, R. E.; Ropero-Miller, J. D., The toxicology of mercury. *Lab. Med.* **2002,** *33* (8), 614-625.
26. Timbrell, J. A., *Principles of Biochemical Toxicology*. Taylor & Francis Group: New York, UNITED STATES, 2008.
27. Clarkson, T. W., The three modern faces of mercury. *Environ. Health Perspect.* **2002,** *110 Suppl 1*, 11-23.
28. Nogara, P. A.; Oliveira, C. S.; Schmitz, G. L.; Piquini, P. C.; Farina, M.; Aschner, M.; Rocha, J. B. T., Methylmercury's chemistry: From the environment to the mammalian brain. *Biochim. Biophys. Acta, Gen. Subj.* **2019,** *1863* (12), 129284.
29. Zahir, F.; Rizwi, S. J.; Haq, S. K.; Khan, R. H., Low dose mercury toxicity and human health. *Environ. Toxicol. Pharmacol.* **2005,** *20* (2), 351-60.
30. Johansson, C.; Castoldi, A. F.; Onishchenko, N.; Manzo, L.; Vahter, M.; Ceccatelli, S., Neurobehavioural and molecular changes induced by methylmercury exposure during development. *Neurotoxic. Res.* **2007,** *11* (3-4), 241-60.
31. Martinez-Finley, E. J.; Chakraborty, S.; Fretham, S.; Aschner, M., Admit One: How Essential and Nonessential Metals Gain Entrance into the Cell. *Metallomics* **2012**, 593-605.
32. Gailer, J., Chronic toxicity of As(III) in mammals: the role of (GS)(2)AsSe(-). *Biochimie* **2009,** *91* (10), 1268-72.
33. Ponomarenko, O.; La Porte, P. F.; Singh, S. P.; Langan, G.; Fleming, D. E. B.; Spallholz, J. E.; Alauddin, M.; Ahsan, H.; Ahmed, S.; Gailer, J.; George, G. N.; Pickering, I. J., Selenium-mediated arsenic excretion in mammals: a synchrotron-based study of whole-body distribution and tissue-specific chemistry. *Metallomics* **2017,** *9* (11), 1585-1595.
34. Pei, K. L.; Gailer, J., Probing the interaction of arsenobetaine with blood plasma constituents in vitro: an SEC-ICP-AES study. *Metallomics* **2009,** *1* (5), 403-8.
35. Jarup, L.; Akesson, A., Current status of cadmium as an environmental health problem. *Toxicol. Appl. Pharmacol.* **2009,** *238* (3), 201-8.
36. Bridges, C. C.; Zalups, R. K., Molecular and ionic mimicry and the transport of toxic metals. *Toxicol. Appl. Pharmacol.* **2005,** *204* (3), 274-308.
37. Namdarghanbari, M. A.; Bertling, J.; Krezoski, S.; Petering, D. H., Toxic metal proteomics: reaction of the mammalian zinc proteome with Cd(2)(+). *J. Inorg. Biochem.* **2014,** *136*, 115-21.
38. Gailer, J., Reactive selenium metabolites as targets of toxic metals/metalloids in mammals: a molecular toxicological perspective. *Appl. Organomet. Chem.* **2002,** *16* (12), 701-707.
39. Roman, M.; Jitaru, P.; Barbante, C., Selenium biochemistry and its role for human health. *Metallomics* **2014,** *6* (1), 25-54.

40. Gailer, J.; George, G. N.; Pickering, I. J.; Prince, R. C.; Ringwald, S. C.; Pemberton, J. E.; Glass, R. S.; Younis, H. S.; DeYoung, D. W.; Aposhian, H. V., A metabolic link between arsenite and selenite: The seleno-bis(S-glutathionyl) arsinium ion. *J. Am. Chem. Soc.* **2000,** *122* (19), 4637-4639.
41. Manley, S. A.; George, G. N.; Pickering, I. J.; Glass, R. S.; Prenner, E. J.; Yamdagni, R.; Wu, Q.; Gailer, J., The seleno bis(S-glutathionyl) arsinium ion is assembled in erythrocyte lysate. *Chem. Res. Toxicol.* **2006,** *19* (4), 601-7.
42. Sarpong-Kumankomah, S.; Gibson, M. A.; Gailer, J., Organ damage by toxic metals is critically determined by the bloodstream. *Coord. Chem. Rev.* **2018,** *374*, 376-386.
43. Haraguchi, H., Metallomics: the history over the last decade and a future outlook. *Metallomics* **2017,** *9* (8), 1001-1013.
44. Haraguchi, H., Metallomics as integrated biometal science. *J. Anal. At. Spectrom.* **2004,** *19* (1), 5-14.
45. Williams, R. J. P., Chemical selection of elements by cells. *Coord. Chem. Rev.* **2001,** *216*, 583-595.
46. Szpunar, J., Metallomics: a new frontier in analytical chemistry. *Anal. Bioanal. Chem.* **2004,** *378* (1), 54-6.
47. Haraguchi, H., Papers based on presentations at the International Symposium on Metallomics 2007 (ISM 2007), 28 November-1 December 2007, Nagoya, Japan Preface. *Pure Appl Chem* **2008,** *80* (12), Iv-Iv.
48. Montes-Bayon, M.; Bettmer, J., 4th International Symposium on Metallomics, 2013. *Metallomics* **2014,** *6* (2), 187-8.
49. Caruso, J. A., 2009 International Symposium on Metallomics. *Metallomics* **2010,** *2* (2), 103.
50. Multiple, A., Fifth International Symposium on Metallomics 2015. *Metallomics* **2016,** *8* (7), 641-643.
51. Sperling, M., The Third International Symposium on Metallomics 2011. *Metallomics* **2011,** *3* (12), 1263-4.
52. The scope of Metallomics. *Metallomics* **2016,** *8* (1), 8.
53. Dey, K. K.; Wang, H.; Niu, M.; Bai, B.; Wang, X.; Li, Y.; Cho, J. H.; Tan, H.; Mishra, A.; High, A. A.; Chen, P. C.; Wu, Z.; Beach, T. G.; Peng, J., Deep undepleted human serum proteome profiling toward biomarker discovery for Alzheimer's disease. *Clin. Proteomics* **2019,** *16*, 16.
54. Anderson, N. L.; Anderson, N. G., The human plasma proteome: history, character, and diagnostic prospects. *Mol. Cell. Proteomics* **2002,** *1* (11), 845-67.
55. Tortorella, S.; Karagiannis, T. C., Transferrin receptor-mediated endocytosis: a useful target for cancer therapy. *J. Membr. Biol.* **2014,** *247* (4), 291-307.
56. Chebotareva, N. A.; Kurganov, B. I.; Livanova, N. B., Biochemical effects of molecular crowding. *Biochemistry* **2004,** *69* (11), 1239-51.
57. Verma, P. K.; Kundu, A.; Cho, M., How Molecular Crowding Differs from Macromolecular Crowding: A Femtosecond Mid-Infrared Pump-Probe Study. *J. Phys. Chem. Lett.* **2018,** *9* (22), 6584-6592.
58. Miyoshi, D.; Sugimoto, N., Molecular crowding effects on structure and stability of DNA. *Biochimie* **2008,** *90* (7), 1040-51.

59. Magyar, J. S.; Godwin, H. A., Spectropotentiometric analysis of metal binding to structural zinc-binding sites: accounting quantitatively for pH and metal ion buffering effects. *Anal. Biochem.* **2003,** *320* (1), 39-54.
60. Manley, S. A.; Byrns, S.; Lyon, A. W.; Brown, P.; Gailer, J., Simultaneous Cu-, Fe-, and Zn-specific detection of metalloproteins contained in rabbit plasma by size-exclusion chromatography-inductively coupled plasma atomic emission spectroscopy. *J. Biol. Inorg. Chem.* **2009,** *14* (1), 61-74.
61. Manley, S. A.; Gailer, J., Analysis of the plasma metalloproteome by SEC-ICP-AES: bridging proteomics and metabolomics. *Expert Rev. Proteomics* **2009,** *6* (3), 251-65.
62. Barri, T.; Dragsted, L. O., UPLC-ESI-QTOF/MS and multivariate data analysis for blood plasma and serum metabolomics: effect of experimental artefacts and anticoagulant. *Anal. Chim. Acta* **2013,** *768*, 118-28.
63. Tsiang, M.; Jain, A. K.; Gibbs, C. S., Functional requirements for inhibition of thrombin by antithrombin III in the presence and absence of heparin. *J. Biol. Chem.* **1997,** *272* (18), 12024-9.
64. Jahromi, E. Z.; Gailer, J., Improved selectivity of ZnNa3DTPA vs. Na5DTPA to abstract Cd2+ from plasma proteins in vitro. *Metallomics* **2013,** *5* (6), 615-8.
65. Sooriyaarachchi, M.; Gailer, J., Removal of Fe3+ and Zn2+ from plasma metalloproteins by iron chelating therapeutics depicted with SEC-ICP-AES. *Dalton Trans.* **2010,** *39* (32), 7466-73.
66. Rai, A. J.; Gelfand, C. A.; Haywood, B. C.; Warunek, D. J.; Yi, J.; Schuchard, M. D.; Mehigh, R. J.; Cockrill, S. L.; Scott, G. B.; Tammen, H.; Schulz-Knappe, P.; Speicher, D. W.; Vitzthum, F.; Haab, B. B.; Siest, G.; Chan, D. W., HUPO Plasma Proteome Project specimen collection and handling: towards the standardization of parameters for plasma proteome samples. *Proteomics* **2005,** *5* (13), 3262-77.
67. Gómez-Ariza, J. L.; Jahromi, E. Z.; González-Fernández, M.; García-Barrera, T.; Gailer, J., Liquid chromatography-inductively coupled plasma-based metallomic approaches to probe health-relevant interactions between xenobiotics and mammalian organisms. In *Metallomics*, 2011; Vol. 3, pp 566-577.
68. Deng, J.; Davies, D. R.; Wisedchaisri, G.; Wu, M.; Hol, W. G.; Mehlin, C., An improved protocol for rapid freezing of protein samples for long-term storage. *Acta Crystallogr., Sect. D: Biol. Crystallogr.* **2004,** *60* (Pt 1), 203-4.
69. Tyler, G.; Yvon, J., ICP Optical Emission Specroscopy Technical Note 05: ICP-OES , ICP-MS and AAS Techniques Compared. Longjumeau, France, 2012; pp 1-11.
70. Cao, E.; Chen, Y.; Cui, Z.; Foster, P. R., Effect of freezing and thawing rates on denaturation of proteins in aqueous solutions. *Biotechnol. Bioeng.* **2003,** *82* (6), 684-90.
71. Jahromi, E. Z.; White, W.; Wu, Q.; Yamdagni, R.; Gailer, J., Remarkable effect of mobile phase buffer on the SEC-ICP-AES derived Cu, Fe and Zn-metalloproteome pattern of rabbit blood plasma. *Metallomics* **2010,** *2* (7), 460-8.
72. Van den Bergh, G.; Arckens, L., Recent advances in 2D electrophoresis: an array of possibilities. *Expert Rev. Proteomics* **2005,** *2* (2), 243-52.
73. Becker, J. S.; Lobinski, R.; Becker, J. S., Metal imaging in non-denaturating 2D electrophoresis gels by laser ablation inductively coupled plasma mass spectrometry (LA-ICP-MS) for the detection of metalloproteins. *Metallomics* **2009,** *1* (4), 312-6.
74. Lee, Y. R.; Li, X.; Ma, W.; Row, K. H., Retention of Large Biological Molecules by Size-Exclusion Chromatography. *Anal. Lett.* **2016,** *50* (6), 905-915.

75. Berek, D., Size exclusion chromatography--a blessing and a curse of science and technology of synthetic polymers. *J. Sep. Sci.* **2010,** *33* (3), 315-35.
76. Kannamkumarath, S. S.; Wrobel, K.; Wrobel, K.; B'Hymer, C.; Caruso, J. A., Capillary electrophoresis-inductively coupled plasma-mass spectrometry: an attractive complementary technique for elemental speciation analysis. *J. Chromatogr. A.* **2002,** *975* (2), 245-66.
77. Montes-Bayon, M.; Profrock, D.; Sanz-Medel, A.; Prange, A., Direct comparison of capillary electrophoresis and capillary liquid chromatography hyphenated to collision-cell inductively coupled plasma mass spectrometry for the investigation of Cd-, Cu- and Zn-containing metalloproteins. *J. Chromatogr. A.* **2006,** *1114* (1), 138-44.
78. Szpunar, J., Advances in analytical methodology for bioinorganic speciation analysis: metallomics, metalloproteomics and heteroatom-tagged proteomics and metabolomics. *Analyst (Cambridge, U. K.)* **2005,** *130* (4), 442-65.
79. Plantz, M. R.; Fritz, J. S.; Smith, F. G.; Houk, R. S., Separation of Trace-Metal Complexes for Analysis of Samples of High Salt Content by Inductively Coupled Plasma Mass-Spectrometry. *Anal. Chem.* **1989,** *61* (2), 149-153.
80. Sarpong-Kumankomah, S.; Gailer, J., Identification of a haptoglobin-hemoglobin complex in human blood plasma. *J. Inorg. Biochem.* **2019,** *201*, 110802.
81. Macintyre, G.; Gutfreund, K. S.; Martin, W. R.; Camicioli, R.; Cox, D. W., Value of an enzymatic assay for the determination of serum ceruloplasmin. *J. Lab. Clin. Med.* **2004,** *144* (6), 294-301.
82. Linder, M. C., Ceruloplasmin and other copper binding components of blood plasma and their functions: an update. *Metallomics* **2016,** *8* (9), 887-905.
83. Ward, G.; Simpson, A.; Boscato, L.; Hickman, P. E., The investigation of interferences in immunoassay. *Clin. Biochem.* **2017,** *50* (18), 1306-1311.
84. Sarpong-Kumankomah, S.; Miller, K.; Gailer, J., Biological Chemsitry of Toxic Metals and Metalloids, Such as Arsenic, Cadmium, and Mercury. In *Encyclopedia of Analytical Chemistry*, John WIley & Sons, Ltd.: 2020.
85. Cid-Barrio, L.; Calderon-Celis, F.; Abasolo-Linares, P.; Fernandez-Sanchez, M. L.; Costa-Fernandez, J. M.; Encinar, J. R.; Sanz-Meder, A., Advances in absolute protein quantification and quantitative protein mapping using ICP-MS. *Trac-Trend Anal Chem* **2018,** *104*, 148-159.
86. Yano, J.; Yachandra, V. K., X-ray absorption spectroscopy. *Photosynth. Res.* **2009,** *102* (2-3), 241-54.
87. A, N., Air Pollution-Related Illness : Effects of Particles. *Science* **2005,** *308*, 804-806.
88. Rai, S.; Gupta, S.; Mittal, P. C., Dietary Intakes and Health Risk of Toxic and Essential Heavy Metals through the Food Chain in Agricultural, Industrial, and Coal Mining Areas of Northern India. *Hum. Ecol. Risk Assess.* **2014,** *21* (4), 913-933.
89. Kampa, M.; Castanas, E., Human health effects of air pollution. *Environ. Pollut.* **2008,** *151* (2), 362-7.
90. El-Kady, A. A.; Abdel-Wahhab, M. A., Occurrence of trace metals in foodstuffs and their health impact. *Trends Food Sci Tech* **2018,** *75*, 36-45.
91. Landrigan, P. J.; Fuller, R.; Acosta, N. J. R.; Adeyi, O.; Arnold, R.; Basu, N. N.; Balde, A. B.; Bertollini, R.; Bose-O'Reilly, S.; Boufford, J. I.; Breysse, P. N.; Chiles, T.; Mahidol, C.; Coll-Seck, A. M.; Cropper, M. L.; Fobil, J.; Fuster, V.; Greenstone, M.; Haines, A.; Hanrahan, D.; Hunter, D.; Khare, M.; Krupnick, A.; Lanphear, B.; Lohani, B.; Martin, K.; Mathiasen, K. V.; McTeer, M. A.; Murray, C. J. L.; Ndahimananjara, J. D.; Perera, F.; Potocnik, J.; Preker,

A. S.; Ramesh, J.; Rockstrom, J.; Salinas, C.; Samson, L. D.; Sandilya, K.; Sly, P. D.; Smith, K. R.; Steiner, A.; Stewart, R. B.; Suk, W. A.; van Schayck, O. C. P.; Yadama, G. N.; Yumkella, K.; Zhong, M., The Lancet Commission on pollution and health. *Lancet* **2018,** *391* (10119), 462-512.
92. Gimeno-Garcia, E.; Andreu, V.; Boluda, R., Heavy metals incidence in the application of inorganic fertilizers and pesticides to rice farming soils. *Environ. Pollut.* **1996,** *92* (1), 19-25.
93. Timbrell, J., Introduction to Toxicology. **2002**.
94. Osibanjo, O.; Nnorom, I. C.; Adie, G. U.; Ogundiran, M. B.; Adeyi, A. A., Global Management of Electronic Wastes: Challenges Facing Developing and Economy-in-Transition Countries. In *Metal Sustainability: Global Challenges, Consequences and Prospects*, Izatt, R. M., Ed. John Wiley & Sons Ltd.: 2016; pp 52-78.
95. Izatt, R. M.; Hagelüken, C., Recycling and Sustainable Utilization of Precious and Specialty Metals. In *Metal Sustainability: Global Challenges, Consequences and Prospects*, Izatt, R. M., Ed. John Wiley & Sons Ltd.: 2016; pp 1-22.
96. Robinson, B. H., E-waste: an assessment of global production and environmental impacts. *Sci. Total Environ.* **2009,** *408* (2), 183-91.
97. Pacyna, J. M., Monitoring and Assessment of Metal Contaminants in the Air. In *Toxicol. Met.*, Chang, L. W., Ed. CRC Press: 1996; pp 9-28.
98. Mandal, B. K.; Suzuki, K. T., Arsenic round the world: a review. *Talanta* **2002,** *58* (1), 201-35.
99. Zhao, F. J.; Zhu, Y. G.; Meharg, A. A., Methylated arsenic species in rice: geographical variation, origin, and uptake mechanisms. *Environ. Sci. Technol.* **2013,** *47* (9), 3957-66.
100. Houlihan, J.; Brody, C. What's in my baby's food? https://www.healthybabyfood.org/sites/healthybabyfoods.org/files/2020-04/BabyFoodReport_ENGLISH_R6.pdf.
101. Darbre, P. D., Underarm cosmetics and breast cancer. *J. Appl. Toxicol.* **2003,** *23* (2), 89-95.
102. Kandimalla, R.; Vallamkondu, J.; Corgiat, E. B.; Gill, K. D., Understanding Aspects of Aluminum Exposure in Alzheimer's Disease Development. *Brain Pathol.* **2016,** *26* (2), 139-54.
103. Jarup, L., Hazards of heavy metal contamination. *Br. Med. Bull.* **2003,** *68*, 167-82.
104. Guney, M.; Zagury, G. J., Heavy metals in toys and low-cost jewelry: critical review of U.S. and Canadian legislations and recommendations for testing. *Environ. Sci. Technol.* **2012,** *46* (8), 4265-74.
105. Rhind, S. M., Anthropogenic pollutants: a threat to ecosystem sustainability? *Philos. Trans. R. Soc., B* **2009,** *364* (1534), 3391-401.
106. Vasto, S.; Candore, G.; Listi, F.; Balistreri, C. R.; Colonna-Romano, G.; Malavolta, M.; Lio, D.; Nuzzo, D.; Mocchegiani, E.; Di Bona, D.; Caruso, C., Inflammation, genes and zinc in Alzheimer's disease. *Brain Res. Rev.* **2008,** *58* (1), 96-105.
107. Adams, J. B.; Audhya, T.; McDonough-Means, S.; Rubin, R. A.; Quig, D.; Geis, E.; Gehn, E.; Loresto, M.; Mitchell, J.; Atwood, S.; Barnhouse, S.; Lee, W., Toxicological status of children with autism vs. neurotypical children and the association with autism severity. *Biol. Trace. Elem. Res.* **2013,** *151* (2), 171-80.
108. Rossignol, D. A.; Genuis, S. J.; Frye, R. E., Environmental toxicants and autism spectrum disorders: a systematic review. *Transl. Psychiatry* **2014,** *4*, e360.
109. Jahromi, E. Z.; Gailer, J., Probing bioinorganic chemistry processes in the bloodstream to gain new insights into the origin of human diseases. *Dalton Trans.* **2010,** *39* (2), 329-36.

110. Rastogi, S. K., Renal effects of environmental and occupational lead exposure. *Indian J. Occup. Health* **2008,** *12* (3), 103-6.
111. Aneni, E. C.; Escolar, E.; Lamas, G. A., Chronic Toxic Metal Exposure and Cardiovascular Disease: Mechanisms of Risk and Emerging Role of Chelation Therapy. *Curr. Atheroscler. Rep.* **2016,** *18* (12), 81.
112. Ord, M. G.; Stocken, L. A., A contribution to chemical defence in World War II. *Trends Biochem. Sci.* **2000,** *25* (5), 253-6.
113. Nicholson, J. P.; Wolmarans, M. R.; Park, G. R., The role of albumin in critical illness. *Br. J. Anaesth.* **2000,** *85* (4), 599-610.
114. Jomova, K.; Valko, M., Advances in metal-induced oxidative stress and human disease. *Toxicology* **2011,** *283* (2-3), 65-87.
115. Shin, S. Y.; Fauman, E. B.; Petersen, A. K.; Krumsiek, J.; Santos, R.; Huang, J.; Arnold, M.; Erte, I.; Forgetta, V.; Yang, T. P.; Walter, K.; Menni, C.; Chen, L.; Vasquez, L.; Valdes, A. M.; Hyde, C. L.; Wang, V.; Ziemek, D.; Roberts, P.; Xi, L.; Grundberg, E.; Multiple Tissue Human Expression Resource, C.; Waldenberger, M.; Richards, J. B.; Mohney, R. P.; Milburn, M. V.; John, S. L.; Trimmer, J.; Theis, F. J.; Overington, J. P.; Suhre, K.; Brosnan, M. J.; Gieger, C.; Kastenmuller, G.; Spector, T. D.; Soranzo, N., An atlas of genetic influences on human blood metabolites. *Nat. Genet.* **2014,** *46* (6), 543-550.
116. Telu, K. H.; Yan, X.; Wallace, W. E.; Stein, S. E.; Simon-Manso, Y., Analysis of human plasma metabolites across different liquid chromatography/mass spectrometry platforms: Cross-platform transferable chemical signatures. *Rapid Commun. Mass Spectrom.* **2016,** *30* (5), 581-93.
117. Gibson, M. A.; Sarpong-Kumankomah, S.; Nehzati, S.; George, G. N.; Gailer, J., Remarkable differences in the biochemical fate of Cd(2+), Hg(2+), CH3Hg(+) and thimerosal in red blood cell lysate. *Metallomics* **2017,** *9* (8), 1060-1072.
118. Rabenstein, D. L.; Isab, A. A.; Reid, R. S., A proton nuclear magnetic resonance study of the binding of methylmercury in human erythrocytes. *Biochim. Biophys. Acta* **1982,** *720* (1), 53-64.
119. Wu, S.; Powers, S.; Zhu, W.; Hannun, Y. A., Substantial contribution of extrinsic risk factors to cancer development. *Nature* **2016,** *529* (7584), 43-7.
120. Gailer, J.; George, G. N.; Pickering, I. J.; Madden, S.; Prince, R. C.; Yu, E. Y.; Denton, M. B.; Younis, H. S.; Aposhian, H. V., Structural basis of the antagonism between inorganic mercury and selenium in mammals. *Chem. Res. Toxicol.* **2000,** *13* (11), 1135-42.
121. Gailer, J.; Madden, S.; Burke, M. F.; Denton, M. B.; Aposhian, H. V., Simultaneous multielement-specific detection of a novel glutathione-arsenic-selenium ion [(GS)2AsSe]? by ICP AES after micellar size- exclusion chromatography. *Appl. Organomet. Chem.* **2000,** *14* (7), 355-363.
122. Korbas, M.; Percy, A. J.; Gailer, J.; George, G. N., A possible molecular link between the toxicological effects of arsenic, selenium and methylmercury: methylmercury(II) seleno bis(S-glutathionyl) arsenic(III). *J. Biol. Inorg. Chem.* **2008,** *13* (3), 461-70.
123. Bernotiene, R.; Ivanoviene, L.; Sadauskiene, I.; Liekis, A.; Ivanov, L., The effects of cadmium chloride and sodium selenite on protein synthesis in mouse liver. *Environ. Toxicol. Pharmacol.* **2013,** *36* (3), 1261-5.
124. Wiechelman, K. J.; Braun, R. D.; Fitzpatrick, J. D., Investigation of the bicinchoninic acid protein assay: identification of the groups responsible for color formation. *Anal. Biochem.* **1988,** *175* (1), 231-7.

125. Bouchet, S.; Bjoern, E., Analytical developments for the determination of monomethylmercury complexes with low molecular mass thiols by reverse phase liquid chromatography hyphenated to inductively coupled plasma mass spectrometry. *J. Chromatogr. A* **2014,** *1339*, 50-58.
126. Bresson, C.; Lamouroux, C.; Sandre, C.; Tabarant, M.; Gault, N.; Poncy, J. L.; Lefaix, J. L.; Den Auwer, C.; Spezia, R.; Gaigeot, M. P.; Ansoborlo, E.; Mounicou, S.; Fraysse, A.; Deves, G.; Bacquart, T.; Seznec, H.; Pouthier, T.; Moretto, P.; Ortega, R.; Lobinski, R.; Moulin, C., An interdisciplinary approach to investigate the impact of cobalt in a human keratinocyte cell line. *Biochimie* **2006,** *88* (11), 1619-29.
127. Thomas, D. J.; Smith, J. C., Effects of coadministered low-molecular weight thiol compounds on short-term distribution of methylmercury in the rat. *Toxicol. Appl. Pharmacol.* **1982,** *62*, 104-110.
128. Kerper, L. E.; Ballatori, N.; Clarkson, T. W., Methylmercury transport across the blood-brain barrier by an amino acid carrier. *Am. J. Physiol.* **1992,** *262*, R761-R765.
129. Simmons-Willis, T. A.; Koh, A. S.; Clarkson, T. W.; Ballatori, N., Transport of a neurotoxicant by molecualr mimicry: the methylmercury-L-cysteine complex is a substrate for human L-type large neutral amino acid transporter (LAT) 1 and LAT 2. *Biochem. J.* **2002,** *367*, 239-246.
130. Hoffmeyer, R. E.; Singh, S. P.; Doonan, C. J.; Ross, A. R.; Hughes, R. J.; Pickering, I. J.; George, G. N., Molecular mimicry in mercury toxicology. *Chem. Res. Toxicol.* **2006,** *19* (6), 753-9.
131. Medvedev, Y. V.; Ramenskaya, G. V.; Shokhin, I. E.; Yarushok, T. A., HPLC and UPLC for Determining Drugs in Blood (A Review). *Pharm Chem J+* **2013,** *47* (4), 225-230.
132. Majorek, K. A.; Porebski, P. J.; Dayal, A.; Zimmerman, M. D.; Jablonska, K.; Stewart, A. J.; Chruszcz, M.; Minor, W., Structural and immunologic characterization of bovine, horse, and rabbit serum albumins. *Mol. Immunol.* **2012,** *52* (3-4), 174-82.
133. Taborskaya, K. I.; Belinskaya, D. A.; Avdonin, P. V.; Goncharov, N. V., Building a three-dimensional model of rat albumin molecule by homology modeling. *J Evol Biochem Phys+* **2017,** *53* (5), 384-393.
134. Irace, C.; Carallo, C.; Scavelli, F.; Esposito, T.; De Franceschi, M. S.; Tripolino, C.; Gnasso, A., Influence of blood lipids on plasma and blood viscosity. *Clin. Hemorheol. Microcirc.* **2014,** *57* (3), 267-74.
135. Wiederin, D. R. Advances in sample introduction for inductively coupled plasma spectrometry. Iowa State University, Ames, Iowa, 1991.
136. Noble, J. E.; Bailey, M. J. A., Chapter 8 Quantitation of Protein. In *Guide to Protein Purification, 2nd Edition*, 2009; pp 73-95.
137. Wastewater Analysis using the Prodigy High Dispersion ICP. Teledyne Instruments, Leeman Labs.
138. Mallet, C. R.; Lu, Z.; Mazzeo, J. R., A study of ion suppression effects in electrospray ionization from mobile phase additives and solid-phase extracts. *Rapid Commun. Mass Spectrom.* **2004,** *18* (1), 49-58.
139. Zhang, J.; Wang, J.; Hu, J.; Zhao, J.; Li, J.; Cai, X., Associations of total blood mercury and blood methylmercury concentrations with diabetes in adults: An exposure-response analysis of 2005-2018 NHANES. *J. Trace Elem. Med. Biol.* **2021,** *68*, 126845.
140. LOD Tables for Plasma Prodigy (Radial View Plasma). Labs, T. L., Ed. Teledyne Technologies.

141. Yun, Z.; Li, L.; Liu, L.; He, B.; Zhao, X.; Jiang, G., Characterization of mercury-containing protein in human plasma. *Metallomics* **2013,** *5* (7), 821-7.
142. Sheinenzon, A.; Shehadeh, M.; Michelis, R.; Shaoul, E.; Ronen, O., Serum albumin levels and inflammation. *Int. J. Biol. Macromol.* **2021,** *184*, 857-862.
143. Clarkson, T. W., The toxicology of mercury. *Crit. Rev. Clin. Lab. Sci.* **1997,** *34* (4), 369-403.
144. Costa, L. G.; Aschner, M.; Vitalone, A.; Syversen, T.; Soldin, O. P., Developmental neuropathology of environmental agents. *Annu. Rev. Pharmacol. Toxicol.* **2004,** *44*, 87-110.
145. Grandjean, P.; Weihe, P.; White, R. F.; Debes, F.; Araki, S.; Yokoyama, K.; Murata, K.; Sorensen, N.; Dahl, R.; Jorgensen, P. J., Cognitive deficit in 7-year-old children with prenatal exposure to methylmercury. *Neurotoxicol. Teratol.* **1997,** *19* (6), 417-28.
146. Schartup, A. T.; Thackray, C. P.; Qureshi, A.; Dassuncao, C.; Gillespie, K.; Hanke, A.; Sunderland, E. M., Climate change and overfishing increase neurotoxicant in marine predators *Nature* **2019,** *572*, 648-650.
147. Clarkson, T. W.; Magos, L.; Myers, G. J., The toxicology of mercury--current exposures and clinical manifestations. *N. Engl. J. Med.* **2003,** *349* (18), 1731-7.
148. Karimi, R.; Vacchi-Suzzi, C.; Meliker, J. R., Mercury exposure and a shift toward oxidative stress in avid seafood consumers. *Environ. Res.* **2016,** *146*, 100-7.
149. Farina, M.; Rocha, J. B.; Aschner, M., Mechanisms of methylmercury-induced neurotoxicity: evidence from experimental studies. *Life Sci.* **2011,** *89* (15-16), 555-63.
150. Nogara, P. A.; Oliveira, C. S.; Schmitz, G. L.; Piquini, P. C.; Farina, M.; Aschner, M.; Rocha, J. B. T., Methylmercury's chemistry: from the environment to the mammalian brain. *Biochim. Biophys. Acta, General Subjects* **2019,** *1863*, 129284.
151. Gibson, M. A.; Sarpong-Kumankomah, S.; Nehzati, S.; George, G. N.; Gailer, J., Remarkable differences in the biochemical fate of Cd^{2+}, Hg^{2+}, CH_3Hg^+ and thimerosal in red blood cell lysate. *Metallomics* **2017,** *9*, 1060-1072.
152. Ballatori, N.; Truong, A. T., Mechanisms of hepatic methylmercury uptake. *J. Toxicol. Environ. Health* **1995,** *46* (3), 343-53.
153. Mellingen, R. M.; Myrmel, L. S.; Lie, K. K.; Rasinger, J. D.; Madsen, L.; Nostbakken, O. J., RNA sequencing and proteomic profiling reveal different alterations by dietary methylmercury in the hippocampal transcriptome and proteome in BALB/c mice. *Metallomics* **2021,** *13* (5), mfab022.
154. Bjorklund, G.; Tinkov, A. A.; Dadar, M.; Rahman, M. M.; Chirumbolo, S.; Skalny, A. V.; Skalnaya, M. G.; Haley, B. E.; Ajsuvakova, O. P.; Aaseth, J., Insights into the potential role of mercury in Alzheimer's disease. *J. Mol. Neurosci.* **2019,** *67*, 511-533.
155. Chapman, L.; Chan, H. M., The influence of nutrition on methyl mercury intoxication. *Environ. Health Perspect.* **2000,** *108 Suppl 1*, 29-56.
156. Trasande, L.; Liu, Y. H., Reducing The Staggering Costs Of Environmental Disease In Children, Estimated At $76.6 Billion In 2008. *Health Affair* **2011,** *30* (5), 863-870.
157. Bridle, T. G.; Kumarathasan, P.; Gailer, J., Toxic Metal Species and 'Endogenous' Metalloproteins at the Blood-Organ Interface: Analytical and Bioinorganic Aspects. *Molecules* **2021,** *26* (11), 3408.
158. Li, Y.; Yan, X. P.; Chen, C.; Xia, Y. L.; Jiang, Y., Human serum albumin-mercurial species interactions. *J. Proteome. Res.* **2007,** *6* (6), 2277-86.
159. Yasutake, A.; Hirayama, K.; Inoue, M., Interaction of methylmercury compounds with albumin. *Arch. Toxicol.* **1990,** *64* (8), 639-43.

160. Pearson, S. A.; Cowan, J. A., Glutathione-coordinated metal complexes as substrates for cellular transporters. *Metallomics* **2021,** *13* (5), mfab015.
161. Wu, G., Methylmercury-cysteine uptake by rat erythrocytes: Evidence for several transport systems. *J. Appl. Toxicol.* **1996,** *16* (1), 77-83.
162. Rabenstein, D. L.; Reid, R. S.; Isab, A. A., ^{1}H nmr study of effectiveness of various thiols for removal of methylmercury from hemolyzed erythrocytes. *J. Inorg. Biochem.* **1983,** *18*, 241-251.
163. Rabenstein, D. L.; Arnold, A. P.; Guy, R. D., ^{1}H-NMR study of the removal of methylmercury from intact erythrocytes by sulfhydryl compounds. *J. Inorg. Biochem.* **1986,** *28* (2-3), 279-87.
164. Isokawa, M.; Kanamori, T.; Funatsu, T.; Tsunoda, M., Analytical methods involving separation techniques for determination of low-molecular-weight biothiols in human plasma and blood. *J. Chromatogr. B: Anal. Technol. Biomed. Life Sci.* **2014,** *964*, 103-15.
165. Refsvik, T.; Norseth, T., Methyl mercuric compounds in rat bile. *Acta Pharmacol. Toxicol.* **1975,** *36* (1), 67-78.
166. Jahromi, E. Z.; White, W.; Wu, Q.; Yamdagni, R.; Gailer, J., Remarkable effect of mobile phase buffer on the SEC-ICP-AES derived Cu, Fe and Zn-metalloproteome pattern of rabbit blood plasma. *Metallomics* **2010,** *2*, 460-468.
167. Refsum, H.; Ueland, P. M.; Nygard, O.; Vollset, S. E., Homocysteine and cardiovascular disease. *Annu. Rev. Med.* **1998,** *49*, 31-62.
168. Grzych, G.; Douillard, C.; Lannoy, J.; Joncquel Chevalier Curt, M., Very High Plasma Homocysteine without Malnutrition or Inherited Disorder. *Clin Chem* **2020,** *66* (11), 1468-1469.
169. Wang, W.; Rusin, O.; Xu, X.; Kim, K. K.; Escobedo, J. O.; Fakayode, S. O.; Fletcher, K. A.; Lowry, M.; Schowalter, C. M.; Lawrence, C. M.; Fronczek, F. R.; Warner, I. M.; Strongin, R. M., Detection of homocysteine and cysteine. *J. Am. Chem. Soc.* **2005,** *127* (45), 15949-58.
170. Barnett, J. P.; Scanlan, D. J.; Blindauer, C. A., Protein fractionation and detection for metalloproteomics: challenges and approaches. *Anal. Bioanal. Chem.* **2012,** *402*, 3311-3322.
171. Gomez-Ariza, J. L.; Jahromi, E. Z.; Gonzalez-Fernandez, M.; Garcia-Barrera, T.; Gailer, J., Liquid chromatography-inductively coupled plasma-based metallomic approaches to probe health-relevant interactions between xenobiotics and mammalian organisms. *Metallomics* **2011,** *3*, 566-577.
172. Grzych, G.; Douillard, C.; Lannoy, J.; Curt, M. J. C., Very High Plasma Homocysteine without Malnutrition or Inherited Disorder. *Clin. Chem.* **2020,** *66* (11), 1468-1469.
173. Ebdon, L.; Fisher, A., The use of ICP-AES as a detector for elemental speciation studies. In *Elemental Speciation. New approaches for trace element analysis*, Caruso, J. A.; Sutton, K. L.; Ackley, K. L., Eds. Elsevier: Amsterdam, 2000; Vol. XXXIII, pp 227-248.
174. Rabenstein, D. L.; Evans, C. A.; Tourangeau, M. C.; Fairhurst, M. T., Methylmercury Species and Equilibria in Aqueous-Solution. *Anal. Chem.* **1975,** *47* (2), 338-341.
175. Rabenstein, D. L.; Reid, R. S., Nuclear Magnetic-Resonance Studies of the Solution Chemistry of Metal-Complexes. 20. Ligand-Exchange Kinetics of Methylmercury(ii) Thiol Complexes. *Inorg. Chem.* **1984,** *23* (9), 1246-1250.
176. Pei, K. L.; Sooriyaarachchi, M.; Sherrell, D. A.; George, G. N.; Gailer, J., Probing the coordination behavior of Hg2+, CH3Hg+, and Cd2+ towards mixtures of two biological thiols by HPLC-ICP-AES. *J. Inorg. Biochem.* **2011,** *105*, 375-381.

177. Ballatori, N.; Clarkson, T. W., Biliary secretion of glutathione and of glutathione-metal complexes. *Fundam. Appl. Toxicol.* **1985,** *5* (5), 816-31.
178. Cheesman, B. V.; Arnold, A. P.; Rabenstein, D. L., Nuclear magnetic resonance studies on the solution chemistry of metal complexes. 25. $Hg(thiol)_3$ complexes and Hg(II)-thiol ligand exchange kinetics. *J. Am. Chem. Soc.* **1988,** *110*, 6359-6364.
179. Majorek, K. A.; Porebski, P. J.; Zimmerman, M. D.; Jablonska, K.; Stewart, A. J.; Chruszcz, M.; Minor, W., Structural and immunogenic characterization of bovine, horse, and rabbit serum albumins. *Mol. Immunol.* **2012,** *52*, 174-182.
180. Harris, H. H.; Pickering, I. J.; George, G. N., The chemical form of mercury in fish. *Science* **2003,** *301* (5637), 1203.
181. Carter, D. C.; Ho, J. X., Structure of serum albumin. *Adv. Protein Chem.* **1994,** *45*, 153-203.
182. Mokrzan, E. M.; Kerper, L. E.; Ballatori, N.; Clarkson, T. W., Methylmercury-Thiol Uptake into Cultured Brain Capillary Endothelial-Cells on Amino-Acid System-L. *J. Pharmacol. Exp. Ther.* **1995,** *272* (3), 1277-1284.
183. Yin, Z. B.; Jiang, H. Y.; Syversen, T.; Rocha, J.; Farina, M.; Aschner, M., The methylmercury-L-cysteine complex conjugate is a substrate for the L-type large neutral amino acid transporter *J. Neurochem.* **2008,** *107*, 1083-1090.
184. Gailer, J.; Lindner, W., On-column formation of arsenic-glutathione species detected by size-exclusion chromatography in conjunction with arsenic-specific detectors. *J. Chromatogr. B: Biomed. Sci. Appl.* **1998,** *716* (1-2), 83-93.
185. Sagmeister, P.; Gibson, M. A.; McDade, K. H.; Gailer, J., Physiologically relevant plasma D, L-homocysteine concentrations mobilize Cd from human serum albumin. *J. Chromatogr. B* **2016,** *1027*, 181-186.
186. Weiss, B.; Clarkson, T. W.; Simon, W., Silent latency periods in methylmercury poisoning and in neurodegenerative disease. *Environ. Health Perspect.* **2002,** *110*, 851-854.
187. Chang, L. W.; Dudley, A. W., Jr.; Dudley, M. A.; Ganther, H. E.; Sunde, M. L., Modification of the neurotoxic effects of methylmercury by selenium. In *Neurotoxicology*, Roizin, L.; Shiraki, H., Eds. Raven Press: New York, 1977; pp 275-282.
188. Hill, A.; Gailer, J., Linking molecular targets of Cd in the bloodstream to organ-based adverse health effects. *J. Inorg. Biochem.* **2021,** *216*, 111279.

Appendix A: Additional Figures

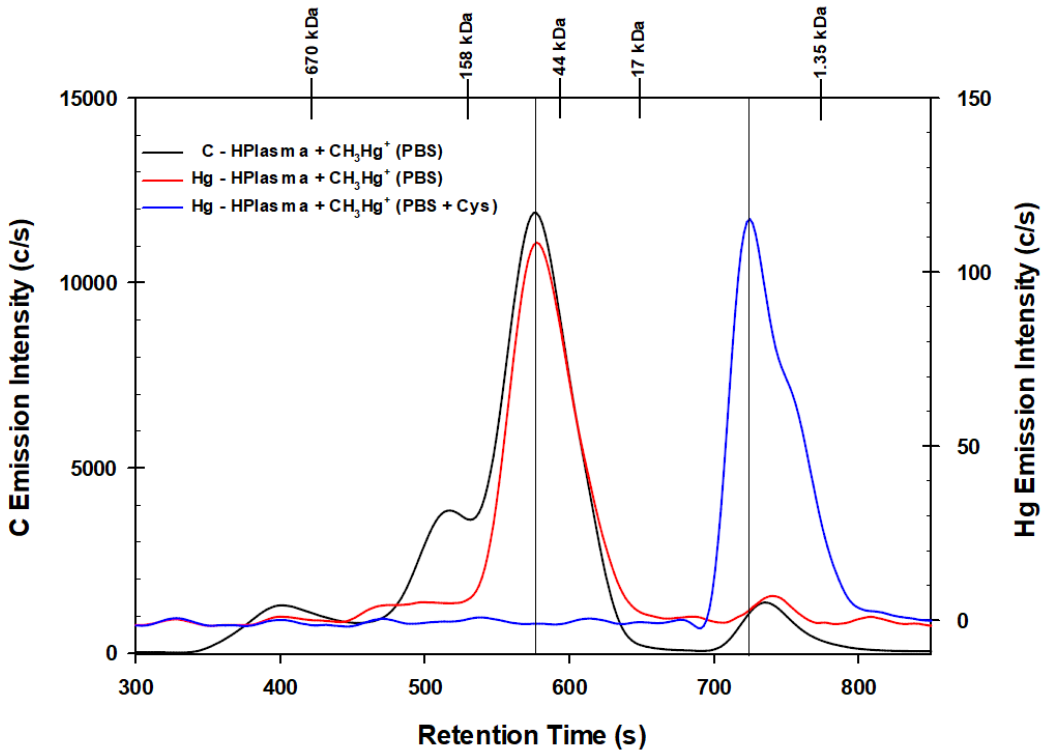

Figure A1: C- and Hg-specific chromatograms obtained by SEC-ICP-AES for the analysis of human blood plasma spiked with 5 µL of 0.01 M CH_3HgOH solution followed by the addition of 495 µL PBS. Column: Sepax SRT-10C SEC-300 column (7.8 × 300 mm I.D. × Length, 10 µm particle size, 300 Å pore size); Mobile phase: 150 mM PBS (pH 7.4); Temperature: 20 °C; Flow rate: 1.0 mL/min; Injection volume: 500 µL (250 µL blood plasma and 250 µL of PBS containing 5 µg Hg, 50 µM CH_3Hg^+); Detector: ICP-AES (C-emission wavelength – 193.091 nm, Hg-emission wavelength – 253.652 nm). The retention times of molecular weight markers are indicated at the top of the figure.

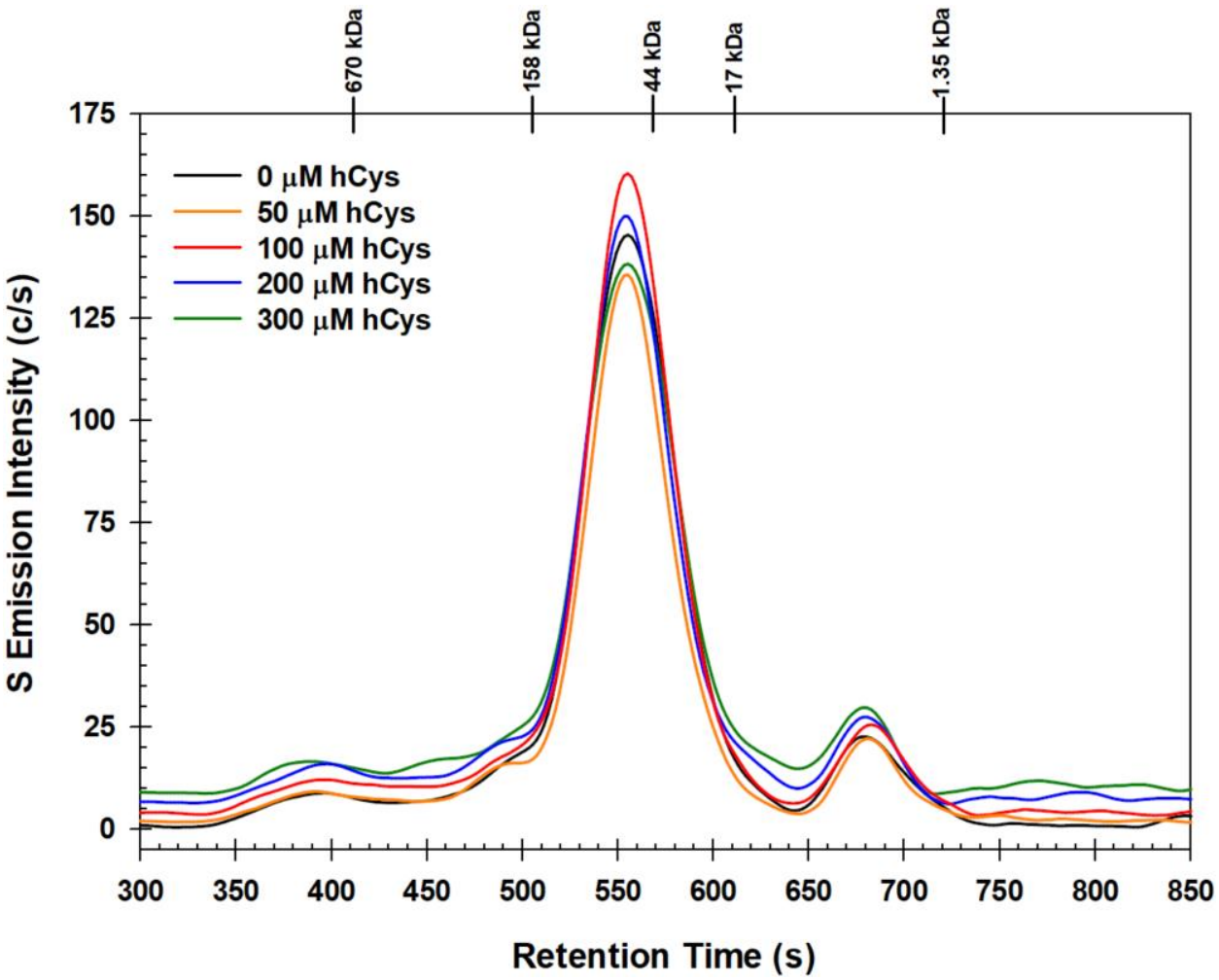

Figure A2: S-specific chromatograms obtained by SEC-ICP-AES for the analysis of rabbit blood plasma spiked with 5 µL of 0.01 M CH_3HgOH solution followed by the addition of 495 µL PBS. Column: Sepax SRT-10C SEC-300 column (7.8 × 300 mm I.D. × Length, 10 µm particle size, 300 Å pore size); Mobile phase: 150 mM PBS (pH 7.4) with 0, 50, 100, 200, 300 µM hCys; Temperature: 20 °C; Flow rate: 1.0 mL/min; Injection volume: 500 µL (250 µL blood plasma and 250 µL of PBS containing 5 µg Hg, 50 µM CH_3Hg^+); Detector: ICP-AES (C-emission wavelength – 193.091 nm, Hg-emission wavelength – 253.652 nm). The retention times of molecular weight markers are indicated at the top of the figure.

Appendix B: Copyright Permissions

Figure B1: Portions of Chapter 1 are used with permission from American Association for the Advancement of Science. Figure 1.2 is modified from Figure 2 in Mertz (1981).

THE AMERICAN ASSOCIATION FOR THE ADVANCEMENT OF SCIENCE LICENSE TERMS AND CONDITIONS

Nov 15, 2021

This Agreement between University of Calgary -- Tristen Bridle ("You") and The American Association for the Advancement of Science ("The American Association for the Advancement of Science") consists of your license details and the terms and conditions provided by The American Association for the Advancement of Science and Copyright Clearance Center.

License Number	5190410145428
License date	Nov 15, 2021
Licensed Content Publisher	The American Association for the Advancement of Science
Licensed Content Publication	Science
Licensed Content Title	The Essential Trace Elements
Licensed Content Author	Walter Mertz
Licensed Content Date	Sep 18, 1981
Licensed Content Volume	213
Licensed Content Issue	4514
Volume number	213
Issue number	4514

Type of Use	Thesis / Dissertation
Requestor type	Scientist/individual at a research institution
Format	Electronic
Portion	Text Excerpt
Number of pages requested	1
Title	Probing the Bioinorganic Chemistry of Methylmercury in Mammalian Blood Plasma
Institution name	University of Calgary
Expected presentation date	Dec 2021
Portions	I want to include a modified version of Figure 2 in my Masters thesis introduction.
Requestor Location	University of Calgary 2500 University Dr NW Calgary, AB T2N 1N4 Canada Attn: University of Calgary
Total	0.00 CAD

Terms and Conditions

American Association for the Advancement of Science TERMS AND CONDITIONS

Regarding your request, we are pleased to grant you non-exclusive, non-transferable permission, to republish the AAAS material identified above in your work identified above, subject to the terms and conditions herein. We must be contacted for permission for any uses other than those specifically identified in your request above.

The following credit line must be printed along with the AAAS material: "From [Full Reference Citation]. Reprinted with permission from AAAS."

All required credit lines and notices must be visible any time a user accesses any part of the AAAS material and must appear on any printed copies and authorized user might make.

This permission does not apply to figures / photos / artwork or any other content or materials included in your work that are credited to non-AAAS sources. If the requested material is sourced to or references non-AAAS sources, you must obtain authorization from that source as well before using that material. You agree to hold harmless and indemnify AAAS against any claims arising from your use of any content in your work that is credited to non-AAAS sources.

If the AAAS material covered by this permission was published in Science during the years 1974 - 1994, you must also obtain permission from the author, who may grant or withhold permission, and who may or may not charge a fee if permission is granted. See original article for author's address. This condition does not apply to news articles.

The AAAS material may not be modified or altered except that figures and tables may be modified with permission from the author. Author permission for any such changes must be secured prior to your use.

Whenever possible, we ask that electronic uses of the AAAS material permitted herein include a hyperlink to the original work on AAAS's website (hyperlink may be embedded in the reference citation).

AAAS material reproduced in your work identified herein must not account for more than 30% of the total contents of that work.

AAAS must publish the full paper prior to use of any text.

AAAS material must not imply any endorsement by the American Association for the Advancement of Science.

This permission is not valid for the use of the AAAS and/or Science logos.

AAAS makes no representations or warranties as to the accuracy of any information contained in the AAAS material covered by this permission, including any warranties of

merchantability or fitness for a particular purpose.

If permission fees for this use are waived, please note that AAAS reserves the right to charge for reproduction of this material in the future.

Permission is not valid unless payment is received within sixty (60) days of the issuance of this permission. If payment is not received within this time period then all rights granted herein shall be revoked and this permission will be considered null and void.

In the event of breach of any of the terms and conditions herein or any of CCC's Billing and Payment terms and conditions, all rights granted herein shall be revoked and this permission will be considered null and void.

AAAS reserves the right to terminate this permission and all rights granted herein at its discretion, for any purpose, at any time. In the event that AAAS elects to terminate this permission, you will have no further right to publish, publicly perform, publicly display, distribute or otherwise use any matter in which the AAAS content had been included, and all fees paid hereunder shall be fully refunded to you. Notification of termination will be sent to the contact information as supplied by you during the request process and termination shall be immediate upon sending the notice. Neither AAAS nor CCC shall be liable for any costs, expenses, or damages you may incur as a result of the termination of this permission, beyond the refund noted above.

This Permission may not be amended except by written document signed by both parties.

The terms above are applicable to all permissions granted for the use of AAAS material. Below you will find additional conditions that apply to your particular type of use.

FOR A THESIS OR DISSERTATION
If you are using figure(s)/table(s), permission is granted for use in print and electronic versions of your dissertation or thesis. A full text article may be used in print versions only of a dissertation or thesis.

Permission covers the distribution of your dissertation or thesis on demand by ProQuest / UMI, provided the AAAS material covered by this permission remains in situ.

If you are an Original Author on the AAAS article being reproduced, please refer to your License to Publish for rules on reproducing your paper in a dissertation or thesis.

FOR JOURNALS:
Permission covers both print and electronic versions of your journal article, however the AAAS material may not be used in any manner other than within the context of your article.

FOR BOOKS/TEXTBOOKS:
If this license is to reuse figures/tables, then permission is granted for non-exclusive world rights in all languages in both print and electronic formats (electronic formats are defined below).

If this license is to reuse a text excerpt or a full text article, then permission is granted for non-exclusive world rights in English only. You have the option of securing either print or electronic rights or both, but electronic rights are not automatically granted and do garner additional fees. Permission for translations of text excerpts or full text articles into other languages must be obtained separately.

Licenses granted for use of AAAS material in electronic format books/textbooks are valid only in cases where the electronic version is equivalent to or substitutes for the print version of the book/textbook. The AAAS material reproduced as permitted herein must remain in situ and must not be exploited separately (for example, if permission covers the use of a full text article, the article may not be offered for access or for purchase as a stand-alone unit), except in the case of permitted textbook companions as noted below.

You must include the following notice in any electronic versions, either adjacent to the reprinted AAAS material or in the terms and conditions for use of your electronic products: "Readers may view, browse, and/or download material for temporary copying purposes only, provided these uses are for noncommercial personal purposes. Except as provided by law,

this material may not be further reproduced, distributed, transmitted, modified, adapted, performed, displayed, published, or sold in whole or in part, without prior written permission from the publisher."

If your book is an academic textbook, permission covers the following companions to your textbook, provided such companions are distributed only in conjunction with your textbook at no additional cost to the user:

- Password-protected website
- Instructor's image CD/DVD and/or PowerPoint resource
- Student CD/DVD

All companions must contain instructions to users that the AAAS material may be used for non-commercial, classroom purposes only. Any other uses require the prior written permission from AAAS.

If your license is for the use of AAAS Figures/Tables, then the electronic rights granted herein permit use of the Licensed Material in any Custom Databases that you distribute the electronic versions of your textbook through, so long as the Licensed Material remains within the context of a chapter of the title identified in your request and cannot be downloaded by a user as an independent image file.

Rights also extend to copies/files of your Work (as described above) that you are required to provide for use by the visually and/or print disabled in compliance with state and federal laws.

This permission only covers a single edition of your work as identified in your request.

FOR NEWSLETTERS:
Permission covers print and/or electronic versions, provided the AAAS material reproduced as permitted herein remains in situ and is not exploited separately (for example, if permission covers the use of a full text article, the article may not be offered for access or for purchase as a stand-alone unit)

FOR ANNUAL REPORTS:
Permission covers print and electronic versions provided the AAAS material reproduced as permitted herein remains in situ and is not exploited separately (for example, if permission covers the use of a full text article, the article may not be offered for access or for purchase as a stand-alone unit)

FOR PROMOTIONAL/MARKETING USES:
Permission covers the use of AAAS material in promotional or marketing pieces such as information packets, media kits, product slide kits, brochures, or flyers limited to a single print run. The AAAS Material may not be used in any manner which implies endorsement or promotion by the American Association for the Advancement of Science (AAAS) or Science of any product or service. AAAS does not permit the reproduction of its name, logo or text on promotional literature.

If permission to use a full text article is permitted, The Science article covered by this permission must not be altered in any way. No additional printing may be set onto an article copy other than the copyright credit line required above. Any alterations must be approved

in advance and in writing by AAAS. This includes, but is not limited to, the placement of sponsorship identifiers, trademarks, logos, rubber stamping or self-adhesive stickers onto the article copies.

Additionally, article copies must be a freestanding part of any information package (i.e. media kit) into which they are inserted. They may not be physically attached to anything, such as an advertising insert, or have anything attached to them, such as a sample product. Article copies must be easily removable from any kits or informational packages in which they are used. The only exception is that article copies may be inserted into three-ring binders.

FOR CORPORATE INTERNAL USE:
The AAAS material covered by this permission may not be altered in any way. No additional printing may be set onto an article copy other than the required credit line. Any alterations must be approved in advance and in writing by AAAS. This includes, but is not limited to the placement of sponsorship identifiers, trademarks, logos, rubber stamping or self-adhesive stickers onto article copies.

If you are making article copies, copies are restricted to the number indicated in your request and must be distributed only to internal employees for internal use.

If you are using AAAS Material in Presentation Slides, the required credit line must be visible on the slide where the AAAS material will be reprinted

If you are using AAAS Material on a CD, DVD, Flash Drive, or the World Wide Web, you must include the following notice in any electronic versions, either adjacent to the reprinted AAAS material or in the terms and conditions for use of your electronic products: "Readers may view, browse, and/or download material for temporary copying purposes only, provided these uses are for noncommercial personal purposes. Except as provided by law, this material may not be further reproduced, distributed, transmitted, modified, adapted, performed, displayed, published, or sold in whole or in part, without prior written permission from the publisher." Access to any such CD, DVD, Flash Drive or Web page must be restricted to your organization's employees only.

FOR CME COURSE and SCIENTIFIC SOCIETY MEETINGS:
Permission is restricted to the particular Course, Seminar, Conference, or Meeting indicated in your request. If this license covers a text excerpt or a Full Text Article, access to the reprinted AAAS material must be restricted to attendees of your event only (if you have been granted electronic rights for use of a full text article on your website, your website must be password protected, or access restricted so that only attendees can access the content on your site).

If you are using AAAS Material on a CD, DVD, Flash Drive, or the World Wide Web, you must include the following notice in any electronic versions, either adjacent to the reprinted AAAS material or in the terms and conditions for use of your electronic products: "Readers may view, browse, and/or download material for temporary copying purposes only, provided these uses are for noncommercial personal purposes. Except as provided by law, this material may not be further reproduced, distributed, transmitted, modified, adapted, performed, displayed, published, or sold in whole or in part, without prior written permission from the publisher."

FOR POLICY REPORTS:

These rights are granted only to non-profit organizations and/or government agencies. Permission covers print and electronic versions of a report, provided the required credit line appears in both versions and provided the AAAS material reproduced as permitted herein remains in situ and is not exploited separately.

FOR CLASSROOM PHOTOCOPIES:
Permission covers distribution in print copy format only. Article copies must be freestanding and not part of a course pack. They may not be physically attached to anything or have anything attached to them.

FOR COURSEPACKS OR COURSE WEBSITES:
These rights cover use of the AAAS material in one class at one institution. Permission is valid only for a single semester after which the AAAS material must be removed from the Electronic Course website, unless new permission is obtained for an additional semester. If the material is to be distributed online, access must be restricted to students and instructors enrolled in that particular course by some means of password or access control.

FOR WEBSITES:
You must include the following notice in any electronic versions, either adjacent to the reprinted AAAS material or in the terms and conditions for use of your electronic products: "Readers may view, browse, and/or download material for temporary copying purposes only, provided these uses are for noncommercial personal purposes. Except as provided by law, this material may not be further reproduced, distributed, transmitted, modified, adapted, performed, displayed, published, or sold in whole or in part, without prior written permission from the publisher."

Permissions for the use of Full Text articles on third party websites are granted on a case by case basis and only in cases where access to the AAAS Material is restricted by some means of password or access control. Alternately, an E-Print may be purchased through our reprints department (brocheleau@rockwaterinc.com).

REGARDING FULL TEXT ARTICLE USE ON THE WORLD WIDE WEB IF YOU ARE AN 'ORIGINAL AUTHOR' OF A SCIENCE PAPER

If you chose "Original Author" as the Requestor Type, you are warranting that you are one of authors listed on the License Agreement as a "Licensed content author" or that you are acting on that author's behalf to use the Licensed content in a new work that one of the authors listed on the License Agreement as a "Licensed content author" has written.

Original Authors may post the 'Accepted Version' of their full text article on their personal or on their University website and not on any other website. The 'Accepted Version' is the version of the paper accepted for publication by AAAS including changes resulting from peer review but prior to AAAS's copy editing and production (in other words not the AAAS published version).

FOR MOVIES / FILM / TELEVISION:
Permission is granted to use, record, film, photograph, and/or tape the AAAS material in connection with your program/film and in any medium your program/film may be shown or heard, including but not limited to broadcast and cable television, radio, print, world wide web, and videocassette.

The required credit line should run in the program/film's end credits.

FOR MUSEUM EXHIBITIONS:
Permission is granted to use the AAAS material as part of a single exhibition for the duration of that exhibit. Permission for use of the material in promotional materials for the exhibit must be cleared separately with AAAS (please contact us at permissions@aaas.org).

FOR TRANSLATIONS:
Translation rights apply only to the language identified in your request summary above.

The following disclaimer must appear with your translation, on the first page of the article, after the credit line: "This translation is not an official translation by AAAS staff, nor is it endorsed by AAAS as accurate. In crucial matters, please refer to the official English-language version originally published by AAAS."

FOR USE ON A COVER:
Permission is granted to use the AAAS material on the cover of a journal issue, newsletter issue, book, textbook, or annual report in print and electronic formats provided the AAAS material reproduced as permitted herein remains in situ and is not exploited separately

By using the AAAS Material identified in your request, you agree to abide by all the terms and conditions herein.

Questions about these terms can be directed to the AAAS Permissions department permissions@aaas.org.

Other Terms and Conditions:

v 2

Questions? customercare@copyright.com or +1-855-239-3415 (toll free in the US) or +1-978-646-2777.

Figure B2: Proof of MDPI Open Access Information and Policy. Figures in Chapter 4 are used with the permission of Multidisciplinary Digital Publishing Institute and Bridle et al. (2021) of which I am an author. Figure 4.1 is taken from Figure 4 in Bridle et al. (2021). Figure 4.5 is modified from Figure 3 in Bridle et al. (2021).

MDPI Open Access Information and Policy

All articles published by MDPI are made immediately available worldwide under an open access license. This means:

- everyone has free and unlimited access to the full-text of *all* articles published in MDPI journals;
- everyone is free to re-use the published material if proper accreditation/citation of the original publication is given;
- open access publication is supported by the authors' institutes or research funding agencies by payment of a comparatively low **Article Processing Charge (APC)** for accepted articles.

Permissions

No special permission is required to reuse all or part of article published by MDPI, including figures and tables. For articles published under an open access Creative Common CC BY license, any part of the article may be reused without permission provided that the original article is clearly cited. Reuse of an article does not imply endorsement by the authors or MDPI.